Chapter 8
Selected Research Findings: Contaminant Partitioning

In the previous chapters of Part III, we discussed various aspects that affect the partitioning of contaminants of anthropogenic origin among the liquid, solid, and gaseous phases in saturated and partially saturated porous media. The partitioning process controls the fate of contaminants in the subsurface, defining their redistribution and transformation. This chapter presents selected research findings that illustrate various aspects of contaminant partitioning in the subsurface. We stress that, although many examples are included here, this chapter does not cover the entire spectrum of contaminant partitioning phenomena that occur in the subsurface.

8.1 Partitioning Among Phases

Under natural conditions, contaminants often reach the earth's surface as a mixture of (potentially) toxic chemicals, having a range of physicochemical properties that affect their partitioning among the gaseous, liquid, and solid phases. As a consequence, contaminant retention properties in the subsurface are highly diverse. Contaminants may reach the subsurface from the air, water, or land surface.

As an introductory example, we consider gasoline (a common and universally used petrochemical product comprising a mixture of about 200 hydrocarbons with different properties) to illustrate contaminant redistribution among phases in relation to their environmental behavior. The recent model of Foster et al. (2005) provides an excellent approach for assessing differential volatilization, dissolution, and retention of various gasoline hydrocarbons in the environment. Based mainly on their volumetric composition, relevant properties (vapor pressure, water solubility, octanol/water partition coefficient K_{ow}), environmental/human hazardous aspects (e.g., toxicity), and persistence (in water, soil, sediments), the authors grouped gasoline hydrocarbons into 24 blocks with a density increasing from 0.564 to 0.837 g/mL. Hydrocarbons were grouped primarily into structural classification including alkanes and alkenes with normal, branched, or cyclic structure; aromatics with one or two rings; and the number of carbon atoms in the

B. Berkowitz et al., *Contaminant Geochemistry*,
DOI: 10.1007/978-3-642-54777-5_8, © Springer-Verlag Berlin Heidelberg 2014

Table 8.1 Component groups for gasoline based on C—number and main chemical composition

Structural class	Number of carbon atoms (C)									
	3	4	5	6	7	8	9	10	11	12
n-alkanes	1		2	3	4			7		
Isoalkanes			5		6					
n-alkenes		8		9		20				
Isoalkenes				10						
Cyclic alkanes			11		13		14			
Cyclic alkenes				15						
Monoaromatics				16	17	19	21			22
Diaromatics								23	24	
Cyclohexane				12						
Ethylbenzene						18				

Reprinted with permission from Foster et al. (2005). Copyright 2005 American Chemical Society

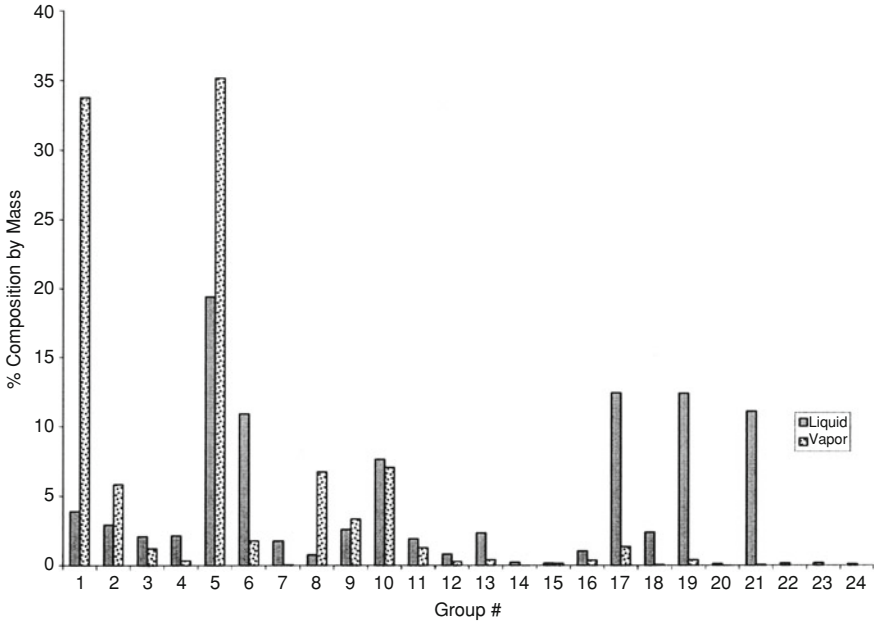

Fig. 8.1 Liquid and vapor gasoline compositions. Reprinted with permission from Foster et al. (2005). Copyright 2005 American Chemical Society

compounds, ranging from 3 to 12. The physicochemical properties are summarized in Table 8.1, and the compositional differences between each compartment and those of the original gasoline mixture are given in Fig. 8.1. These data provide an overview of the multiple properties of a contaminant mixture; these properties control its partitioning among the subsurface phases.

The mode of entry to the subsurface environment affects partitioning among subsurface components. Considering that the composition of gasoline depends on the nature of the emission process, Foster et al. (2005) developed a model scenario where a known amount of gasoline emission was divided equally among air (gas), water, and soil. The composition of gasoline in the air phase was assumed to be in the form of a fugitive vapor from liquid gasoline, while emissions to soil or to water were considered as liquid gasoline. Figure 8.2 exhibits a four by four set of charts displaying the relative gasoline composition by mass in air, water, soil, and sediment as a result of three modes of entry and the total simultaneous emission. For each mode of entry, the percentage of gasoline by mass and the concentration in each of the 24 compartments was calculated and the contribution of the mode of entry estimated.

When the emission of gasoline is mainly into the air phase, more than 99 % of the contaminant remains in the air. In this case, the gasoline emission consists predominantly of alkanes (70 % of the total gasoline composition) with a lower number of carbon atoms. When gasoline emission is mainly to water, 85 % remains in the aqueous phase, including groups 5, 6, 7, 19, and 21 (see Fig. 8.1), about 8 % partitions into sediment, and less than 1 % into soil. The mode of entry only into soil leads to retention of about 91 %. From Fig. 8.2, we see that simultaneous entry of a total emission of gasoline leads to a partitioning of 52 % in soil, 31 % in water, 14 % in air, and 3 % in sediments. This scenario and calculation provide a representative overview of contaminant partitioning among the gaseous, aqueous, and solid phases, as affected by the properties of the contaminants, the surrounding phase, and their mode of entry into the environment.

8.2 Contaminant Volatilization

Contaminant volatilization from subsurface solid and aqueous phases may lead, on the one hand, to pollution of the atmosphere and, on the other hand, to contamination (by vapor transport) of the vadose zone and groundwater. Potential volatility of a contaminant is related to its inherent vapor pressure, but actual vaporization rates depend on the environmental conditions and other factors that control behavior of chemicals at the solid–gas–water interface. For surface deposits, the actual rate of loss, or the proportionality constant relating vapor pressure to volatilization rates, depends on external conditions (such as turbulence, surface roughness, and wind speed) that affect movement away from the evaporating surface. Close to the evaporating surface, there is relatively little movement of air and the vaporized substance is transported from the surface through the stagnant air layer only by molecular diffusion. The rate of contaminant volatilization from the subsurface is a function of the equilibrium distribution between the gas, water, and solid phases, as related to vapor pressure solubility and adsorption, as well as of the rate of contaminant movement to the soil surface.

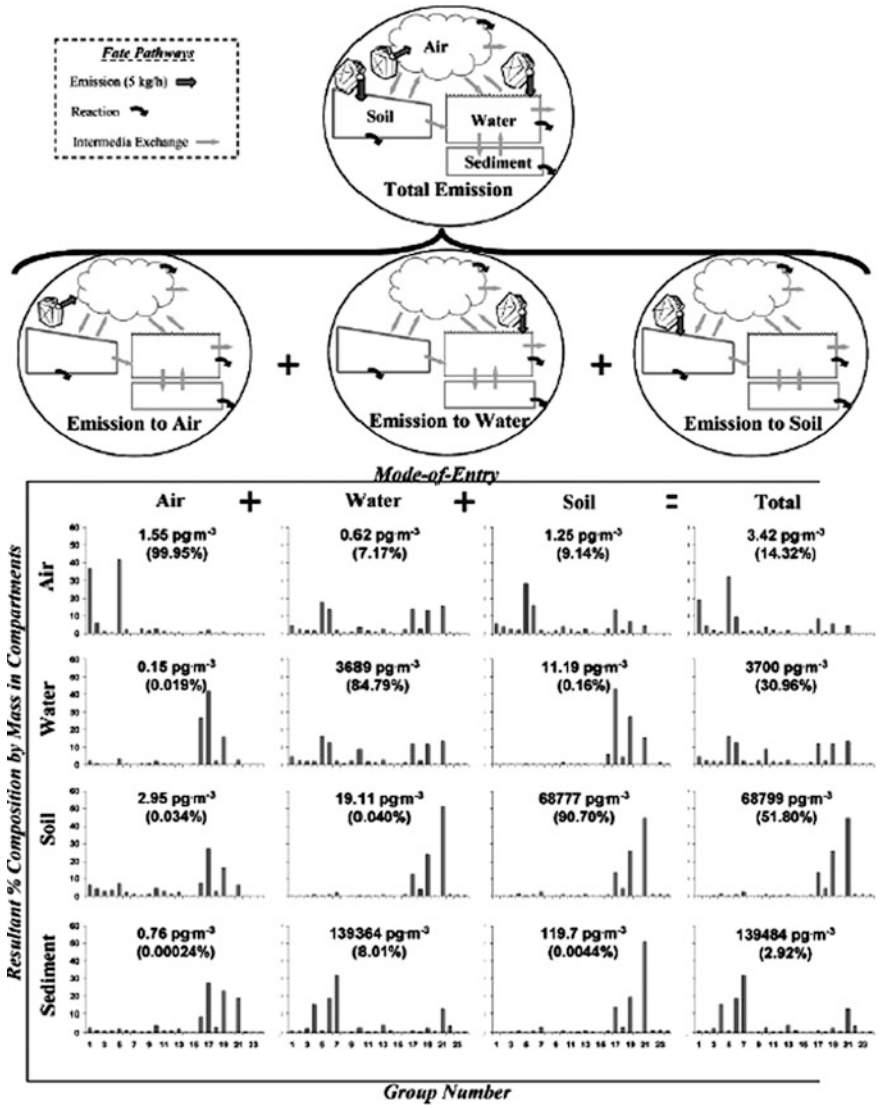

Fig. 8.2 Gasoline composition in environmental compartments as a result of emissions to air, water, soil, and sediment, individually at an arbitrary rate of 5 kg/ha, and simultaneously. Reprinted with permission from Foster et al. (2005). Copyright 2005 American Chemical Society

To illustrate these phenomena, we discuss relevant examples of volatile chemical products that originate mainly from agricultural and industrial–municipal practices. The rates and extent of volatilization of these chemicals are presented in relation to subsurface environmental conditions.

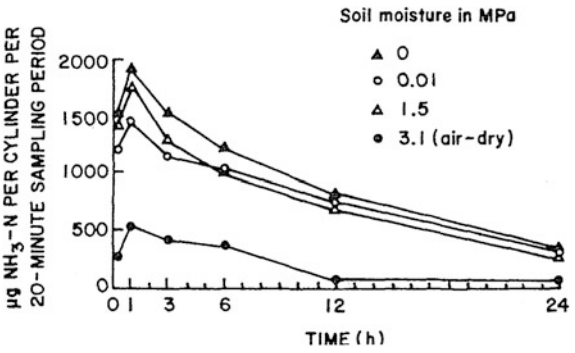

Fig. 8.3 Ammonia-N volatilization as a function of time from sewage sludge applied to soils at 0, 0.01, and 1.5 MPa, and air-dry initial moisture levels (Donovan and Logan 1983)

8.2.1 Inorganic Contaminants

Ammonia volatilization illustrates the behavior of inorganic chemicals in the subsurface under aerobic or anaerobic conditions. It is recognized that ammonia volatilization is affected by the time and depth of release, pH, temperature, and moisture content as well as by the cation exchange capacity (CEC).

The relative concentrations of NH_3 and NH_4^+ in an aqueous solution are pH dependent, in accordance with the following reaction equilibrium:

$$NH_4^+ \rightleftharpoons NH_{3(aq)} + H^+ \tag{8.1}$$

$$[NH_{3(aq)}][H^+]/[NH_4^+] = K = 10^{-9.5} \tag{8.2}$$

$$\log\left([NH_{3(aq)}]/[NH_4^+]\right) = -9.5 + \text{pH}, \tag{8.3}$$

where $NH_{3(aq)}$ is NH_3 in solution. According to these equations, the concentrations of $NH_{3(aq)}$ at pH 5, 7, and 9 are 0.0036, 0.36, and 36 %, respectively, of the total ammonia-N in solution.

Loss of NH_3 from calcareous subsurface media is considerably greater than from noncalcareous media and involves production of $(NH_4)_2CO_3$ or NH_4HCO_3. The fate of $(NH_4)_2SO_4$ added to calcareous material is expressed by the reaction between $(NH_4)_2SO_4$ and $CaCO_3$, and as a result, volatile ammonia is produced according to the equation

$$CaCO_3 + (NH_4)_2SO_4 \rightleftharpoons 2NH_3 + CO_2 + H_2O + CaSO_{4\,(solid)}. \tag{8.4}$$

A similar pattern of ammonia formation and volatilization occurs when sewage effluent is disposed on the land surface or in sludge-enriched soils. Donovan and Logan (1983) showed that ammonia loss increases with increasing pH and temperature and is affected by the type of sludge added to the land surface. Loss from air-dry soil is much lower than from a soil at moisture tension <1.5 MPa, the kinetics of volatilization with time being depicted in Fig. 8.3. Donovan and Logan

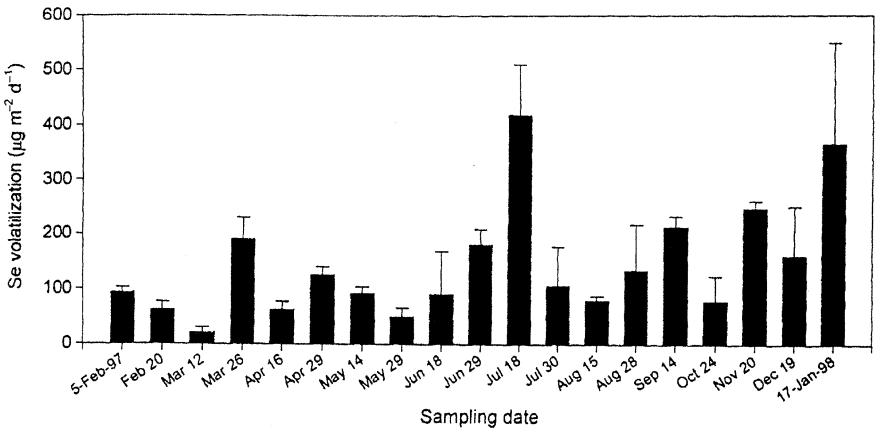

Fig. 8.4 Rates of selenium volatilization from soil versus time (Lin et al. 2000)

(1983) also report that NH_3 volatilization losses are greater from lime-stabilized sludge with pH = 12 than from aerobic or anaerobic sludge. A linear relationship between volatilization decrease and temperature decrease also characterizes NH_3 behavior in the sludge-amended lands.

A special case is given by ammonia volatilization from flooded land surfaces, which involves a more complex pathway. This is because the kinetics and extent of the volatilization are affected by water quality, type of land, and biological and environmental factors. In this particular case, the rate of NH_3 volatilization is mainly a function of ammonia concentration in the flooding water (Jayaweera and Mikkelsen 1991).

Nitrite formation may lead to nitrous oxide (N_2O) emission. An example of such a process under reclaimed effluent disposal on the land surface is reported by Master et al. (2004). Irrigating a grumosol (<60 % clay content) with fresh and reclaimed effluent water, it was found that, under effluent irrigation, the amount of N_2O emissions was double the amount emitted under freshwater treatment, at 60 % w/w. The N_2O emission from effluent-treated bulk soil was more than double the amount formed from large aggregates.

Plant-mediated volatilization of inorganic compounds is an accepted method for reclaiming selenium-contaminated lands. Volatile Se is formed mostly from dimethyl selenide, evolving from the land surface. For example, dimethyl selenide produced more than 90 % of the total volatile Se in the San Joachim Valley, California (Karlson and Frankenberger 1988). Lin et al. (2000) report on Se volatilization from a *Salicornia bigelovii* field which occurs as a result of Se methylation by plants. In their experiment, Lin et al. (2000) found that biological volatilization removed 62 mg Se m/yr, which accounted for 6.5 % of the total annual Se input to the *S. bigelovii* field. The fluctuation of Se volatilization rates during a 12-month study period is presented in Fig. 8.4. Linear regression analysis

Table 8.2 Saturation vapor pressures and densities of selected pesticides (modified after Taylor and Spencer 1990)

Pesticide	Molecular weight (g)	Temperature (°C)	Vapor pressure (MPa)	Vapor density (μg/L)
Alachlor	270	25	2.9	3.2×10^{-1}
Atrazine	216	25	9.0×10^{-2}	8.0×10^{-3}
Bromacil	261	25	2.9×10^{-2}	3.0×10^{-3}
DDT	354	25	4.5×10^{-2}	6.0×10^{-3}
Dieldrin	381	25	6.8×10^{-1}	1.0×10^{-1}
Diuron	233	25	2.1×10^{-2}	2.0×10^{-3}
Lindane	291	25	8.6	1.0
Malathion	330	20	1.3	1.8×10^{-1}
Parathion	291	25	1.3	1.5×10^{-1}
Trifluralin	335	20	1.5×10^{1}	2.0

of all 57 measurements, conducted during the study period, yielded the relationship $y = 51.96 \pm 9.42x$ ($r^2 = 0.252$), where x denotes the time during the year and y is the rate of Se volatilization. The regression shows a general increase in Se volatilization from spring to winter.

8.2.2 Organic Contaminants

Organic contaminants can be released to the surface in different ways, and contamination can be classified as point source and nonpoint source (or diffuse source). As an example of a *nonpoint source*, we discuss the case of pesticides applied during agricultural activity over large areas; an example of *point source* contamination is given by the behavior of petroleum products that reach the subsurface as a result of leakage (or a spill) from pipes or from a gas station.

Pesticides are characterized by a range of (saturation) vapor pressure and densities (Table 8.2); they therefore evaporate from the land surface in different patterns. Peck and Hornbuckle (2005) studied atmospheric concentrations of currently used pesticides in Iowa (United States) during the years 2000–2002. The average detected concentrations of five heavily used herbicides were 0.52 ng/m^3 for trifluralin, 4.6 ng/m^3 for acetoclor, 2.3 ng/m^3 for metolaclor, 1.7 ng/m^3 for pendimethalin, and 1.2 ng/m^3 for atrazine. The survey considered about 45 organic pesticides (herbicides and insecticides) used in the field; only seven of them were not detected in the air phase. A similar study was performed on herbicides used on the Canadian prairies (Waite et al. 2004), focusing on five main products: bromoxynil, dicamba, diclofop, MCPA, and trifluralin. Figure 8.5, which depicts the atmospheric concentration of trifluralin in three dugouts (Waite et al. 2004), clearly shows the seasonal variation of herbicide presence. In general, none of the herbicides was detected continuously throughout the sampling period.

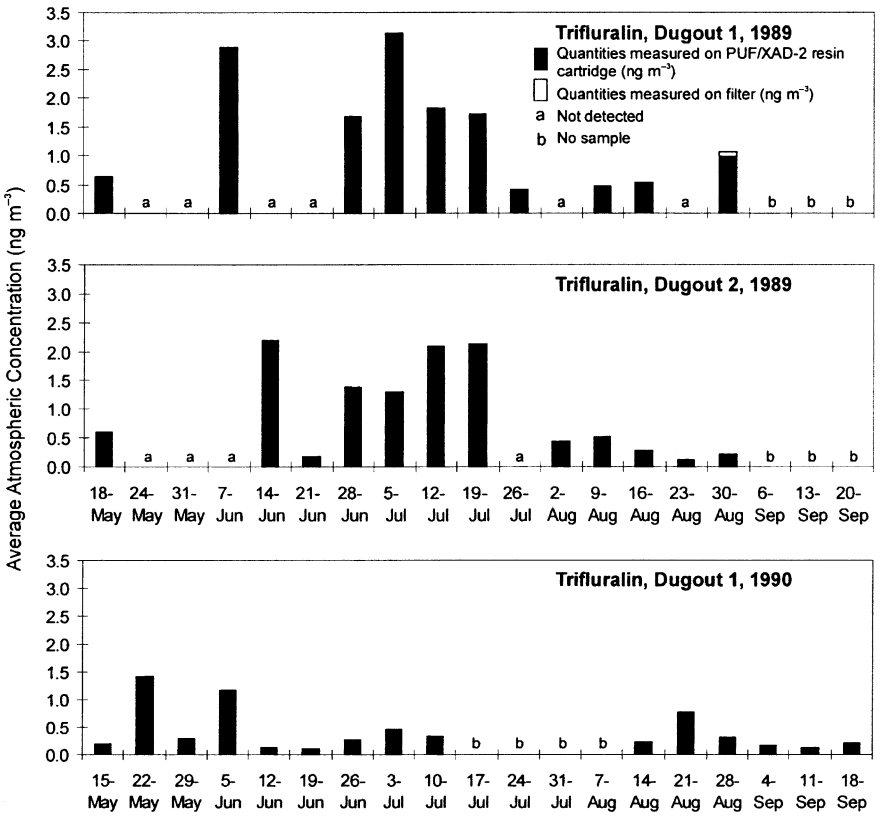

Fig. 8.5 Atmospheric concentrations of trifluralin in three dugouts on the Canadian Prairies during 1989–1990 (Waite et al. 2004)

Because each herbicide may degrade during volatilization, it is interesting to compare the cumulative volatilization of the parent contaminant and its metabolites. This behavior was studied in a wind-tunnel experiment by Wolters et al. (2003) for a mixture of parathion, terbuthylazine, and fenpropimorph, as well as for the metabolites fenpropimorph acid and desethyl-terbuthylazine. Figure 8.6 shows the volatilization dynamics of these pesticides and their metabolites when the products were applied initially on the surface of Gleyic Cambisol (~73 % clay, 23 % silt, 4 % clay). The volatilization, however, is controlled not only by the properties of the molecules but also by the properties of the subsurface composition, moisture content, and environmental factors.

Spencer and Cliath (1969, 1973) studied the effect of organic matter (OM) and clay content on vapor density of various pesticides. In general, they found that subsurface OM content and partition coefficients are of primary importance in describing the rate of volatilization for compounds having a high affinity for OM.

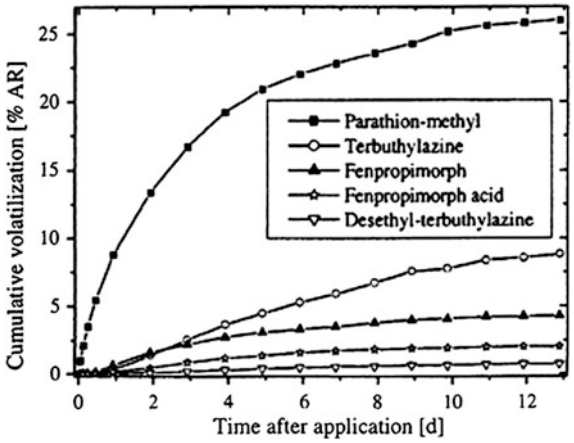

Fig. 8.6 Cumulative volatilization of ^{14}C-labeled pesticides and metabolites after soil surface application on gleyic cambisol (Wolters et al. 2003)

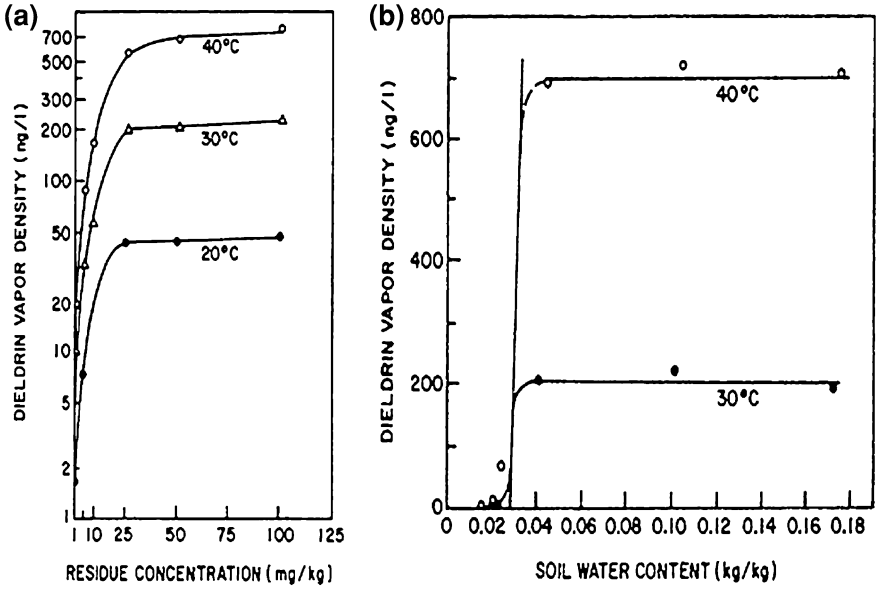

Fig. 8.7 Effect of **a** temperature and **b** soil moisture content on dieldrin vapor density (Taylor and Spencer 1990)

Temperature and moisture content are other important factors that control volatilization of organic contaminants in the subsurface. Spencer and Cliath (1969, 1973) showed that a temperature increase from 20 to 40 °C led to an increase in dieldrin vapor density from 45 to 700 ng/L (Fig. 8.7a). It also may be observed that a reduction in the soil moisture content caused a large reduction in the dieldrin

vapor densities, even when the pesticide concentration in the moist soil was high enough to yield vapor densities approaching those of the pure compound. These results explain why reduction in pesticide volatilization in dry soils was observed over many years.

Wolters et al. (2003) observed that volatilization kinetics of the fungicide fenpropimorph express a clear correlation between volatilization rates and soil moisture content. Volatilization rates reached a maximum 24 h after application under moist conditions and decreased with the decrease in soil moisture over following days.

8.2.3 Mixtures of Organic Contaminants

Volatilization from mixtures of organic contaminants brings about changes in both the physical and the chemical properties of the residual liquid. We consider data on kerosene volatilization, as summarized in Yaron et al. (1998). Kerosene is an industrial petroleum product composed of more than 100 hydrocarbons, which may become a subsurface contaminant.

The differential volatilization of neat kerosene components from a liquid phase, directly into the atmosphere during volatilization up to 50 % (w/w), is presented in Fig. 8.8. Ten kerosene components were selected, and their composition was depicted as a function of gas chromatograph peak size (%), which is linearly related to their concentration. It may be seen that the lighter fractions evaporate at the beginning of the volatilization process. Increasing evaporation causes additional components to volatilize, which leads to a relative increase in the heavier fractions of kerosene in the remaining liquid.

In the subsurface, kerosene volatilization is controlled by the physical and chemical properties of the solid phase and by the water content. Porosity is a major factor in defining the volatilization process. Galin et al. (1990) reported an experiment where neat kerosene at the saturation retention value was recovered from coarse, medium, and fine sands after 1, 5, and 14 days of incubation. The porosity of the sands decreased from coarse to fine. Figure 8.9 presents gas chromatographs obtained after kerosene volatilization. Note the loss of the more volatile hydrocarbons by evaporation in all sands 14 days after application and the lack of resemblance to the original kerosene. It is clear that the pore size of the sands affected the chemical composition of the remaining kerosene. For example, the C_9–C_{12} fractions disappeared completely 14 days after their application, except for the saturated fine sand case, where 5 % of the initially applied C_{12} remained.

The effect of aggregation of the subsurface solid phase on kerosene volatilization was studied by Fine and Yaron (1993), who compared the rate of aggregation in two size fractions of a vertisol soil: the <1 mm fraction and 2 mm aggregates. The total porosity of these two fractions was similar (53 and 55 % of the total volume, respectively). Differences in aggregation are reflected in the air

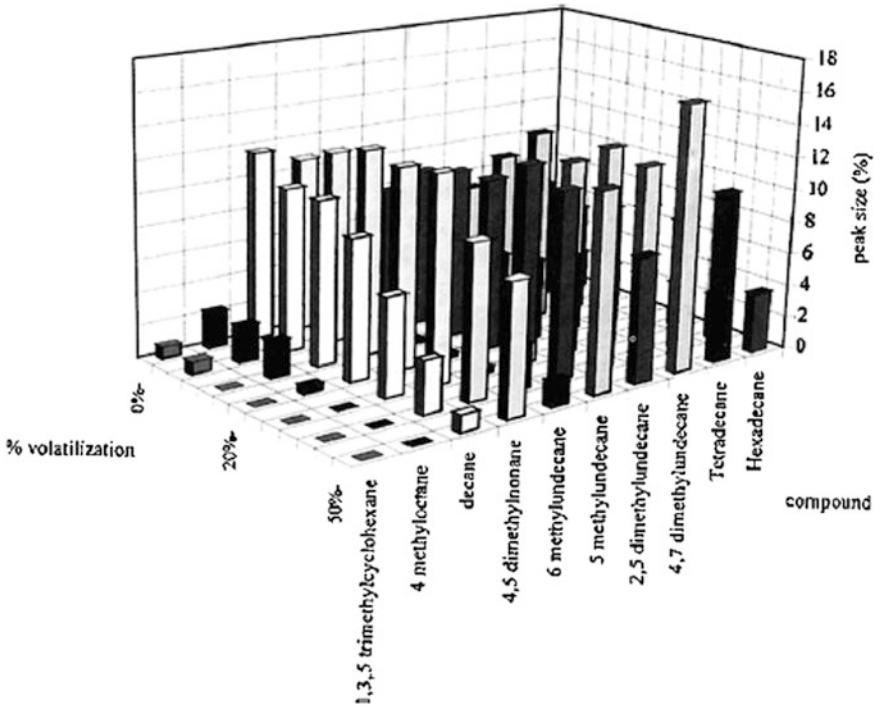

Fig. 8.8 Major remaining components of kerosene during the volatilization process (Yaron et al. 1998)

permeability; that is, their respective values were 0.0812 ± 0.009 and 0.145 ± 0.011 cm^2. Figure 8.10 presents the volatilization of kerosene as affected by the soil aggregation, when the initial amount applied was equivalent to the retention capacity. The more permeable fraction releases kerosene faster and thus enhances volatilization.

These examples indicate that aggregation and pore size distribution parameters affect volatilization of petroleum products from a contaminated subsurface. Fine and Yaron (1993) report that kerosene volatilization depends on the type of soil. Tests on four soils with a clay content increasing from 0.3 to 74.4 %, and OM content ranging from 0.01 to 5.1 % (Fig. 8.11), showed significant variations in rate and amount of volatilization over an 18-day period. This effect was attributed not only to the soil composition but also to the soil porosity and aggregation status.

Changes in the chemical composition of residual kerosene, resulting from volatilization of the light fractions, cause changes in the physical properties of the remaining product. Table 8.3 shows the effect of the differential volatilization on kerosene viscosity, surface tension, and density. When 20, 40, and 60 % of the initial amount of kerosene was removed by the transfer of light fractions to the atmosphere, the viscosity of the remaining kerosene was affected strongly. Negligible effects on liquid density and on surface tension were observed.

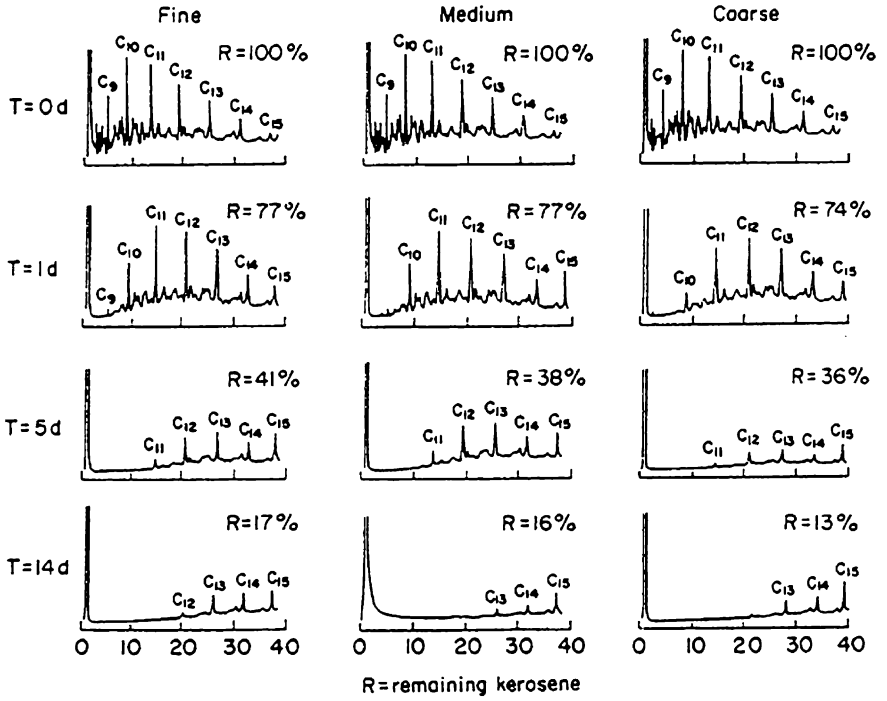

Fig. 8.9 Effect of porosity on composition of kerosene during 14 days of volatilization from fine, medium, and coarse sand, as seen from gas chromatograph analyses. Reprinted from Galin et al. (1990). Copyright 1990 with permission of Elsevier

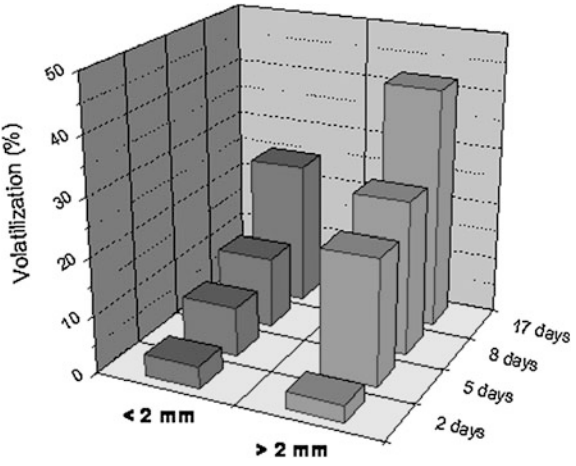

Fig. 8.10 Volatilization of kerosene from vertisol as affected by aggregate size. Reprinted from Fine and Yaron (1993). Copyright 1994 with permission of Elsevier

Differential volatilization, as affected by properties of the subsurface and its environmental conditions, leads to changes in residual composition of the hydrocarbon mixture. Jarsjo et al. (1994) investigated volatilization of kerosene

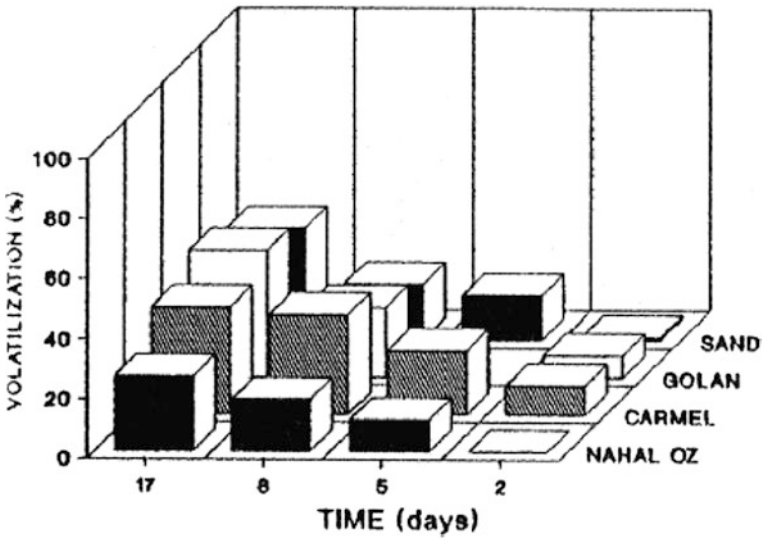

Fig. 8.11 Volatilization of kerosene as affected by soil type: sand (dune), chromoxeret (Golan), pelloxeret (Carmel), and calcic haploxeralf (Nahal Oz). Reprinted from Fine and Yaron (1993). Copyright 1994 with permission of Elsevier

Table 8.3 Effect of volatilization on physical properties of residual kerosene

Amount volatilized (%)	Density (g/cm^3)	Surface tension (1/Nm)	Viscosity (Pa s $\times$ 10^{-3})
0	0.805	2.75	1.32
20	0.810	2.78	1.48
40	0.818	2.80	1.78
60	0.819	2.78	1.96

Reprinted from Galin et al. (1990). Copyright 1990 with permission of Elsevier

from glacial and post-glacial soils. The composition of the residual kerosene mixture recovered from sand, sandy loam, and peat materials, after volatilization at 5 and 27 °C, for 7 and 30 days, respectively, is shown in Fig. 8.12. From this figure, we see that all the lighter components disappeared from the sand and the sandy loam and the residual kerosene percentages are similar regardless of temperature. The relative concentration of the light fraction, C_{10}–C_{12}, diminished with time in all soils, while those of the heavy fractions, C_{14} and C_{15}, increased.

Volatilization of an organic mixture of contaminants, distributed vertically in the subsurface, may induce not only a decrease in the component concentrations but also an enrichment of the deeper layers during the volatilization process. Figure 8.13 shows the actual content of three representative hydrocarbons—m-xylene (C_8), n-decane (C_{10}), and hexadcane (C_{16})—which originated from the applied kerosene found along a 20-cm soil column, 18 days after application on

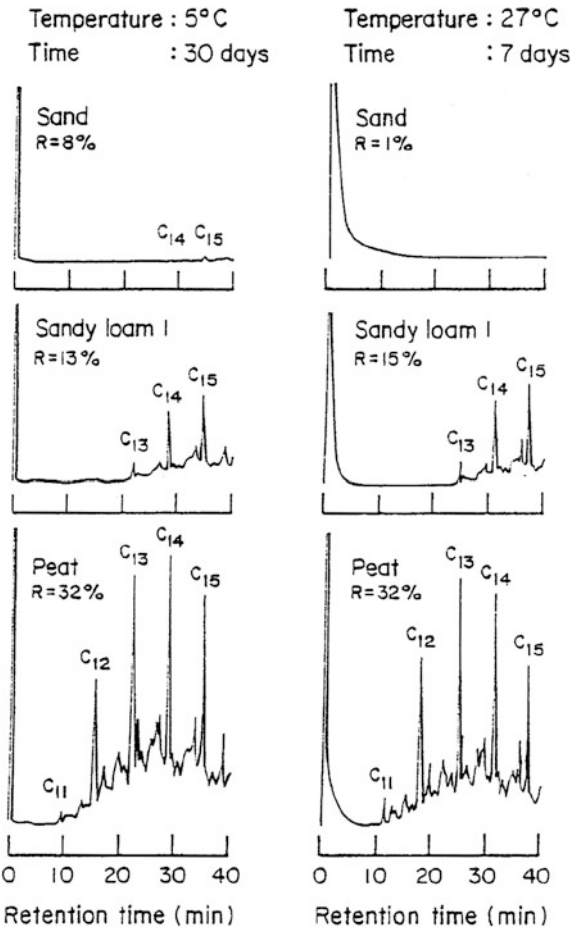

Fig. 8.12 Gas chromatographs of residual kerosene recovered from glacial and post-glacial earth materials after volatilization at 5 and 27 °C, for 30 and 7 days, respectively. *R* denotes the total remaining kerosene (percentage of initial amount). Reprinted from Jarsjo et al. (1994). Copyright 1994 with permission of Elsevier

dry soil. Roughly 30 % of the initial content of m-xylene still remained in the soil after 18 days. Furthermore, the content of m-xylene increased somewhat after the third day; a similar trend was found for the n-decane distribution. Hexadecane was partially removed from deeper layers and redistributed near the soil surface.

8.3 Solubility and Dissolution

The solubility of contaminants in subsurface water is controlled by (1) the molecular properties of the contaminant, (2) the porous media solid-phase composition, and (3) the chemistry of the aqueous solution. The presence of potential cosolvents or other chemicals in water also affects contaminant solubility. A number of relevant examples selected from the literature are presented here to illustrate various solubility and dissolution processes.

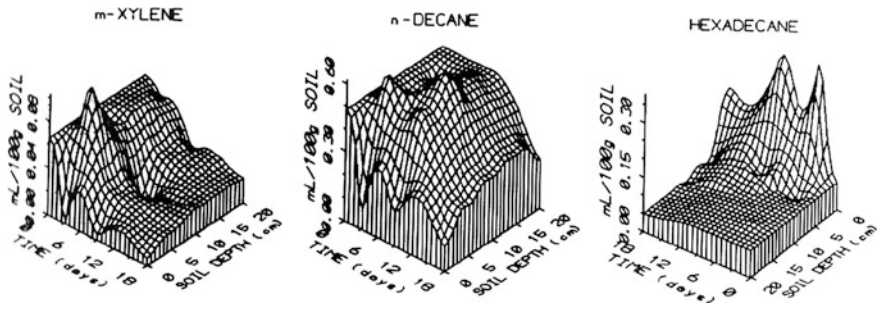

Fig. 8.13 Concentration of selected petroleum hydrocarbons (mL/100 g soil) during volatilization of kerosene from air-dry vertisol. Reprinted from Fine and Yaron (1993). Copyright 1994 with permission of Elsevier

8.3.1 Acidity and Alkalinity Effects

Hydrogen ion regulation in subsurface water is provided by numerous homogeneous or heterogeneous buffer systems. A buffer system is characterized by a range of pH within which it is efficient, relative to its acid- or base-neutralizing capacity. In a natural environment, the pH of the subsurface water does not generally correspond to an equilibrium state; this results in instability of pH values, which is reflected in short-term fluctuations due to seasonal variations and anthropogenic processes. The effects of low and high pH on dissolution of a number of earth minerals are discussed here.

Aluminum dissolution under acid rain is the outcome of an anthropogenically induced effect on the subsurface acid–base equilibrium. As a result of acidic atmospheric pollutants (e.g., HCl, HNO_3, H_2SO_4), rainwater becomes acidic; and when it reaches the subsurface, where buffering by existing bases is missing, the acidity of the subsurface water increases. Soil acidification usually is a long-term process. For example, Johnston et al. (1986) report a decrease from pH 7.2 to pH 4.2 after 100 years at the Rothamsted agricultural experimental station (United Kingdom).

Dissolution of Al, which has devastating effects on soil biological populations, is the main consequence of acidic atmospheric deposition in the forest environment in large areas of northern and central Europe and North America (Mulder et al. 1987). In a study of acid effects on sandy soils, van Grunsven et al. (1992) observed that the logarithm of Al dissolution rates in individual earth samples follows an inverse linear relationship with pH. Hargrove (1986) investigated Al dissociation from mica–OM complexes, observing that Al concentrations in water solutions reach minimum values in a pH range of about 4–5 (Fig. 8.14).

Trace element dissolution from soils surrounding abandoned waste incinerators, as a combined effect of pH and speciation, was reported by Bang and Hesterberg (2004), who determined the concentration of dissolved metals eluted from soil samples as a function of pH. In parallel, the speciations of Cu and Zn were analyzed using X-ray absorption and near-edge structure spectroscopy analysis

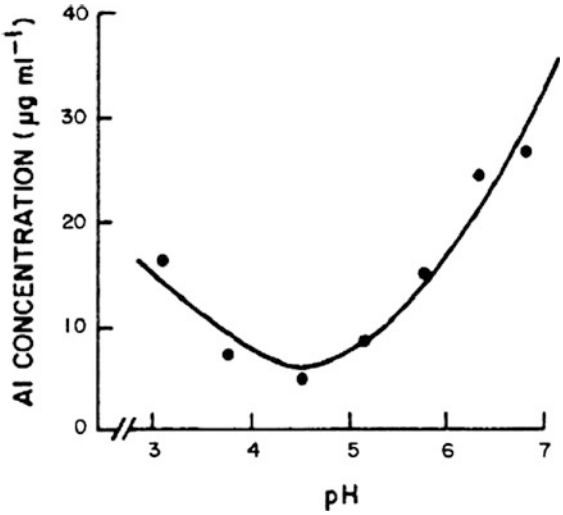

Fig. 8.14 Effect of pH on dissolution from Al–mica–organo matter complexes (Hargrove 1986)

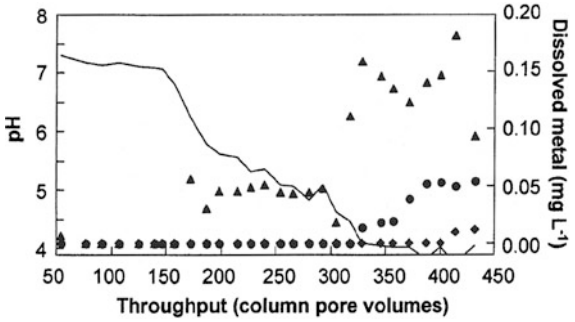

Fig. 8.15 Typical trends of dissolved Cu (*black circle*), Pb (*black diamond*), and Zn (*black up-pointing triangle*) concentrations and pH (−) in effluent solutions collected during a flow column experiment on soil samples from the Bogue site (USA), as a function of the throughput volume of acidified, 0.01 M $CaCl_2$ solution (Bang and Hesterberg 2004)

(XANES). Typical trends for dissolution of Cu, Pb, and Zn, as affected by pH, are presented in Fig. 8.15. The maximum dissolved concentration of these compounds occurred at the lowest pH. Dissolved Cu, Pb, and Zn concentrations increased as pH declined, compensating for the Na^+. This phenomenon occurs below pH threshold levels of pH ∼4 for Cu and Pb and pH ∼5 for Zn. The Cu and Zn results were consistent with synchrotron (XANES) spectroscopy data, suggesting that Cu was bound mainly to soil OM, while Zn was associated with Al- and Fe-oxide-type minerals.

Another key process involves gypsum dissolution; gypsum is found in the subsurface as a natural constituent or as an added reclamation material. In cases

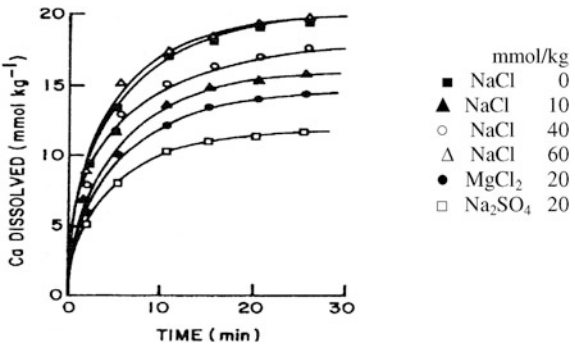

Fig. 8.16 Kinetics of Ca dissolution from a gypsum sample in various salt solutions (Gobran and Miyamoto 1985)

where human actions enhance subsurface alkalinity, as a result of irrigation with alkali water or poor management of irrigation and drainage, the distribution of gypsum with depth may be changed by gypsum dissolution. The effective solubility of gypsum depends only on the subsurface water chemistry and the exchange-phase composition of the solid matrix. The dissolution exchange reaction is

$$2NaX + CaSO_4 \rightleftharpoons CaX_2 + 2Na^+ + SO_4^{2-} \tag{8.5}$$

where X is one equivalent of exchanger and indicates that cation exchange removes Ca^{2+} from subsurface water and allows additional gypsum dissolution. Disposal of alkali water or alkali effluents on land brings an increase in the exchangeable Na^+ in the solid phase. Under such conditions, the dissolution of $CaSO_4$ in the subsurface increases to compensate for the Na^+ that exchanges with Ca^{2+}.

Effective gypsum solubility is enhanced through ion-pair formation and electrolyte effects. The amount of water required for dissolution of gypsum in an alkaline subsurface is likely to be much less than commonly inferred for gypsum solubility in water. When the alkalinity is associated with an increase in the total salt content, gypsum dissolution is affected by the presence of electrolytes. An example is given in Fig. 8.16, which shows dissolution kinetics of gypsum samples from Egypt in NaCl and $MgCl_2$ solutions (Gobran and Miyamoto 1985). It appears that the dissolved amounts at equilibrium are related to the ionic composition of the aqueous solution. We see that the dissolution in the subsurface water apparently increases with increasing salt content, as expected from ionic strength considerations.

8.3.2 Redox Processes

Redox processes affect contaminant solubility and may result from fluctuating saturation and drying processes in the subsurface due to natural or anthropogenic

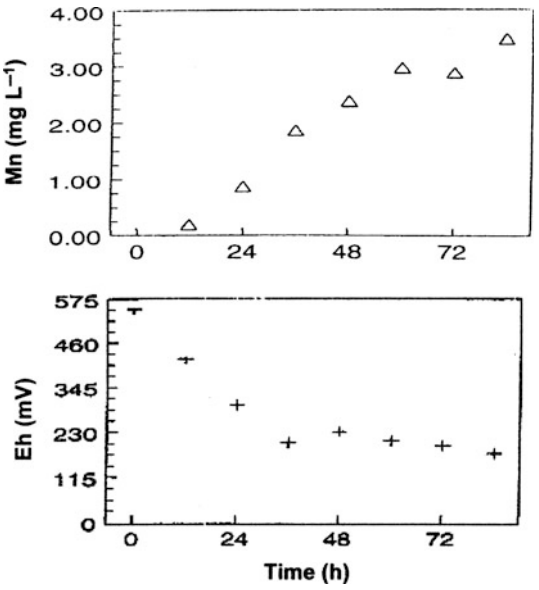

Fig. 8.17 Changes with time in soluble Mn (*increment*) and Eh (+). (Green et al. 2003)

factors. Reduction and oxidation processes also may occur simultaneously in a partially saturated soil matrix at the aggregate level: reduction into the solid-phase aggregate and oxidation at the aggregate surface. The reduction–oxidation process may be enhanced by biological activity or by chemical catalysis, which affects heavy metal solubility.

Examples of the ability of Mn oxides to oxidize metals directly or to catalyze metal oxidation have been reported widely (e.g., Lindsay 1979; McBride 1989, 1994; Stumm and Morgan 1996; Xiang and Banin 1996; Charlatchka and Cambier 2000). As an example, we consider a case study by Green et al. (2003) on solubilization of manganese and other trace metals from soils irrigated previously with water affected by acid mine runoff. The experiment was designed to simulate waterlogged irrigated soils, saturated for short-term periods of up to 5 days. Increases in soluble Mn were observed, which are associated with a decrease in redox potential (Eh; see Sect. 2.2.2). Dissolved Mn concentrations in the soil water solutions, studied after 84 h of saturation, exceeded US EPA drinking water quality standards of 0.05 mg/L. Changes in soluble Mn and in Eh as obtained in one replicate of the experiment are presented in Fig. 8.17.

As seen in Fig. 8.17, Mn was released into solution after the Eh decreased below approximately 450 mV. Once the critical Eh ($\sim$450–500 mV) needed for dissolution of Mn was reached, time became the limiting factor in determining soluble Mn concentration. The soluble Mn concentration continued to increase throughout the duration of the experiment, suggesting that equilibrium conditions were not reached. Concentrations of Zn and Ni also increased following soil reduction. Lack of significant correlation for Cu was explained by the formation of complexes with dissolved organic matter (DOM). Increases in the soluble

concentration of Zn and Ni at values greater than those expected from the dissolution of metal-bearing Mn oxides are due to exchangeable trace elements. These elements can be released due to changes in the electrolyte concentration, for example, as a result of the reduction process.

8.3.3 Dissolution from Mixtures of Organic Contaminants

Dissolution of volatile organic mixtures was observed by studying the behavior of kerosene. Dror et al. (2002) compared the gas chromatographs of neat kerosene to those of the fraction of kerosene dissolved in an aqueous electrolyte solution of 0.01 M NaCl, at an ambient temperature of 22 °C (Fig. 8.18). Aliphatic and branched aliphatic hydrocarbons in the range C_9–C_{16} constitute the major group of components in neat kerosene, with only a minor set of aromatic components. In aqueous electrolyte solutions, on the other hand, aromatic compounds, especially branched benzene and naphthalene, make up the majority of compounds. The C_9–C_{16} aliphatic and branched aliphatic components do not appear in the gas chromatograph of the aqueous electrolyte solution. The reason for the difference between the neat and aqueous dissolved kerosene is the wide range of aqueous solubility typical of the different kerosene components. Aromatic compounds usually are much more soluble than aliphatic components. Therefore, aromatic components, which are minor constituents of neat kerosene, dissolve in a water solution much more readily than the major group of aliphatic compounds.

Gasoline commonly contains appreciable amounts of aniline, phenol, and their alkyl substituted homologs as well as many other polar compounds. Schmidt et al. (2002) measured the fuel–water partitioning coefficients, K_{fw}, of several polar compounds during a batch experiment. The K_{fw} values for the investigated phenols, anilines, benzotriazoles, and S-heterocycles ranged from 0.2 to 1,700; these values are up to three orders of magnitude lower than the K_{fw} of benzene. The nonaqueous-phase liquid (NAPL)–water partitioning of anilines and phenols depends strongly on the structure of the compound as well as on the pH of the gasoline composition. Due to their polarity, anilines and phenols associated with the gasoline, after a spill on the land surface, may reach groundwater ahead of the benzene and may be used as a marker to predict groundwater contamination.

8.3.4 Apparent Solubility

The “apparent solubility” of contaminants can be defined when the theoretical solubility deviates from the initial value, as a result of a number of factors encountered in the subsurface environment. Waste and sludge disposal sites usually contain a mixture of salts, toxic trace metals, and organic contaminants. When the disposal site is leached by rain or irrigation water, a solution containing soil

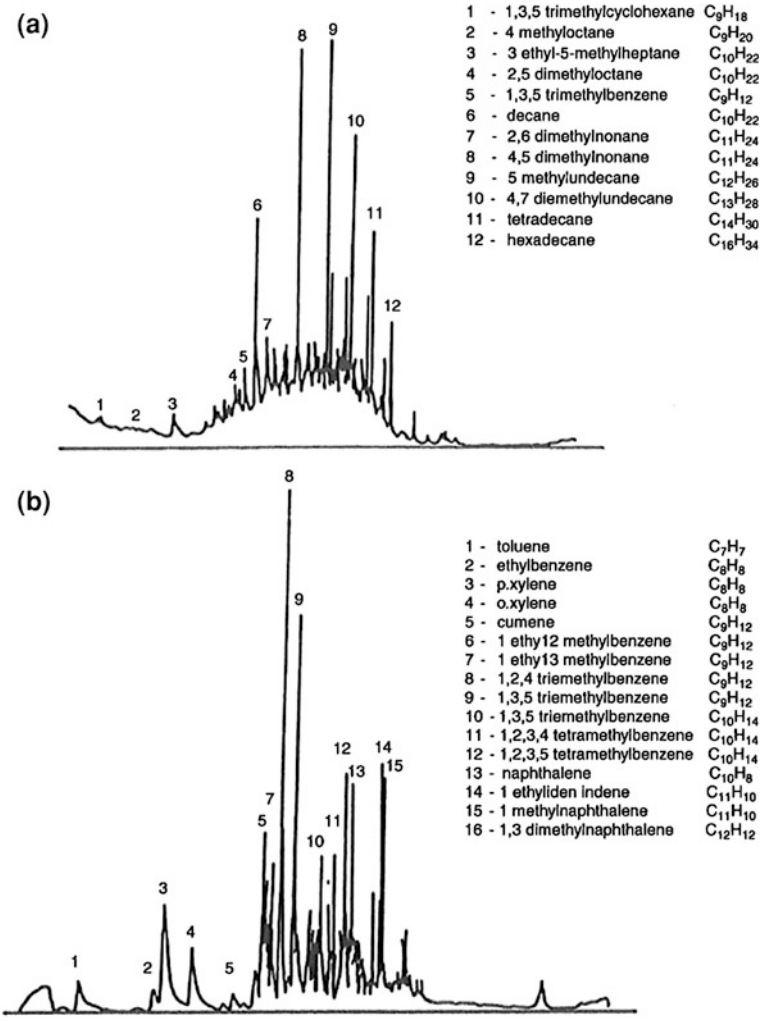

Fig. 8.18 Gas chromatographs of **a** neat kerosene and **b** kerosene dissolved in aqueous solution. Reprinted from Dror et al. (2002). Copyright 2002 with permission of Elsevier

and dissolved or suspended waste and sludge is obtained. The solubility of the contaminants in the water solution is affected by the presence of potential organic ligands and surfactants, electrolytes, and cosolvents; therefore, measurements represent an "apparent solubility" that differs from the theoretical solubility.

Surfactants are major compounds that reach the subsurface alone or accompanying other contaminants. Their effect depends highly on the solution chemistry. For example, Park and Bielefeldt (2003) report the partitioning of Tergitol, a nonionic surfactant, and pentachlorophenol (PCP), from NAPL to an aqueous

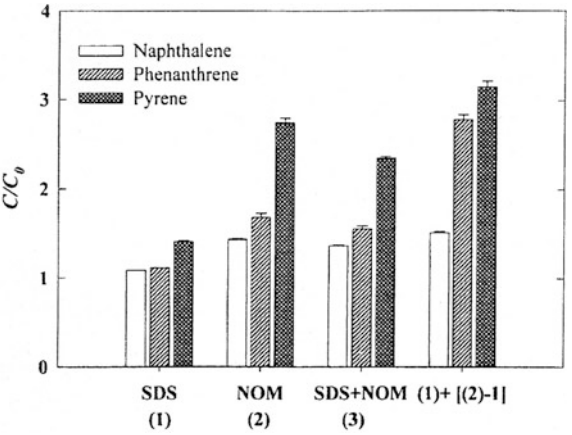

Fig. 8.19 Solubility of polycyclic aromatic hydrocarbons (*PAH*) in sodium dodecyl sulfate (*SDS*, 10 mg/L) and Suwannee River natural organic matter (*NOM*, 10 mg/L) solution. *C* denotes increased solubility in SDS and NOM solutions, and C_0 is the solubility in water (Cho et al. 2002)

solution. Enhanced PCP dissolution into water from the NAPL was achieved at aqueous Tergitol concentrations >200 mg/L. Surfactant addition of 1,200 mg/L increased the aqueous PCP concentration by 14-fold at pH 5 and by twofold to threefold at pH 7. This result is explained by the ionizable nature of PCP and the effect of pH and ionic strength on equilibrium partitioning. The significant response at the lower pH may be explained by the greater hydrophobicity of PCP molecules at a low pH. To the ionizable nature of PCP and the effect of pH on the equilibrium partitioning, one must also add the effect of ionic strength. These results can be used to improve the use of surfactants for remediation of subsurface sites contaminated by NAPLs.

A combined effect of natural organic matter (NOM) and surfactants on the apparent solubility of polycyclic aromatic hydrocarbons (PAHs) is reported in the paper of Cho et al. (2002). Kinetic studies were conducted to compare solubilization of hydrophobic contaminants such as naphthalene, phenanthrene, and pyrene into distilled water and aqueous solutions containing NOM and sodium dodecyl sulfate (SDS) surfactant. The results obtained after 72-h equilibration are reproduced in Fig. 8.19. The apparent solubility of the three contaminants was higher in SDS and NOM solutions than the solubility of these compounds in distilled water. When a combined SDS–NOM aqueous solution was used, the apparent solubility of naphthalene, phenanthrene, and pyrene was lower than in the NOM aqueous solution.

Properties of surfactant and cosolvent additives affect the rate of apparent solubilization of organic contaminants in aqueous solutions and may serve as a tool in remediation of subsurface water polluted by NAPLs. Cosolvents (synthetic or natural) are organic solutes present in sufficient quantities in the subsurface water to render the aqueous phase more hydrophobic. Surfactants allow NAPLs to partition into the micelle core, when present at levels above the critical micelle concentration, causing an apparent solubility increase. An extensive discussion of surfactant- and cosolvent-induced dissolution of NAPLs in porous media is given

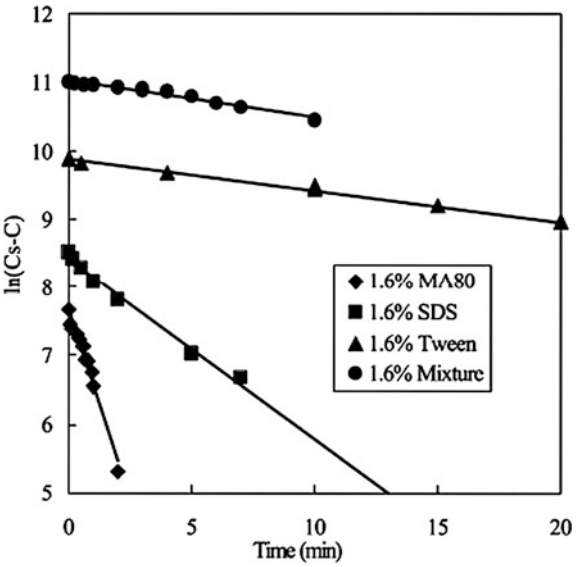

Fig. 8.20 Solubilization rate of trichloroethylene as affected by surfactant type and concentration; *Cs* and *C* denote surfactant concentration and initial surfactant concentration, respectively. Reprinted from Zhong et al. (2003). Copyright 2003 with permission of Elsevier

by Khachikian and Harmon (2000). Here, we discuss selected examples to illustrate this phenomenon.

Zhong et al. (2003) studied the apparent solubility of trichloroethylene in aqueous solutions, where the experimental variables were surfactant type and cosolvent concentration. The surfactants used in the experiment were sodium dihexyl sulfosuccinate (MA-80), SDS, polyoxyethylene 20 (POE 20), sorbitan monooleate (Tween 80), and a mixture of Surfonic PE-2597 and Witconol NP-100. Isopropanol was used as the alcohol cosolvent. Figure 8.20 shows the results of a batch experiment studying the effects of type and concentration of surfactant on solubilization of trichloroethylene in aqueous solutions. A correlation between surfactant chain length and solubilization rate may explain this behavior. However, the solubilization rate constants decrease with surfactant concentration. Addition of the cosolvent isopropanol to MA-80 increased the solubility of isopropanol at each surfactant concentration but did not demonstrate any particular trend in solubilization rate of isopropanol for the other surfactants tested. In the case of anionic surfactants (MA-80 and SDS), the solubility and solubilization rate increase with increasing electrolyte concentration for all surfactant concentrations.

Speciation of transition metals by "natural" organic substances that behave as complexing ligands may occur in the subsurface following waste and sludge disposal. As a result, metal solubility increases, favoring metal mobility with depth. Haitzer et al. (2002) report binding of mercury(II) to DOM as a function of the Hg–DOM concentration ratio. Humic and fulvic acids, which were isolated from water originating from a site in the Florida Everglades, were used as DOM binding material. Comparing the Hg binding capacity of natural DOM to a chelate (ethylenediamine tetraacetic acid, EDTA), the natural DOM ligand was observed

to have a limited number of strong Hg binding sites. Haitzer et al. (2002) suggest that the binding of Hg to DOM under natural conditions (very low Hg–DOM ratios) is controlled by a small functional fraction of DOM molecules containing a thiol functional group. Therefore, Hg–DOM distribution coefficients used in modeling biogeochemical behavior of Hg in natural systems must be determined at low Hg–DOM ratios.

Contaminants bound to colloids also may lead to an increase in the apparent solubility of the compounds. Most colloidal phases are effective sorbents of low-solubility contaminants, due to their large surface area. For example, Fig. 8.21 depicts the solubilization of *p*-nitrophenol into hydrophobic microdomains, which defines the trace metal level in the groundwater of a coastal watershed (Sanudo-Wilhelmy et al. 2002). The authors emphasize that the (heavy) metals contained in the colloidal size fraction in some instances may reach more than 50 % of what is considered "dissolved" metal; this should be considered to properly understand the cycling of metals and carbon in the subsurface water.

Babiarz et al. (2001) examined total mercury (Hg) and methylmercury (Me–Hg) concentrations in the colloidal phase of 15 freshwaters from the upper Midwest and southern United States. On average, Hg and Me–Hg forms were distributed evenly between the particulate (0.4 μm), colloidal, and dissolved (10 kDa) phases. The amount of Hg in the colloidal phase decreased with increasing specific electric conductance. Furthermore, experiments on freshwater with artificially elevated electric conductance suggest that Hg and Me–Hg may partition to different subfractions of colloidal material. The two colloidal Hg phases act differently with the same type of adsorbent. For example, the colloidal phase Hg correlates poorly with organic carbon (OC), but a strong correlation between Me–Hg and OC was observed.

Once reaching a water system, the components of a crude oil or a petroleum hydrocarbon are "truly dissolved" at a molecular level or "apparently soluble" at a colloidal level when droplets characterized by radii of tens to hundreds of microns are formed. The apparent solubility of PAHs from oil in an aquatic system is reported by Sterling et al. (2003), who consider that the colloidal concentration of a given hydrocarbon contaminant in aqueous phase, C, is described by the equation

$$\mathrm{C} = \phi \mathrm{X}/\mathrm{v} \tag{8.6}$$

where ϕ denotes the volume fraction of oil emulsion in water (vol. emulsion/vol. water), X is a (dimensionless) chemical mole fraction in the organic phase, and v is average molar volume of component in the petroleum product.

Figure 8.22 highlights the fraction of naphthalenes present in water due to colloidal entrainment. As the compound molecular weight increases, the relative fraction of the compound in the colloidal phase increases. This occurs regardless of the level of entrainment. Sterling et al. (2003) suggest that this behavior has

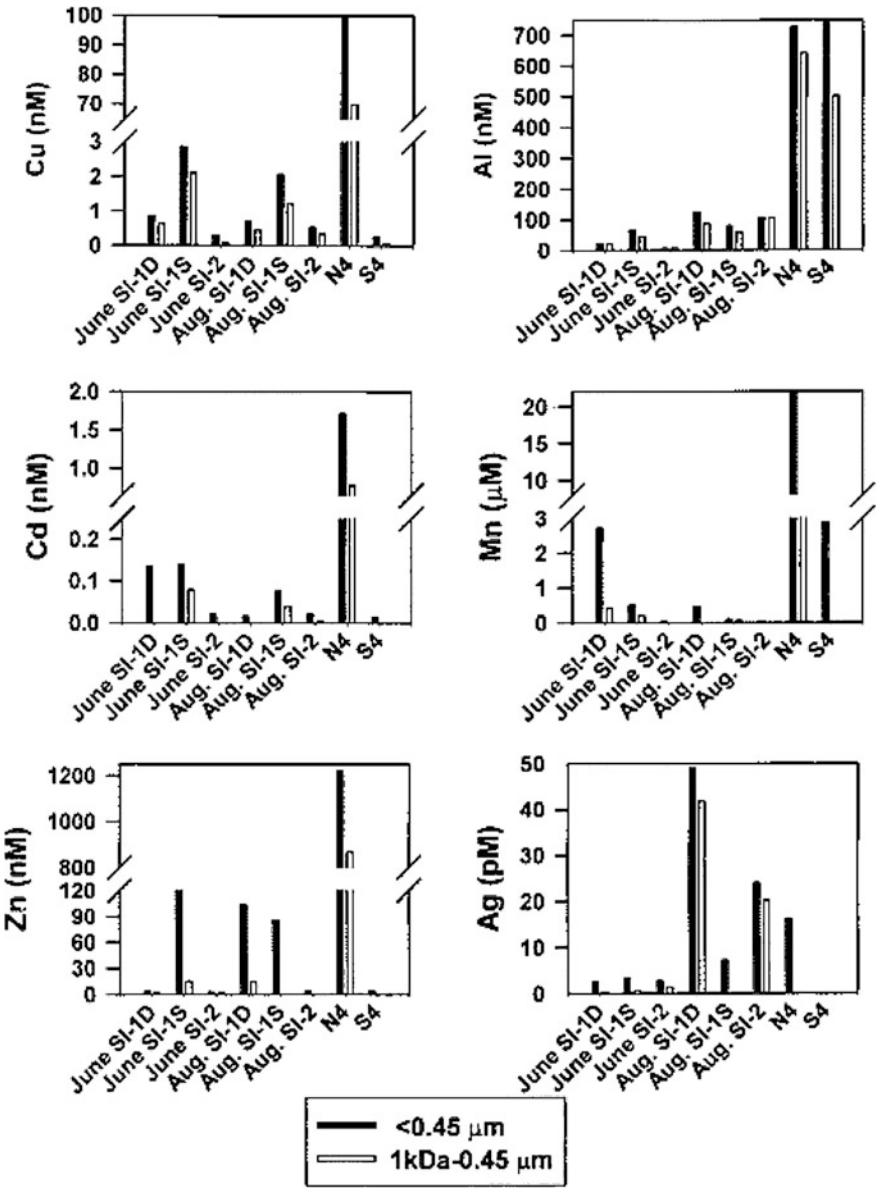

Fig. 8.21 Dissolved and colloidal concentrations of metals measured in the groundwater of Shelter Island and in the Peconics (North and South Forks of Long Island). Reprinted with permission from Sanudo-Wilhelmy et al. (2002). Copyright 2002 American Chemical Society

significant implications for the fate and transport of PAHs in natural aquatic systems, where the majority of PAH transport is due to water-entrained oil droplets.

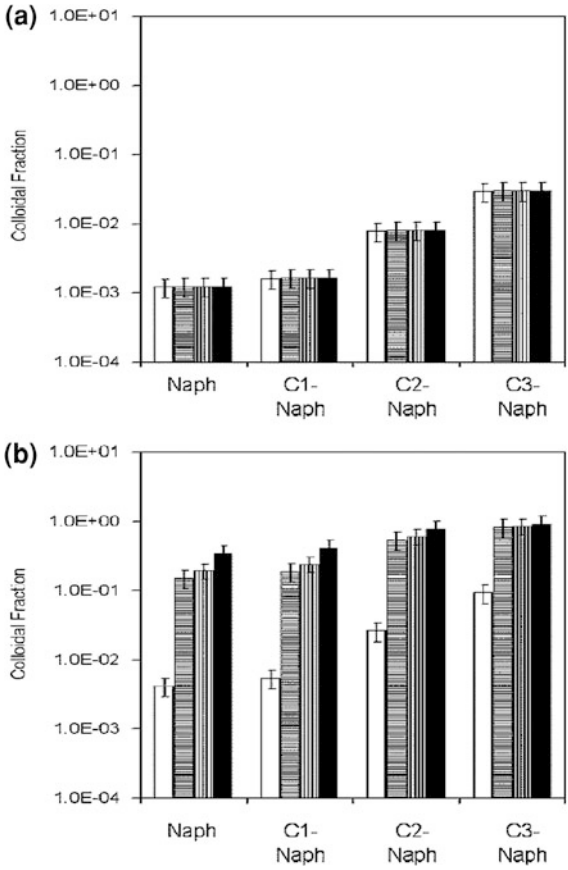

Fig. 8.22 Fraction of naphthalene concentration due to colloidal entrainment at **a** $G_m = 5\ s^{-1}$ and **b** $G_m = 20\ s^{-1}$, for naphthalene and naphthalene compounds containing 1, 2, or 3 C as side chains, where G_m is the mean shear rate. Reprinted with permission from Sterling et al. (2003). Copyright 2003 American Chemical Society

The salting-out effect (see Sect. 6.5) may lead to lower solubility of organic or organo-metallic contaminants in saline waters compared to those obtained in pure water. The solubility decreases with an increase in salt concentration in water. An extreme example may be found in Sorensen et al. (2002), who examined solubility of gaseous methane in pure and saline water. Referring to their experimental results, saline solutions of NaCl (up to 2.5 molality and $\sim$11 wt%) were used with $CaCl_2$ (up to 2 molality and $\sim$20 wt%). Figure 8.23 shows the decrease in solubility in saline water in the gas–water–salt system. Because methane dissolution in NaCl and $CaCl_2$ saline water occurred at different pressure and temperature, the results cannot be compared directly. However, the decreasing trend is obvious in both cases.

The electrolyte concentration in an aqueous solvent may affect dissolution of petroleum products, which are composed of a mixture of hydrocarbons. Dror et al. (2000) considered increasing concentrations of NaCl in water, up to a value approaching the salinity of seawater, and showed that kerosene dissolution decreases as the electrolyte concentration in water increases, according to the

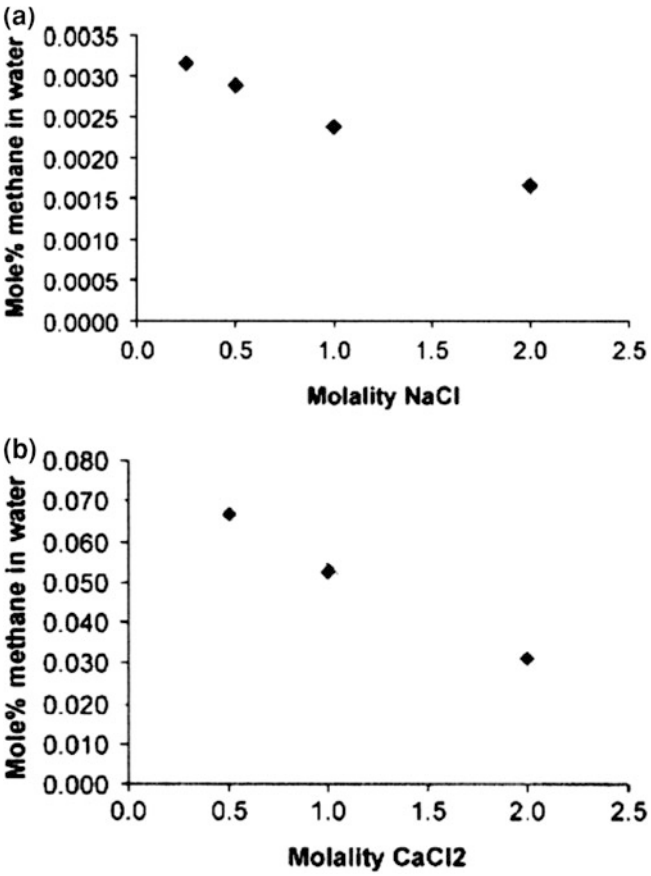

Fig. 8.23 Solubility of methane **a** in NaCl at 1 atm and 283.15 °K and **b** in $CaCl_2$ solutions at 37.4 atm and 298.15 °K. Reprinted from Sorensen et al. (2002). Copyright 2002 with permission of Elsevier

salting-out effect (Fig. 8.24). More data on effects of salts on the solubility of a large number of organic compounds are presented in Table 6.3.

The partitioning behavior of alkylphenols in crude oil–brine subsurface systems was reported by Bennett and Larter (1997). Partition coefficients were measured in the laboratory for simulated environmental conditions, from the near to the deep subsurface, as a function of pressure (25–340 bar), temperature (25–150 °C), and water salinity (0–100,000 mg/L sodium chloride) for a variety of oils. Alkylphenol partition coefficients between crude oil and brines decreased with increasing temperature, increased with water salinity and concentration of nonhydrocarbon compounds in the crude oil, and showed little change with varying pressure. The results of Bennett and Larter (1997) clearly show that, with increasing salt addition, the partition coefficient of alkylphenols increases, indicating increased phenol preference for the petroleum phase at higher brine salinity.

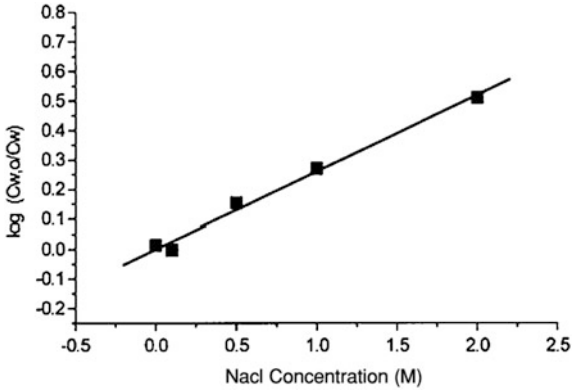

Fig. 8.24 Decrease in kerosene solubility in a NaCl aqueous solutions of various concentration as result of the salting-out effect (Dror et al. 2000). $C_{w,0}$ and C_w denote concentrations at initial maximum solubility and at various salinities

Table 8.4 K_{salt} values for three tested drugs

Solute	Experimental K_{salt}	logK_{ow}	Calculated[a] K_{salt}
Phenytoin	0.191	2.08	0.198
Theophylline	0.100	−0.06	0.115
Cytosine	−0.005	−1.65	0.053

[a] Based on $K_{salt} = 0.039 \log K_{ow} + 0.117$ (Ni et al. 2000)

Pharmaceuticals and personal care products represent potential contaminants; we consider it appropriate to include an example of the salting-out effect on drug solubility in aqueous solutions. Ni et al. (2000) examined the relation between the Setschenow constant (K_{salt}) of a nonelectrolyte in a NaCl solution and the logarithm of its octanol–water partition coefficient, log K_{ow}. The relation $K_{salt} = A \log K_{ow} + B$, where A and B are constants, was tested for 15 compounds including a number of drugs. The values of A (=0.039) and B (=0.117) were determined empirically from the literature data for 62 organic compounds. This linear relationship provides a simple and accurate method to predict the salting-out effect on organic compound solubility and was used to determine the K_{salt} for the drugs phenytoin, theophylline, and cytosine; the results are presented in Table 8.4.

When a NAPL is "mixed" with saline water, the coupled effects of salting out and droplet formation can occur. Despite an expected decrease in concentration due to the salting-out effect, a higher total organic concentration may be found. This phenomenon is explained by formation of a pseudo "oil-in-water" emulsion, with droplets of various sizes leading to increased apparent solubilities that may be up to several times greater than those known theoretically. This phenomenon also contradicts the salting-out effect. These droplets, which are not visible to the naked eye, are observed by optical microscope and detected by gas chromatography analysis.

Examples of NAPL droplet formation in water are described by Yaron-Marcovich et al. (2007). Solutions of benzene, toluene, xylene, trichloroethylene, and a mixture of them were prepared in excess in freshwater and saltwater, and solution stability was examined. High organic concentrations were found to remain stable in both freshwater and saltwater. In saltwater, for example, toluene and xylene concentrations remained as high as 14 and 26 times their theoretical solubilities, respectively, over a period of six days, while in freshwater, their concentrations remained 8 and 30 times their solubilities over the same period. This phenomenon is attributed to the presence of stable organic droplets. An image of organic droplets in saline solution captured by optical microscope is presented in Fig. 8.25.

A similar effect was observed in experiments reported by Dror et al. (2003) in a saline solution simulating seawater. They found that the concentration of a mixture of organic contaminants may be much higher than expected from theoretical considerations, accounting for the salting-out effect (Table 8.5). This is because the total concentration of organic mixture in natural saline (or sea) water is given not only by the dissolved contaminant and electrolyte concentration but also by the presence of mechanically dispersed organic droplets formed under various environmental conditions. This apparent solubility and concentration is called the *carrying capacity of the aqueous solution* (CCAS). It may be observed from Table 8.5 that, in saline water, the low-density hydrocarbons (benzene and toluene) have a CCAS value much greater than the CCAS in freshwater.

8.4 Contaminant Retention in the Subsurface

As mentioned previously, the retention of contaminants on geosorbents may occur by surface adsorption on or into the colloid fraction of the solid phase and by physical retention as liquid ganglia or as precipitates into the porous media. The type of retention is defined by the properties of the solid phase and the contaminants as well as by the composition of the subsurface water solution and the ambient temperature.

8.4.1 Contaminant Adsorption

Contaminant adsorption includes retention on the porous medium solid phase, as a result of cation exchange processes, and surface retention of neutral molecules, due to van der Waals forces.

Sodic water reaching the land surface through irrigation or disposal of sewage effluent leads to soil deterioration, caused by the exchange process between Na^+ from the water and clay-saturating cations. The sodium–calcium exchange process leads to retention of Na^+ in the solid phase, affecting not only the earth material

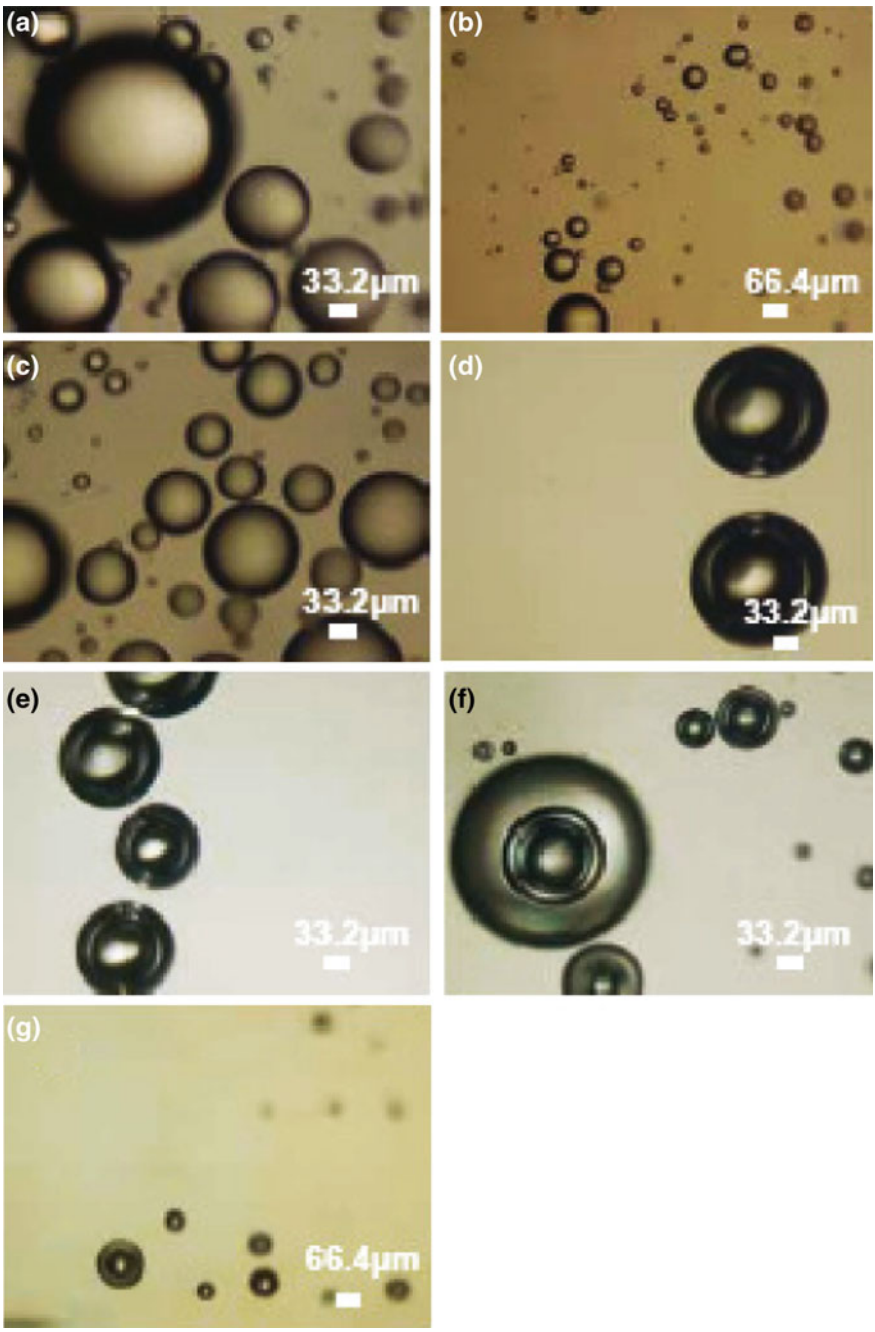

Fig. 8.25 Organic compound droplets in saline (30 g/L NaCl) water as captured by optical micrographs: **a** benzene; **b** toluene; **c** xylene; **d** TCE; **e** benzene and TCE; **f** xylene and TCE; and **g** organic compound mixture. Reprinted from Yaron-Marcovich et al. (2007). Copyright 2007 with permission of Elsevier

Table 8.5 Carrying capacity of aqueous solution (CCAS) for hydrocarbons as a result of droplet formation (Dror et al. 2003)

Compound	Distilled water solubility (mg/L)	Seawater solubility (mg/L)	Freshwater CCAS (mg/L)	Saline water CCAS (mg/L)
Benzene (C_6H_6)	1,740	1,391	1,940	3,340
Toluene (C_7H_8)	535	379	1,345	7,461
Trichloroethylene (C_2HCl_3)	1,100	769	1,520	1,306

Table 8.6 Effect of SAR and Na^+ concentration in water on the ESP of soils with different mineralogy

Location	Clay distribution		Clay mineralogy		SAR	Na^+ concentration, mEq/L	ESP
	<0.2 μm	0.2−2 μm	<0.2 μm	0.2−2 μm			
Burleson	71	29	$M_1Mi_3K_3$	$M_2MiK_2Q_2$	28	11.0	18.9
						33.0	20.4
Houston black	78	22	M_1	$M_2K_2Mi_2Q_2$	28	11.0	16.0
						33.0	16.0
Miller	49	51	$M_1Mi_2K_3$	$M_2Mi_2K_2Q_2F_3$	28	11.0	25.8
						33.0	37.9
Pullman	41	59	Mi_2K_2 M_2	$Mi_2K_2Q_2F_3$	28	11.0	31.7
						33.0	32.5

Legend: Mi = mica, K = kaolinite, M = montmorillonite, Q = quartz, and F = feldspar. Estimated quantities: 1: >40 %; 2: 10–40 %; and 3: <10 % (Thomas and Yaron 1968)

chemical composition but also soil physical properties, such as porosity, aggregation status, and water infiltration capacity.

When Na^+ from saline irrigation or wastewater disposal first flows through a soil, there is no significant correlation between the sodium adsorption ratio (SAR) of the water and the exchangeable sodium percentage (ESP) of soil. In a column experiment by Thomas and Yaron (1968) on a series of Texas soils of differing mineralogy, the total electrolyte concentration of the saline water was observed to influence the rate of sodium adsorption. At equilibrium, the ESP in the soil was influenced more by the soil mineralogy than by the cationic composition of the water and the total electrolyte concentration (Table 8.6).

Characteristic data for the adsorption of Na^+ are shown in Fig. 8.26. Three synthetic aqueous solutions with a total electrolyte concentration of 11 mEq/L and SAR values of 7.5, 14.0, and 28.0 were passed through a Burleson soil column. At equilibrium, a solution with SAR = 7.5 gave an ESP of 8.1, and a solution with SAR = 28 exhibited an ESP of 18.0. We see from Fig. 8.26 that the quantity of aqueous solution that had to be passed through the soil column to achieve a constant Na^+ content in the entire profile increased with SAR. In other words, for a given applied volume of solution, greater SAR values led to larger depths where a constant ESP was achieved.

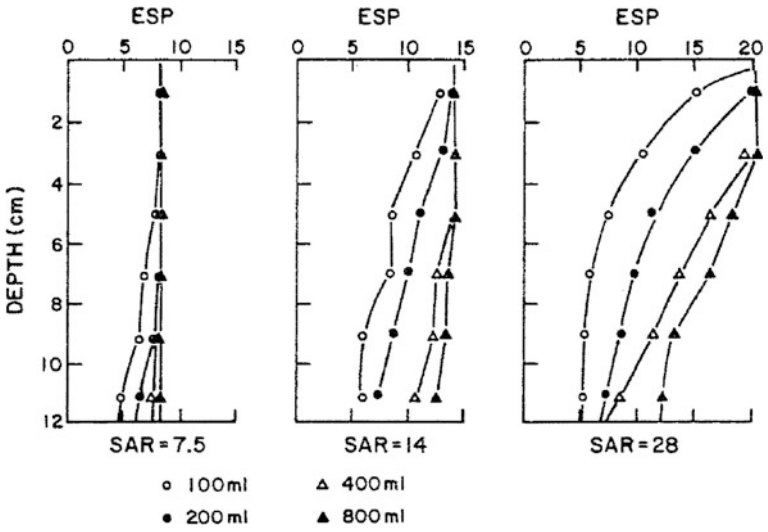

Fig. 8.26 Exchangeable sodium percentage (*ESP*) along a Burleson soil column, as a function of the sodium adsorption ratio (*SAR*) of irrigation water. The values were obtained by percolating the soil columns with sodic water (total electrolyte concentration of 11 mEq/L). Each curve corresponds to a given applied volume of solution (Thomas and Yaron 1968)

Heavy metal sorption on soil constituents may occur by one of the two mechanisms: (1) in a two-step mechanism where a rapid chemical reaction takes place on the surface of soil mineral followed by a long-time process recognized as a film diffusion route; (2) a three-step mechanism including (a) rapid adsorption of heavy metals on the external surface of the soil constituents, (b) delayed move of the heavy metal from the external to internal sites by solid-state film diffusion, and (c) binding and fixation of heavy metal at positions in the internal phase of the soil/mineral particle.

Sparks (2005) illustrated these adsorption mechanisms by comparing kinetics of some heavy metal sorption on a soil and various soil minerals. In this study, Ni, Pb, and As sorption on kaolinite, pyrophylite, gibbsite, montmorillonite, and Matapeake soil was compared as shown in Fig. 8.27. The sorption process was controlled by both sorbent and sorbate properties. An example of the three-step mechanism was demonstrated for As(V) adsorption on ferrihydrite where a great part of applied contaminant was sorbed within the first 5 min followed by slow sorption during $\sim$200 h (Fig. 8.27c).

The desorption of heavy metals may exhibit an hysteretic pathway, the hysteresis being controlled by residence (contact) time with the sorbent. An example of the residence time effect on desorption of Pb sorbed on Matapeake soil is given in Table 8.7. By extrapolating the data of Strawn and Sparks (2000), we can assume that Pb adsorption under specific environmental conditions may become irreversible on a lifetime scale.

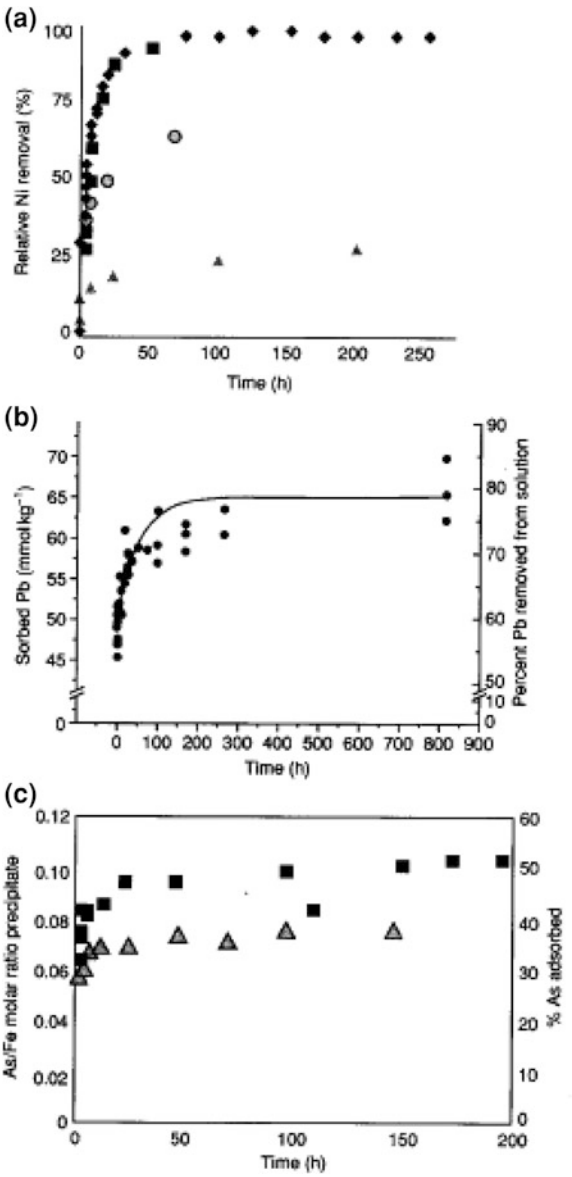

Fig. 8.27 Kinetics of metal and oxyanions on soil minerals and soil. **a** Kinetics of Ni sorption (%) on pyrophylite (*black diamond*), kaolinite (*black square*), gibbsite (*black up-pointing triangle*), and montmorillonite (*open circle*) from a 3 $mmol^{-1}$ Ni solution, an ionic strength $I = 0.1$ mol^{-1} $NaNO_3$ and a pH of 7.5; **b** kinetics of sorption on a Matapeake soil from a 12.25 $mmol^{-1}$ Pb solution, an ionic strength $I = 0.05$ mol^{-1} and a pH of 5.5; **c** kinetics of As(v) sorption on ferrihydrite at pH 8.0 and 9.0. As(v) total 1×10^{-4} mol^{-1}; Fe (III) total 5×10^{-4} mol^{-1} (*black square*) adsorption at pH 8.0 (*black up-pointing triangle*) adsorption at pH 9.0 (Sparks 2005)

Sparks (2005) notes that in addition to diffusion processes, the formation of metal hydroxide surface precipitates on phyllosilicates, metal oxides, and soils, together with residence time effects, can greatly affect the release of heavy metal and the hysteresis pattern. Aging of the metal hydroxide surface precipitate affects metal release, enhancing metal stability on soil minerals. With time, heavy metal sorption on soil minerals may develop a chain of processes leading to soil

Table 8.7 Effect of residence time on Pb desorption from a Matapeake soil (Strawn and Sparks 2000)

Residence time (days)	Sorbed Pb (mmol/kg)	Desorbed Pb (mmol/kg)	Percentage Pb desorbed (mmol/kg)
1	54.9	27.9	50.8
10	60	28.7	47
32	66.1	30.5	46.1

Table 8.8 Influence of the resident cation on the adsorption of diquat and paraquat by homoionic-exchanged clays (Hays and Mingelgrin 1991) indicates data for incomplete cation exchange

Clay	Resident inorganic cation	CEC (μEq/g)	Organic adsorption (μEq/g)		Enthalpy change ΔH (kJ/mol)	
			Diquat	Paraquat	Diquat	Paraquat
Montmorillonite	Na^+	999	950	970	−32	−48
	K^+	850	920	940	−31	−51
	Ca^{2+}	950	940	950	−36	−51
Vermiculite	Na^+	1,440	1,210	1,130	26	42
	K^+		270	230	1.6	−0.9
	Ca^{2+}	1130	(870)	(630)	(−9.2)	(−5.2)
Illite	Na^+	230	240	230	−13	−22
	K^+	ND	220	220	−6.8	−17
	Ca^{2+}	240	230	220	−16	−24
Kaolinite	Na^+	30	36	36	0	−11
	K^+		35	34	1.3	−4.9
	Ca^+	60	36	36	−18	−25

solid-phase transformation. Xu et al. (2008) confirm that Ni^{2+} adsorption on montmorillonite and fulvic–humic momtmorillonite complexes may be irreversible and that the adsorption–desorption pattern is not affected by the presence of humic substances.

Pesticides are used widely in plant protection practices, by dispersal on agricultural lands, and generally are cationic or nonionic organic compounds. After application, these products may volatilize, being transported in the groundwater as solutes or retained on the porous medium solid phase. Pesticide retention is controlled by the molecular properties of the compound, the solid-phase constituents, and environmental factors. Diquat and paraquat organo-cationic herbicides exhibit sorption isotherms of the *L* type according to the Giles et al. (1960) classification (Sect. 5.2.2), with the data fitting well to the Langmuir equation. Kookana and Aylmore (1993) noted that the sorption capacities of Australian soils studied for diquat ranged from very high in clay soil (146,400 μmol/kg) to very low in sand (1,765 μmol/kg). The clay soil showed the highest value of the Langmuir coefficient, indicating a high bonding energy. Table 8.8 shows the adsorption of these cationic pesticides by four types of homoionic-exchanged clays: montmorillonite,

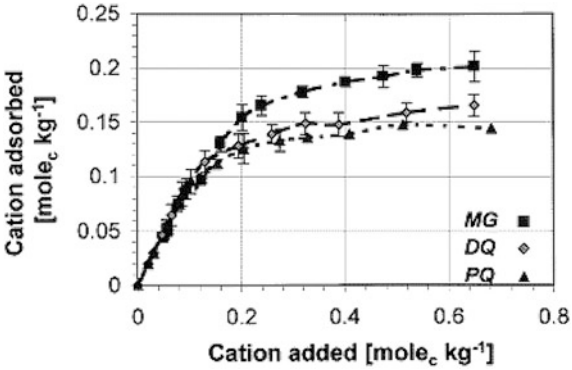

Fig. 8.28 Adsorption isotherms of methyl green (*MG*), diquat (*DQ*), and paraquat (*PQ*) on sepiolite. Reprinted from Rytwo et al. (2002). Copyright 2002 with permission of Elsevier

vermiculite, illite, and kaolinite. We see from these data that the cations can have a significant influence on the extent and energy of the adsorption processes. Exchange of the resident cations by both of the organo-cations was essentially complete in the case of kaolinite, montmorillonite, and illite clays, although there was a slight preference for paraquat over diquat in homoionic montmorillonite. The affinities were reversed in the case of adsorption by Na^+-vermiculite and illite clays.

Competitive adsorption between the organo-cationic herbicides diquat and paraquat and salts or a monovalent organic compound also was considered by Kookana and Aylmore (1993). An increase in the salt concentration of the soil solution from 0.005 to 0.05 M $CaCl_2$ resulted in decreases in sorption capacities for the studied herbicides.

The effect of NaCl concentration on the rate of paraquat adsorption on activated clays is reported by Tsai et al. (2003). The rate constant increases with an increase in salts in the aqueous paraquat solution: from 0.046 (g/mg/min) at a NaCl concentration of 0.05 M, to 0.059 (g/mg/min) at a solution concentration of 2.50 M NaCl. Studying the effect of various alkali metals ions on paraquat adsorption capacity on activated clay surfaces, Tsai et al. (2003) found the order Li^+ (32.79 mg/g) > Na^+ (31.25 mg/g) > K^+ (24.75 mg/g). Moreover, the rate constant appears to be inversely proportional to the adsorption capacity.

Competitive adsorption on sepiolite clay of a monovalent dye (e.g., methyl green or methyl blue) and of the divalent organo-cationic herbicides diquat and paraquat was studied by Rytwo et al. (2002). To evaluate a possible competitive adsorption between the two organic compounds, separate aqueous solutions of each cation were used and adsorption isotherms were obtained. Figure 8.28 shows the amount of diquat, paraquat, and methyl green adsorbed on sepiolite as a function of total added divalent cation. It may be observed that, when the added amounts were lower than the CEC of the sepiolite (0.14 mol_c/kg), all cations were completely adsorbed.

Rytwo et al. (2002) also found that, when the added amounts were higher than the CEC, the adsorbed amounts of methyl green and diquat increased up to 140

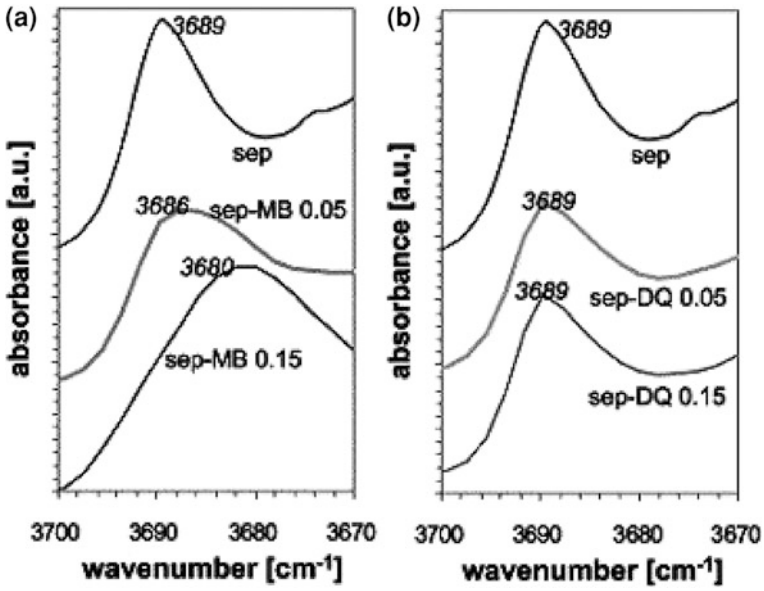

Fig. 8.29 IR spectra of the Si–OH vibration in **a** pure sepiolite (sep), sepiolite with 0.05 and 0.15 mol_c methylene blue (MB)/kg clay (sep-MB 0.05 and sep-MB 0.15, respectively) and **b** pure sepiolite (sep), sepiolite with 0.05 and 0.15 mol_c diquat/kg clay (sep-DQ 0.05 and sep-DQ 0.15, respectively). Reprinted from Rytwo et al. (2002). Copyright 2002 with permission of Elsevier

and 115 % of CEC, respectively, while paraquat adsorption reached only a value close to the CEC level. These behaviors were examined using Fourier transform infrared (FTIR) measurements. Pure sepiolite exhibits two clear peaks at 789 and 764 cm^{-1}. Adsorption of monovalent organic cations such as methylene blue (MB) leads to a considerable deformation of the peaks at high adsorption loads, but the peaks are not affected when the adsorption is smaller than one-third of the CEC. A divalent cation compound such as diquat or paraquat does not affect the O–H doublet at any adsorbed load. When both diquat and MB are coadsorbed up to CEC, the peak deformation appears but is ascribed to the binding of the monovalent organic cation to the neutral sites. Similar effects are observed for the main Si–OH vibration at 3,700 cm^{-1}. The effects of adsorption of MB and diquat on sepiolite IR spectra are presented in Fig. 8.29. With increasing amounts of adsorbed MB, the peak shift is observed (Fig. 8.29a); no shift is observed when diquat is adsorbed (Fig. 8.29b).

Rytwo et al. (2002) show that diquat and paraquat adsorb on neutral sites of sepiolite; the authors speculate that this might be a general pattern for organic cation contaminants interacting with sepiolite.

Competitive adsorption on clay and soil surfaces between a heavy metal contaminant (Cu) and a cationic herbicide (chlordimeform) was reported by Maqueda et al. (1998) and Undabeytia et al. (2002). In the presence of herbicides, Cu

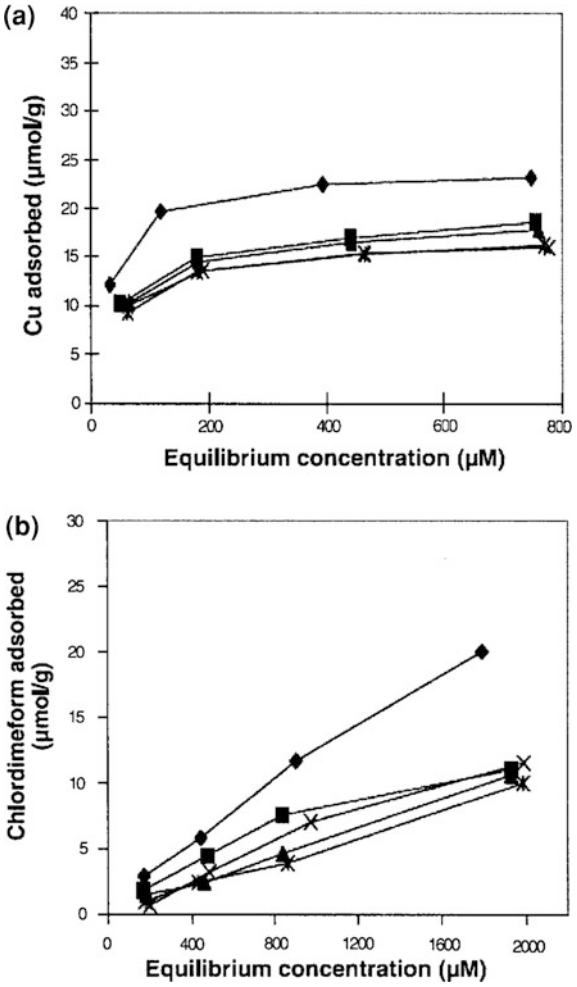

Fig. 8.30 Adsorption isotherms of chlordimeform on Cu-treated soil **a** at several chlordimeform initial concentrations (mM): 0 (*black diamond*), 0.2 (*black square*), 0.5 (*black up-pointing triangle*), 1.0 (×), and 2.0 (*black star*) and **b** at several Cu concentrations (mM): 0 (*black diamond*), 0.16 (*black square*), 0.31 (*black up-pointing triangle*), 0.63 (×), and 0.94 (*black star*) (Undabeytia et al. 2002)

adsorption on clay minerals decreases due to competition for the same adsorption sites. Preadsorption of Cu on soil surfaces leads to a decrease in chlordimeform adsorption, also as a result of competition for the adsorption sites. This behavior is shown in Fig. 8.30, including adsorption isotherms of chlordimeform at several Cu concentrations and for Cu adsorption with increasing chlordimeform values on an Ultic Haploxeralf soil derived from shales of Devonian-age parent material. The soil adsorbent is characterized by 1.9 % OM and a CEC of 9.8 mol_c/kg.

Considerable attention has been given to the adsorption of diquat and paraquat by humic acids. On the basis of data from Burns et al. (1973), Hayes and Mingelgrin (1991) explained how the exchangeable cations on humic macromolecules can influence the adsorption of paraquat. Adsorption decreased according to the order Ca^{2+}-humate > H^{+}-humic acid > Na^{+}-humate. Adsorption by the Na^{+}-

humate approached the CEC of the polyelectrolyte. This can be explained, in part, by the preference of the ion exchanger for mineral ions of higher valence. However, the effects of macromolecules are more important in this instance than consideration of valence. Adsorbed organo-cations bridge negative charges within strands and between strands, and the interstrand binding causes the macromolecules to shrink; water is then excluded from the matrix and precipitation of the paraquat–humate complex may occur. This behavior was observed for Na^+-smectite uptake of paraquat by Na^+-humate, approaching the CEC value of the polyelectrolyte. Adsorption by the Ca^{2+}- and H^+-exchanged humic acids was significantly less than the CEC of the preparation. Comparisons of the isotherms in Fig. 8.31 indicate a high affinity for adsorption of paraquat by the H^+-humic acid in water and by the Ca^{2+}-humate. These isotherms are representative of adsorption occurring on readily available sites or close to exteriors of macromolecular structures. The presence of $CaCl_2$ reduces the adsorption, due to the competition from the excess Ca^{2+} ions in solution.

In a review on the effects of OM heterogeneity on sorption of organic contaminants, Huang et al. (2003) emphasized the possible presence of matured kerogen and black carbon or soot particles as a fraction of soils and sediments. For example, analyzing the naturally occurring total organic matter (TOC) in a sediment, Song et al. (2002) found 8 % humic acid, 52 % black carbon, and 40 % kerogen materials. The molecular structures of kerogen and black carbon are very different from those of humic acids, so their interaction with organic contaminants in the subsurface are different. Kerogen, for example, has a three-dimensional structure with aromatic nuclei cross-linked by aliphatic chainlike bridges. The nuclei appear to be formed mainly from clusters (about 100 nm in diameter) of 24 or more parallel aromatic sheets, separated by gaps or voids of 30–40 nm, and therefore are capable of trapping small hydrophobic organics. The aromatic sheets contain up to 10 condensed aromatic homocyclic or heterocyclic rings. Bridges are linear or branched aliphatic chains or O- or S-containing functional groups (Engel and Macko 1993). Absorption capacities of TOC components in a pond sediment vary, for example, with a lower sorption capacity for phenanthrene compared to that calculated only for humic acid (Xiao et al. 2004). The lower sorption capacity is explained by the presence of particulate kerogen and black carbon associated with the sediment; because these surfaces (in soil/sediment aggregates) are coated with metal oxides and hydroxides, the TOC components are not fully accessible by phenanthrene.

The charge characteristics of many pesticides are pH dependent. Some anionic species are formed through dissociation of protons, and cationic compounds may be formed by the uptake of protons. Compounds with carboxylic acid groups are characteristic of anionizable compounds, although phenolic groups rise to anionic species in alkaline subsurface conditions. The s-triazine family of herbicides applied to soil is considered the classical representative of the cationizable species. Several compounds containing carboxylic acid groups enter the subsurface when sprayed on the vegetation canopy or directly onto the land surface. These act as neutral molecules when pH values are well below their pK_a values but become

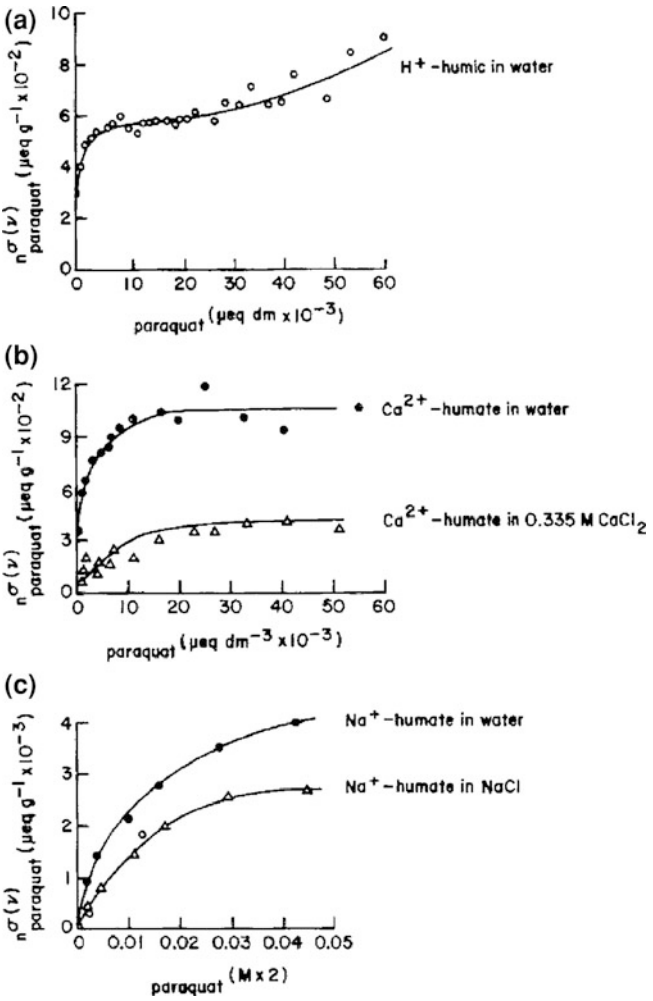

Fig. 8.31 Isotherms for the adsorption of paraquat **a** by H^+-humic acid, **b** by Ca^{2+}-humate in water and 0.335 M $CaCl_2$ solution, and **c** by Na^+-humate solution in water and dilute NaCl solutions (Burns et al. 1973)

increasingly anionic as pK_a is reached and exceeded. Table 8.9 shows the adsorption from aqueous solution of a series of compounds from the s-triazine family onto Na^+-smectites, as affected by the solution pH. Hayes and Mingelgrin (1991) emphasize that, under low pH conditions, prometone adsorption can take place through association of triazine with carboxyl groups in the humic substances, followed by electrostatic binding to the conjugate carboxylate base of the proton donor.

Table 8.9 Adsorption from aqueous solutions of s-triazine compounds by Na^+-montmorillonite (Hayes and Mingelgrin 1991)

Compound	pK_a	Water solubility (ppm)	Adsorption (μmol/g)			
			pH 2	pH 3	pH 4	pH 5
Atrazine	1.68	33	275	200	115	70
Atratone	4.20	1,654	410	450	475	400
Ametryne	3.12	193	520	610	650	560
Propazine	1.85	9	150	110	20	20
Hydroxypropazine	5.20	310	150	220	240	245
Prometone	4.30	750	290	380	400	350
Prometryn	3.08	48	460	490	490	415

Sposito et al. (1996) analyzed a broad set of data and suggested two general complexation mechanisms to characterize the retention of s-triazines on humic acids: Proton transfer is favored for humic acids of high acidic functional groups and for s-triazine with low basicity; electron transfer mechanisms are favored for humic acids of low acidic functional group content and for s-triazines of high basicity.

The effect of initial pH (3–11) on paraquat intake rate by activated clay adsorption also is reported by Tsai et al. (2003). As the pH increased, the amount of adsorbed cationic paraquat increased in response to the increasing number of negatively charged sites, which are available due to the loss of H^+ from the surfaces. The surface of activated clay at pH > 3.0 exhibited negative charges due mainly to the variable charge from pH-dependent surface hydroxyl sites. With the increase in pH, the negative charges increased, which in turn increased paraquat sorption. The distribution coefficient, K_d, decreased as pH decreased, for example, from 3,521 (L/kg) at pH 11.0 to 981 (L/kg) at pH 3.0. In fact, the rates of adsorption for all of the studied pH values decreased with time, until they gradually approached a plateau.

Barriuso et al. (1992) analyzed the relationship between soil properties and adsorption behavior of cationic, anionic, and neutral herbicides. Atrazine, terbutryn, and 2,4-D from the triazine herbicides family were considered. The study included 58 soils, covering a wide range of pH values, OC contents, and mineralogical compositions. For this range of soils and pH, atrazine was in a neutral form, 2,4-D in an anionic form, and terbutryn in either neutral or cationic form. Based on the adsorption measurements, the authors concluded that (1) K_d for atrazine is strongly related to the OC content but not correlated to the soil pH; (2) K_d for terbutryn is less correlated to the OC content and is correlated to the soil pH; and (3) K_d for 2,4-D is not correlated to the OC content, but it is inversely correlated to the soil pH.

Because pesticides in the subsurface can reach layers with different properties, as they are redistributed with depth, it is interesting to examine their adsorption on earth materials during vertical transport. Dror et al. (1999) report adsorption of two s-triazines (atrazine and terbuthylazine), as they are redistributed in a 120-cm-deep

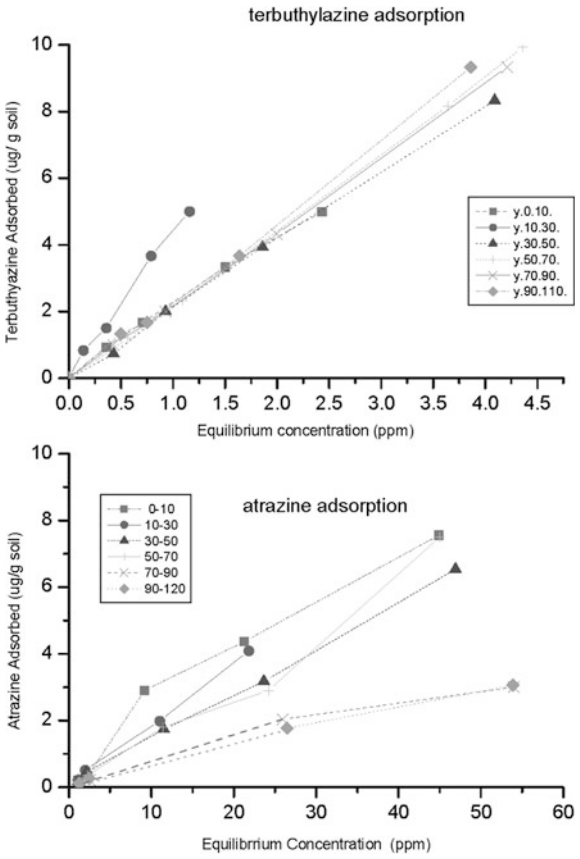

Fig. 8.32 Adsorption isotherms of terbuthylazine and atrazine at different depths along the soil profile, as affected by the *vertical* variability of soil properties (Dror et al. 1999)

soil profile, following surface application and subsequent leaching by irrigation or rainfall. Figure 8.32 shows adsorption isotherms of these two herbicides as affected by the vertical variability of the soils. The adsorption isotherms are linear along the soil profile. The K_d coefficients of atrazine range from 0.10 to 0.21 mL/g, while those of terbuthylazine range from 1.9 to 2.9 mL/g. The vertical variability of K_d, quantified in terms of the mean and standard deviation (SD), is $K_d = 0.15$ with an SD of 0.04 for atrazine and $K_d = 2.17$ with an SD of 0.36 for terbuthylazine. The effect of soil OM on herbicide adsorption is given by the distribution coefficient on OC, K_{oc}, obtained from the relation $K_{oc} = K_d/OC \times 100$, assuming that OC = OM/1.7. The vertical spatial variability of K_{oc} is similar to those of K_d.

Organophosphorus pesticides are used as an example of the adsorption of nonpolar (nonionic) or slightly polar toxic chemicals. The phosphoric acid ester group has a general formula $(RO)_2PO(OX)$, where R is an alkyl group and X is a leaving group (see Sect. 4.1.2). In contact with clay surfaces or other earth materials, such organic nonpolar molecules are retained on the surface. These

Table 8.10 Percent of adsorption from aqueous solution of organophosphorus pesticides by clays (Yaron 1978)

Insecticides	Solution equilibrium concentration (ppm)	Clays		
		Ca^{2+}-montmorillonite (%)	Ca^{2+}-kaolinite (%)	Ca^{2+}-attapulgite (%)
Parathion ($C_{10}H_{14}NO_5PS$)	6.5	73	14	87
Pirimiphos-methyl ($C_{11}H_{20}N_3O_3PS$)	16.0	94	30	
Pirimiphos-methyl ($C_{13}H_{24}N_3O_3PS$)	16.0	92	75	
Menazon ($C_6H_{12}N_5O_2PS_2$)	16.0	16	5	

esters are stable at neutral or acidic pH but susceptible to hydrolysis in the presence of alkali compounds, where the P–O–X ester bond breaks down. The rate of hydrolysis is related to the nature of the constituent X, the presence of catalytic agents, pH, and temperature. Because the solubilities of organophosphorus compounds in water are low, their adsorption from water solutions also is low. Table 8.10 shows the percentage of some organophosphorus compounds adsorbed from aqueous solution onto clay surfaces. The maximum adsorption capacity of clays for organophosphorus pesticides is achieved only when the chemical reaction occurs in an appropriate organic solvent. The maximum adsorption capacity of parathion, for example, on a monoionic clay surface from a hexane solution is 10 % of the initial concentration on montmorillonite, 8 % on attapulgite, and less than 0.5 % on kaolinite.

The amount of adsorbed chemical is controlled by both properties of the chemical and of the clay material. The clay-saturating cation is a major factor affecting the adsorption of the organophosphorus pesticide. The adsorption isotherm of parathion from an aqueous solution onto montmorillonite saturated with various cations (Fig. 8.33) shows that the sorption sequence ($Al^{3+} > Na^{+} > Ca^{2+}$) is not in agreement with any of the ionic series based on ionic properties. This shows that, in parathion-montmorillonite interactions in aqueous suspension, such factors as clay dispersion, steric effects, and hydration shells are dominant in the sorption process. In general, organophosphorus adsorption on clays is described by the Freundlich equation, and the K_d values for parathion sorption are 3 for Ca^{2+}-kaolinite, 125 for Ca^{2+}-montmorillonite, and 145 for Ca^{2+}-attapulgite.

The hydration status of the clay or earth material may affect the adsorption capacity of nonpolar (or slightly polar) toxic chemicals. Continuing with parathion as a case study, Fig. 8.34 shows the increase adsorbed parathion on attapulgite from a hexane solution, as the adsorbed water on the clay surface decreases. This behavior may be explained by the competition for adsorption sites between the polar water and the slightly polar parathion. Possibly, however, the reduction in adsorption due to the presence of water is caused by the increased time required for parathion molecules to diffuse through the water film to the adsorption sites.

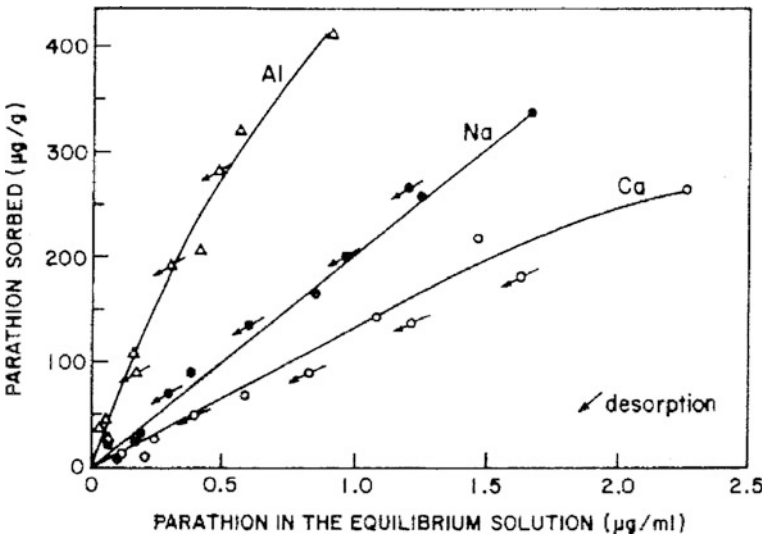

Fig. 8.33 Adsorption from aqueous solutions of parathion onto montmorillonite saturated with various cations (Yaron and Saltzman 1978)

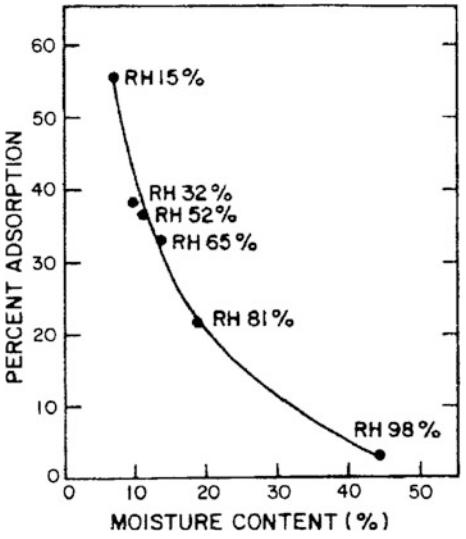

Fig. 8.34 Adsorption of parathion by attapulgite from hexane solution, as affected by initial hydration status of mineral; RH = relative humidity (Gerstl and Yaron 1981)

In a dry attapulgite–parathion–hexane system, parathion molecules compete effectively with nonpolar hexane molecules for the adsorption sites. In partially hydrated systems, parathion molecules cannot replace the strongly adsorbed water molecules, so that parathion adsorption occurs only on water-free surfaces and a decrease in adsorption per total surface area may be observed. Infrared studies lead

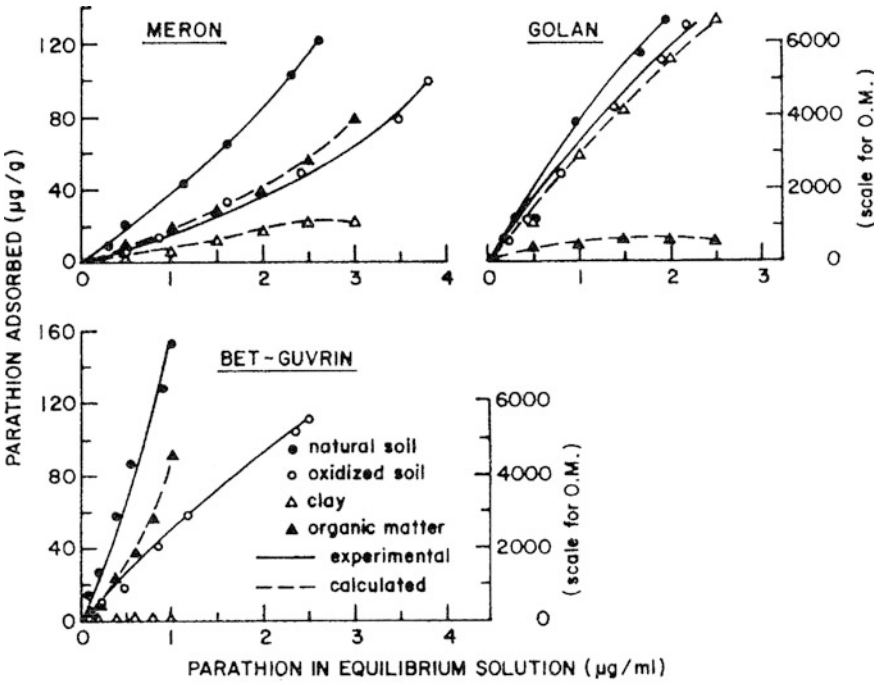

Fig. 8.35 Parathion adsorption from aqueous solutions by three soils, before and after oxidation, as well as on clay and organic matter. Reprinted with permission from Saltzman et al. (1972). Copyright 1972 American Chemical Society

to an understanding of the adsorption mechanism of organophosphorus compounds on clay surfaces. For example, IR spectra indicate that, on both montmorillonite and attapulgite, parathion was sorbed by clay coordinates through water molecules to the metallic cations. When clay–parathion complexes are dehydrated, parathion becomes coordinated directly, and the type of cation determines the structure of the complex. The main interaction is through the oxygen atoms of the nitro group. Interactions through the P=S group have also been observed, especially for complexes saturated by polyvalent cations (Saltzman and Yariv 1976; Prost et al. 1977).

Subsurface adsorption of nonpolar or slightly polar toxic chemicals also was found to be related to the solid-phase OM and mineralogy. Saltzman et al. (1972) studied the importance of mineral and organic surfaces in parathion adsorption on semiarid soils characterized by low OM content and different mineralogy. They found that parathion adsorption depends on the type of association with organic and mineral colloids. Following removal of OM by soil treatment with hydrogen peroxide, the adsorptive affinity of mineral soils decreases, mainly due to a decrease in the OM content and not due to other soil modifications that may occur during OM oxidation. Figure 8.35 presents the isotherms of parathion adsorption on three semiarid soils, before and after oxidation, as well as on clay and OM.

Steroid hormones form a group of pollutants that includes natural hormones such as estradiol, testosterone, and their metabolites as well as several synthetic analogs. Steroid hormones used as growth promoters have already been found in water and sediments (Lai et al. 2000; Thorpe et al. 2003), and their adsorption properties on earth materials have been considered. Lee et al. (2003) report batch experiments where simultaneous sorption of three hormones (17-β-estradiol, 17-α-ethyl estradiol (EED), and testosterone) on four Midwestern US soils and a freshwater sediment was performed. Apparent sorption equilibria were reached within a few hours. Sorption isotherms generally were linear for the chemicals studied; on one of these soils (Drummer soil), K_d ranged from 23.4 to 83.2 L/kg and logK_{oc} ranged from 2.91 to 3.46. The distribution coefficients on OC, K_{oc}, indicate that hydrophobic partitioning was consistent with the aqueous solubilities and octanol–water partition coefficients.

Endocrine disruptor compounds (EDCs), which are hormone and hormone-like substances, may enter the subsurface through agricultural practices or urban and industrial effluents, or through improper sludge and waste disposal. Loffredo and Senesi (2006) reported adsorption–desorption of four EDCs—bisphenol A (BPA), octyphenol (OP), 17-α-EED, and 17-β-estradiol (17ED)—onto two acidic soils, with the adsorptive material being collected from depths of 0–30 and 30–90 cm. The surface samples were characterized by a higher content of OM (6.3–16.0 g/kg) than those collected from the deeper layer (1.8–3.3 g/kg) and a clay content ranging from 1.5 to 26 %. Adsorption of EDCs on the soils was relatively fast, occurring mainly during the first hours of contact. Over the concentration range tested, no limiting adsorption was observed for BPA, OP, or EED, whereas adsorption of 17ED reached a saturation level. In general, EDC adsorption in the upper layer is greater than on the samples collected from a 30–90 cm depth. The type of adsorption isotherm (e.g., *C* or *L* type) is controlled by both the characteristics of the EDCs and the properties of the earth material. Based on their experimental results, Loffredo and Senesi (2006) suggested that, in addition to the OC content, EDC adsorption is affected by the nature of the OC and its association with other colloidal fractions (such as clay materials).

EDC desorption rates and amounts define their distribution in the subsurface. The adsorption of OP and EED is mostly pseudo-irreversible, with a partial desorption that occurs very slowly; OP and EED thus are likely to accumulate in the upper soil layers. In contrast, BPA adsorption is reversible; desorption occurs quickly and is completed after a few steps of leaching. As a consequence, BPA released to the soil environment is more likely to be transported to deeper layers, leading eventually to groundwater contamination.

Inorganic trace element retention on earth materials is illustrated in several case studies, where selected contaminants (e.g., fluoride, cesium, Hg, lead, and cadmium) interact with rocks, clays, soils, and sediments under different environmental conditions (e.g., pH, presence of organic ligands, and salinity).

Fluoride in minor concentrations is beneficial for animals and humans, but it becomes toxic when ingested in excessive amounts. Bar-Yosef et al. (1989) investigated adsorption kinetics and isotherms of K^+-montmorillonite and a series

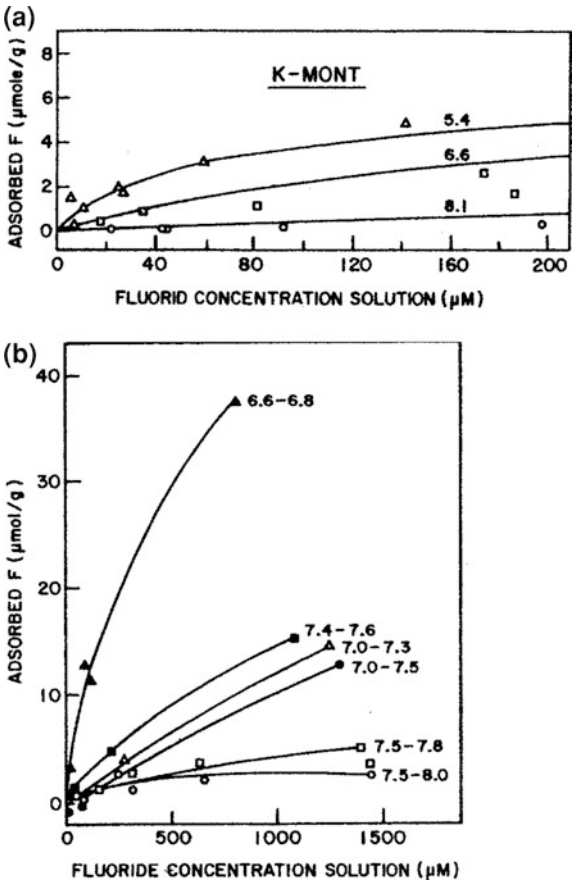

Fig. 8.36 Fluoride adsorption from aqueous suspensions as affected by pH **a** on K^+-montmorillonite and **b** on six soils (Bar-Yosef et al. 1989)

of soils (clay, 4–61 %; OM, 2–7 %), as affected by solution pH. The fluoride adsorption isotherms are shown in Fig. 8.36. In all cases, fluoride adsorption is a function of its concentration at the selected pH values. Soil pH is correlated inversely to the maximum number of fluoride adsorption sites, and this correlation stems from the effect of pH on the charge density of the clay edges. No significant correlation was found between the OM content and the maximum fluoride adsorption. Fluoride partitioning between solid and liquid phases of neutral and high pH is in accord with the earlier results of Flühler et al. (1982). The time needed to attain quasi-equilibrium in fluoride sorption reactions is satisfactorily described by a Langmuir adsorption isotherm model.

Cesium is a radionuclide found in radioactive wastes intended for storage in underground repositories; it is used as a standard marker for highly radioactive and long-lived materials. Argillaceous or clay media are considered potential earth materials for inclusion as barriers in radioactive waste repositories, due to their favorable properties for confinement: low permeability, high retention capacity,

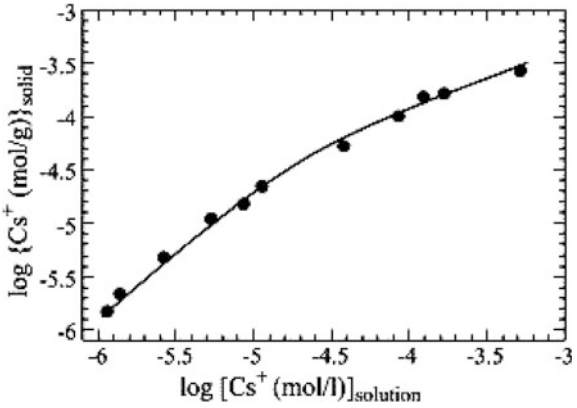

Fig. 8.37 Cs^+ adsorption isotherm on Na^+-loess clay. Reprinted from Bergaoui et al. (2005). Copyright 2005 with permission of Elsevier

and chemical buffering effect. Bergaoui et al. (2005) studied cesium adsorption on a Na^+-loess clay, where batch experiments were analyzed by X-ray diffraction and infrared and far-infrared measurements. The adsorption isotherm (Fig. 8.37) shows that loess clay is selective for cesium cations. The raw material contained a large amount of quartz, and the clay material was a mixture of kaolinite and an interstratified illite–smectite mineral; as a result, equilibrium Cs^+ adsorption data are not consistent with a single-site Langmuir model. Cesium adsorption on this particular soil clay occurs by cation exchange on sites with various cesium affinities. At low concentration, far-infrared spectroscopy shows the presence of very selective adsorption sites that correspond to internal collapsed layers. At high concentration, 133 Cs MAS-NMR shows that cesium essentially is adsorbed to external sites that are not very selective.

Variation of Cs^+ adsorption with depth, as a function of changes in clay content, is reported by Melkior et al. (2005); the study aimed to test the efficiency of a host rock for radionuclide confinement. Mudrock samples were collected from Callovo-Oxfordian layers in Bure (France), at depths between −422 and −478 m. The total clay content increases with depth by a factor of two to three between the measured depths. Figure 8.38 depicts the K_d of Cs^+ as a function of its concentration in solution at equilibrium.

Soil and sediment samples collected from Fukushima prefecture were investigated for Cs content using a sequential extraction (EXAFS) procedure by Qin et al. (2012). The investigations revealed that 94 % of ^{137}Cs was retained in the interlayer of the phyllosilicate mineral (Fig. 8.39). The $k^3\chi(k)$ spectra of vermiculite, soil, and sediments showed significantly different oscillations in frequency and amplitude compared to those for the CsCl solution, suggesting that inner-sphere complexes were formed on contaminated vermiculate and soil–sediment materials were formed on vermiculite. However, the Cs–soil/sediment complexes were smaller than those formed on vermiculite. The authors attribute these differences to the OM content of the soil–sediment samples.

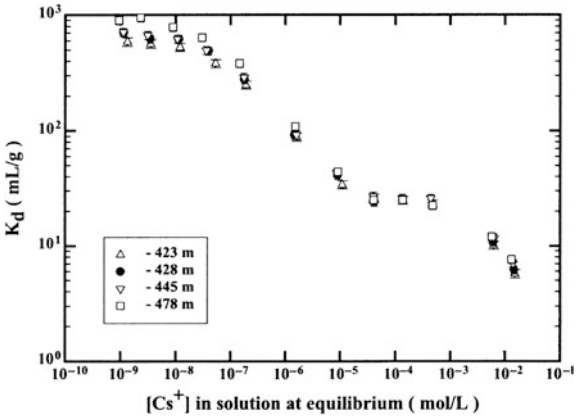

Fig. 8.38 Cesium sorption on Bure mudrock samples: K_d as a function of concentration in solution at equilibrium, at four different depths (Melkior et al. 2005)

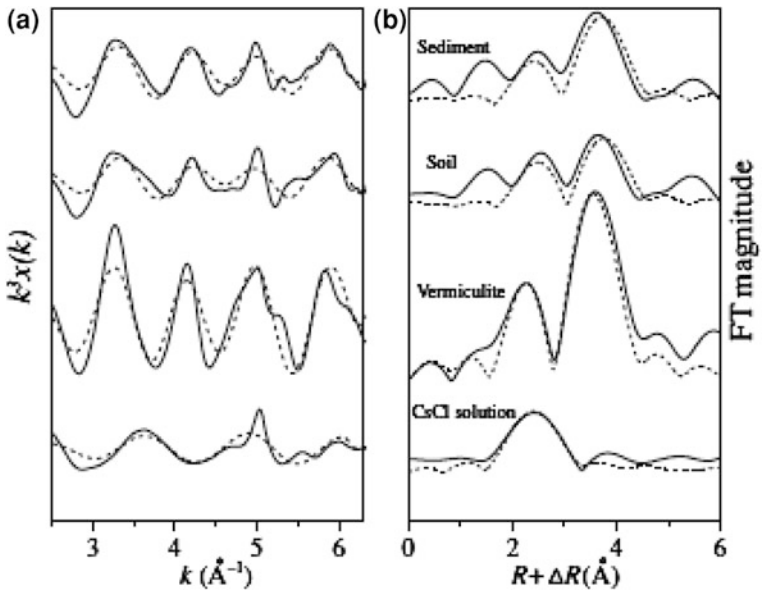

Fig. 8.39 Adsorption of cesium on vermiculite compared to CsCl solution. Cesium L_{III}-edge EXAFS spectra of reference material, Cs-adsorbed samples. **a** k^3-weighted $\chi(k)$ spectra and **b** RSF of (**a**) (phase shift not corrected). *Solid lines* are spectra obtained by experiments, and *dotted lines* are fitted spectra by curve-fitting analysis (Qin et al. 2012)

Buerge-Weirich et al. (2002) examined copper and nickel adsorption on a goethite surface in the presence of organic ligands, in natural groundwater samples from an infiltration site of the river Glatt at Glattfelden (Switzerland). Figure 8.40 exhibits Cu and Ni adsorption isotherms at pH 7.35, in the presence of

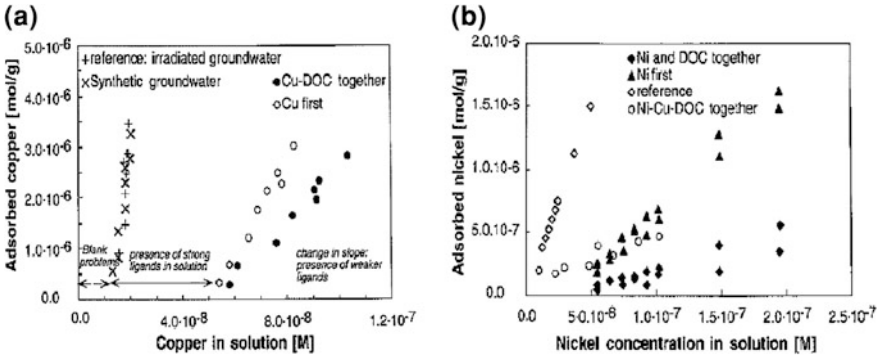

Fig. 8.40 Experimental results for **a** Cu and **b** Ni adsorption isotherms on goethite, at pH 7.35, in the presence of groundwater containing natural organic ligands, as compared to irradiated natural groundwater and synthetic groundwater. Reprinted with permission from Buerge-Weirich et al. (2002). Copyright 2002 American Chemical Society

groundwater containing natural organic ligands, as compared to irradiated natural and synthetic groundwater. Clearly, less Cu and Ni were adsorbed in the presence of organic ligands than in the reference systems. In both cases, the isotherms do not intercept the x-axis at the origin but at a value near 5×10^{-8} M. This behavior indicates the presence of strong complexing ligands in solution. When these ligands were saturated, the amount of adsorbed metal increased linearly with total metal concentration.

Dissolved inorganic trace metal (e.g., Hg, Ag, Cd, Ni, Zn) speciation and the tendency to form stable soluble complexes in saline water was considered by Turner (1996) and Turner et al. (2001, 2002), who developed an empirical equation to describe the direct relationship between the sediment–water distribution coefficient (K_d) and salinity. We focus on Hg sediment–water partitioning as a result of a coupled speciation and a salting-out process, as reported by Turner et al. (2001). Hg has the tendency to form chloro-complexes. In a natural aqueous system characterized by the presence of dissolved humic materials and salts, Hg is complexed by the abundant cation or has a strong affinity for particulate OM. Turner et al. (2001) designed their study recognizing that the nature and extent of sediment–saline water partitioning of Hg(II) are governed by the hydrophobic characteristics in the presence of OM, including a tendency to be salted out of solution by seawater ions. They found that the increase in K_d with increasing salinity is at least partially the result of an increase in the proportion of the relatively hydrophobic and lipophilic $HgCl_2$ complex, which is subject to salting out.

Distribution coefficients (K_d) and (K_{oc}) defining ^{203}Hg(II) sorption to three estuarine sediments are plotted against salinity in Fig. 8.41. Despite different Hg(II) concentrations and K_{oc} values in each location, a common exponential increase is evident. Salting out did not occur when Hg(II) is only in an ionic form, so that an increase in Hg(II) dissolution in estuarine water may be explained by the

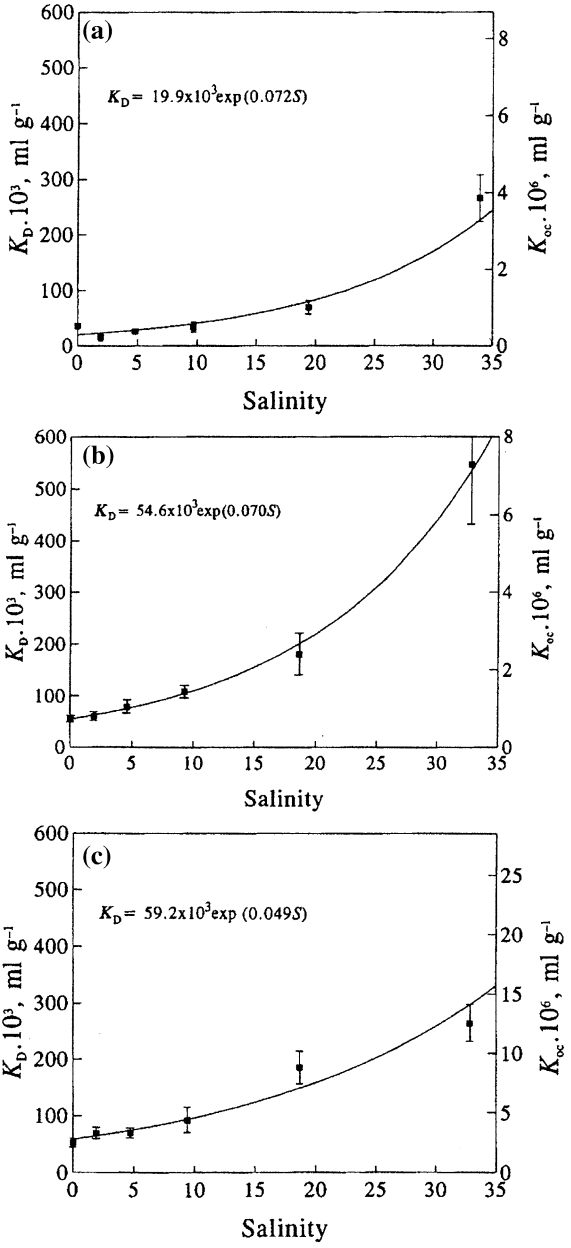

Fig. 8.41 Distribution coefficients (K_d and K_{oc}) defining the sorption of inorganic Hg(II) to estuarine particles versus salinity (S, in g/L) in the **a** Beaulieu, **b** Mersey, and **c** Plym estuaries. Reprinted with permission from Turner et al. (2001). Copyright 2001 American Chemical Society

formation of organically complexed Hg(II), due to the presence of dissolved or particulate OM. In particular, Hg(II) tends to form uncharged complexes with Cl^- that are covalent, nonpolar, and lipophilic. An increase in dissolved Hg(II) with increasing salinity may be explained by an increase in the proportion of the

Table 8.11 Range of selected trace element concentrations in dry, digested sewage sludge, and in comparison with element concentrations in median sludges and in soils (Chaney 1989)

Element	Reported range (mg/kg)		Typical median sludge	Typical soil
	Minimum	Maximum		
As	1.1	230	10	
Cd	1	3,410	10	0.1
Cu	84	17,000	800	15
Cr	10	99,000	500	25
F	80	33,500	260	200
Hg	0.6	56	6	
Ni	2	5,300	80	25
Pb	13	26,000	250	15
Se	1.7	17.2	5	
Zn	101	49,000	1,700	50

relatively hydrophobic and lipophilic $HgCl_2$ complex, which is more prone to salting out than other, more hydrophilic, complexes. Based on this study, Turner et al. (2001) consider that neutral methylated forms of Hg(II) behave in a similar fashion because they have a strong affinity for particulate OM and are known to be salted out from aqueous solution. Extending this finding to other trace metals, Turner et al. (2002) suggest that such contaminants are complexed by and subsequently neutralize organic ligands and the resulting neutral assemblages are salted out, possibly by electrostriction.

8.4.2 Nonadsorptive Retention

Nonadsorptive retention of contaminants may occur when chemicals reach the subsurface as a separate liquid phase or are adsorbed on suspended particles or organic residues. Contaminated suspended particles originating from sludge disposal or polluted runoff, for example, can represent a substantial hazard to the subsurface environment.

Table 8.11 shows the concentration range of potential toxic trace elements in US sewage sludges, as summarized by Chaney (1989). In this table, data on maximum concentration of toxic trace elements in dry, digested sewage sludges are compared to concentrations of the elements in median sludges and in soils. The subsurface contamination that may result from uncontrolled disposal on land surfaces is evident. In a laboratory study carried out by Vinten et al. (1983), the distribution of suspended particles from a sewage effluent on various types of soils was studied. If, for example, heavy metals in the concentration range of the values shown in Table 8.11 are adsorbed on transported sludge, a highly concentrated aggregate of polluted solid material is formed. Vinten et al. (1983) examined the effect of subsurface properties on the vertical redistribution of deposited solids and

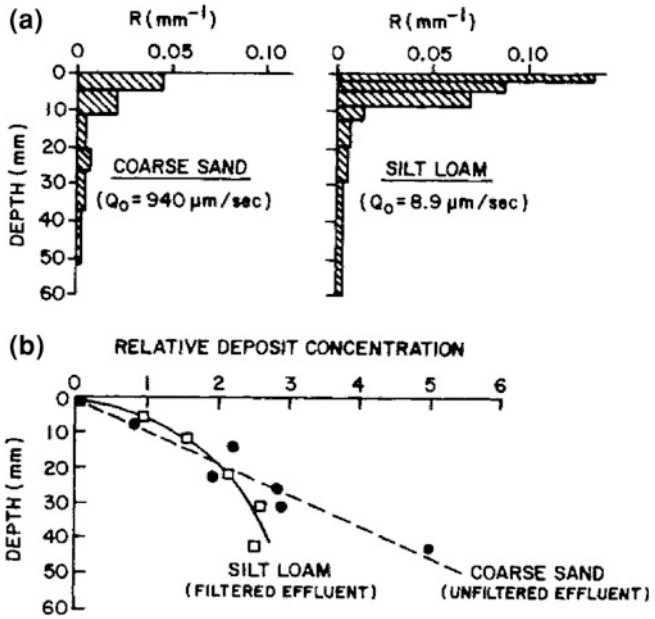

Fig. 8.42 Retention (R, defined as deposited solids per unit length of section/total added suspended solids, mm^{-1}) of suspended solids in the soil subsurface: **a** distribution of deposited solids in coarse sand and silt loam and **b** relative deposition (defined as—$\ln(\sigma/\sigma_i)$, where σ denotes initial amount of applied suspended solids and σ_i denotes measured amount of deposited solid mass per unit length of section at each depth) of suspended solids in silt loam and coarse sand leached by filtered and unfiltered effluents (Vinten et al. 1983)

on the resulting change in flow rate (Fig. 8.42). In the experiment, coarse sand was leached with unfiltered effluent, and silt loam was leached with filtered effluent. Passing unfiltered effluent through the coarse sand resulted in retention of 43 % of the total suspended solids, and the flow rate declined by less than 25 %. The relatively low retention is caused by the coarseness of the porous medium; finer suspended solids remain highly mobile. In a heavier silt loam, a very large relative reduction in flow rate occurred in the silt loam; after 400 mm of filtered effluent were added, the flow rate declined to 20 % of its initial value. A very small fraction of suspended solids was present in the leachate; most of the deposit was in the top 10 mm of soil.

Nonadsorptive retention of contaminants can also be beneficial. For example, oil droplets in the subsurface are effective in developing a reactive layer or decreasing the permeability of a sandy porous medium. Coulibaly and Borden (2004) describe laboratory and field studies where edible oils were successfully injected into the subsurface, as part of an in situ permeable reactive barrier. The oil used in the experiment was injected in the subsurface either as a NAPL or as an oil-in-water emulsion. The oil-in-water emulsion can be distributed through sands

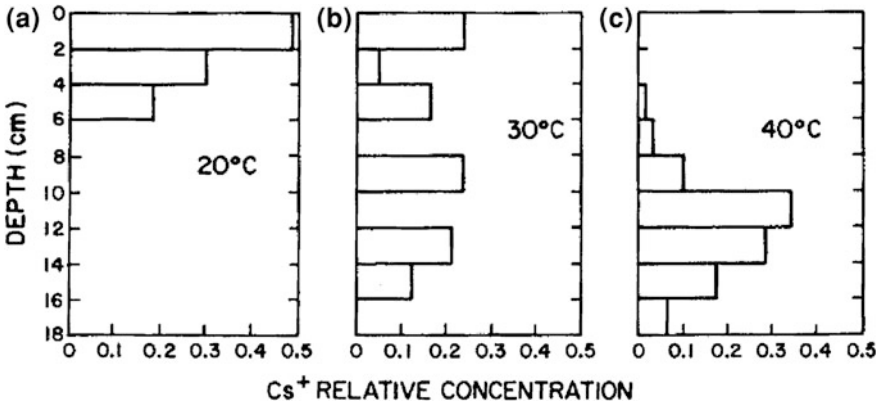

Fig. 8.43 Simulated Chernobyl Cs^+ distribution in the soil ecosystem in soil columns when the microbial decomposition of the organic material is enhanced by an increase in ambient temperature **a** 20 °C, **b** 30 °C, **c** 40 °C (Tengen et al. 1991)

without excessive pressure buildup, contrary to NAPL injection, which requires introduction to the subsurface by high pressure.

Subsurface organisms and organic residues also may affect vertical migration of contaminants. In a laboratory experiment by Tengen et al. (1991), the influence of microbial activity on the migration of Cs^+ and the effect of OM residue on Cs^+ retention were illustrated. These experiments were performed to understand the consequences of the Chernobyl accident in 1986. Figure 8.43 shows the distribution of Cs^+ in soil columns leached at temperatures of 20, 30, and 40 °C. Based on these results, Tengen et al. (1991) note the dominant role of the turnover of nondecomposed soil OM on Cs^+ retention in the subsurface: After deposition on land surface, the contaminant is fixed mainly by nondecomposed organic material and subsequently redistributed with depth as a result of microbial decomposition. This process is induced by an increase in temperature and the dissolution of organic C compounds in the infiltrating water. While the organic material is not decomposed, the Cs^+ is retained in the top layer of the subsurface. By decomposition of OM, the Cs^+ is complexed and transported to deeper layers.

The residual content of immiscible liquids can be defined by the amount of NAPL remaining in the subsurface when pore geometry permits NAPL flow greater than the retention capacity. In an outdoor pilot experiment, Fine and Yaron (1993) studied the effect of soil constituents and soil moisture contents on the retention of kerosene in the subsurface. This retention is termed the kerosene residual content (KRC). Ten soils were studied, with a broad spectrum of clay and OM contents, together with four soil moisture contents corresponding to oven-dried, air-dried, 33 kPa tension and 199 kPa tension. The KRC of the soils, studied as a function of clay content and moisture content, is presented in Fig. 8.44. The KRC of oven-dried soils ranged from 3.5 to 18.1 mL/100 g. It is affected by the

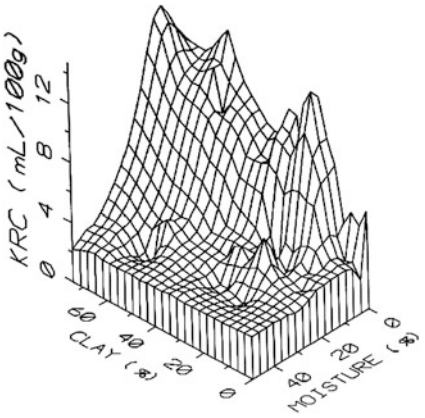

Fig. 8.44 Kerosene residual content (KRC) of soils as a function of clay and moisture contents. Reprinted from Fine and Yaron (1993). Copyright 1994 with permission of Elsevier

clay content of the soils, with KRC values of clayey soils being 1.5 times greater than for less clayey ones.

The OM content also contributes to the KRC. The relationship between clay, OM, and moisture contents and KRC is described by

$$\mathrm{KRC} = 0.13[\%\mathrm{clay}] + 1.48[\%\mathrm{OM}] - 0.32[\%\mathrm{moisture}] + 4.31. \qquad (8.7)$$

KRC exhibits a linear relationship toward the combination of clay and OM contents and an inverse correlation to moisture content. The range of values of the three independent variables was clay, 0.3–74 %; OM, 0–5.2 %; and moisture content, 0–49 %. The crucial effect of moisture content on KRC of the soils was demonstrated by comparing the fine clay material to dune sand. The respective KRCs were 14.8 and 3.2 mL/100 g for air-dried materials and 2.17 and 1.84 mL/100 g for moist materials at 33 % pK_a tension. Hayden et al. (1997) investigated the influence of NOM on the residual content of another petroleum product, gasoline, and found that higher organic content leads to a higher residual saturation under air-dried environmental conditions. Contamination with gasoline when the soils are water saturated leads to a virtually identical gasoline residual content value, despite the differences in the soil OM content.

8.5 Contaminant Release

Contaminant release can result from a change in physicochemical characteristics of the liquid phase surrounding the retaining solid phase. Such a release usually is obtained by lowering the contaminant concentration in the solution, which previously reached equilibrium with the solid phase. Changes in the liquid phase concentration can occur as a result of physicochemical or biologically induced processes. Moreover, the release of trace elements can occur following a decrease

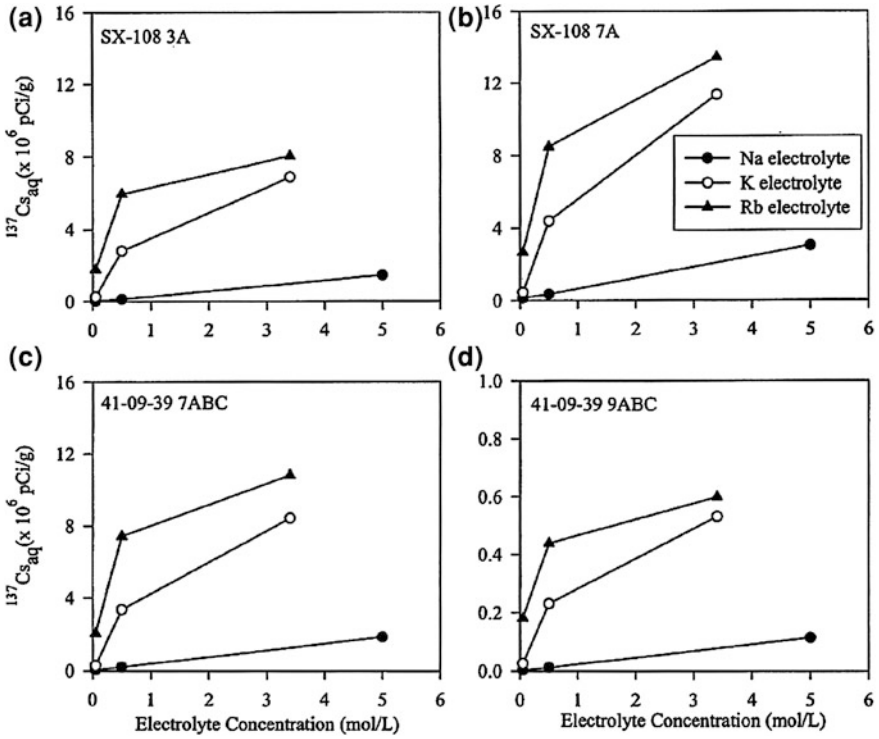

Fig. 8.45 $^{137}Cs^+$ desorption from the contaminated Hanford sediments after 6 days of equilibration, as a function of exchanging cations and their concentrations. Reprinted from Liu et al. (2003). Copyright 2003 with permission of Elsevier

in the concentration of metallic cations in solution, even if there is no modification in the background electrolyte concentration. Release may also result from the addition of protons or complexing molecules to the background electrolyte. This process sometimes is used as an extraction technique for metallic cations, which render mobile some strongly sorbed cations; but their passage into the solution implies partial destruction of the solid phase.

Liu et al. (2003) studied radiocesium desorption from subsurface pristine and contaminated micaceous sediments at the Hanford site, United States. Some of these sediments were, in the past, contaminated accidentally by nuclear wastes containing alkaline $^{137}Cs^+$. The desorption of $^{137}Cs^+$ was measured in solutions of Na^+, K^+, Rb^+, and NH_4 electrolytes of variable concentration and pH and in the presence of a strong Cs^+-specific sorbent. Desorption of $^{137}Cs^+$ from the contaminated sediment exhibits two distinct phases: an initial instantaneous release followed by a slow kinetic process (Fig. 8.45). The extent of $^{137}Cs^+$ desorption increases with increasing electrolyte concentration, following the trend $Rb^+ > K^+ > Na^+$ at a neutral pH. The extent and rate of $^{137}Cs^+$ desorption is

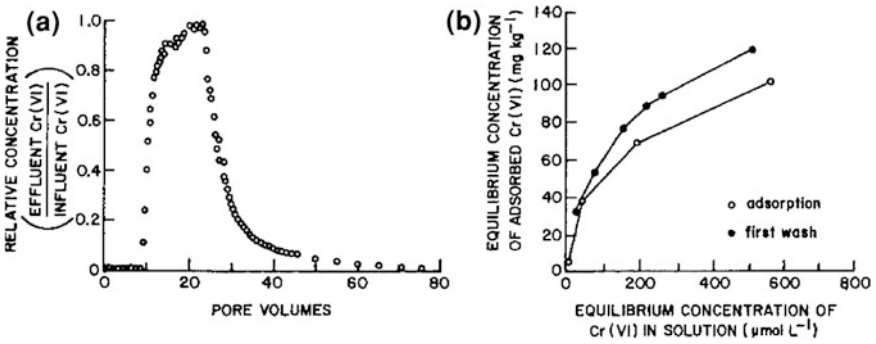

Fig. 8.46 Adsorption and desorption of Cr(VI) by a telluride alluvium in **a** a flow-through column experiment and **b** on alluvium under batch conditions (Stollenwerk and Grove 1985)

influenced by surface configuration, intraparticle diffusion, and the collapse of edge-interlayer sites in solutions of K^+, Rb^+, and NH_4. Moreover, Liu et al. (2003) showed that only 40 % of the $^{137}Cs^+$ adsorbed in a subsurface sediment, contaminated over a 30-year period, was desorbed by exchange with the electrolyte solutions. This value increased up to 80 % after long-term contact with acidified ammonium oxalate. Desorption studies with Cs^+-spiked pristine sediment, equilibrated over short duration, indicated that adsorbed Cs^+ is fully exchangeable with Na^+ solution but becomes less exchangeable when placed in K^+ and Rb^+ electrolyte solutions. This effect was attributed to the collapses of edges and partially expanded interlamellar regions, which result from saturation of the exchange complex with poorly hydrated Rb^+ and K^+ cations.

In many cases, a trace element retained on the subsurface solid phase may undergo chemical reactions that induce a hysteresis phenomenon during the release process. A relevant example of hysteresis due to precipitation of some of the initial contaminants is given by the behavior of Cr(VI), an industrial contaminant, which in the subsurface environment may be subject to reduction reactions. When an available source of electrons is present, such as OM, Cr(VI) is reduced to Cr(III); the rate of this reaction increases with decreases in pH (Ross et al. 1981).

Stollenwerk and Grove (1985) report the adsorption and desorption of Cr(VI) in an alluvial aquifer. From Fig. 8.46a, we see that, over the first $\sim$10 pore volumes, all the Cr(VI) in water contaminant was adsorbed by the alluvium. A rapid increase in the effluent concentration of Cr(VI) then occurred, until the capacity of alluvium for contaminant retention was exhausted ($\sim$25 pore volumes). Leaching the alluvium column with 10 pore volumes of Cr-free water caused the release of about 50 % of the adsorbed Cr(VI), and further leaching with 80 pore volumes of groundwater, over 232 days, removed only an additional 34 % of the adsorbed contaminant. Stollenwerk and Grove (1985) attributed the difficulty in removing part of the adsorbed Cr(VI) to the presence of specific adsorption sites and possible reduction to Cr(III) followed by precipitation.

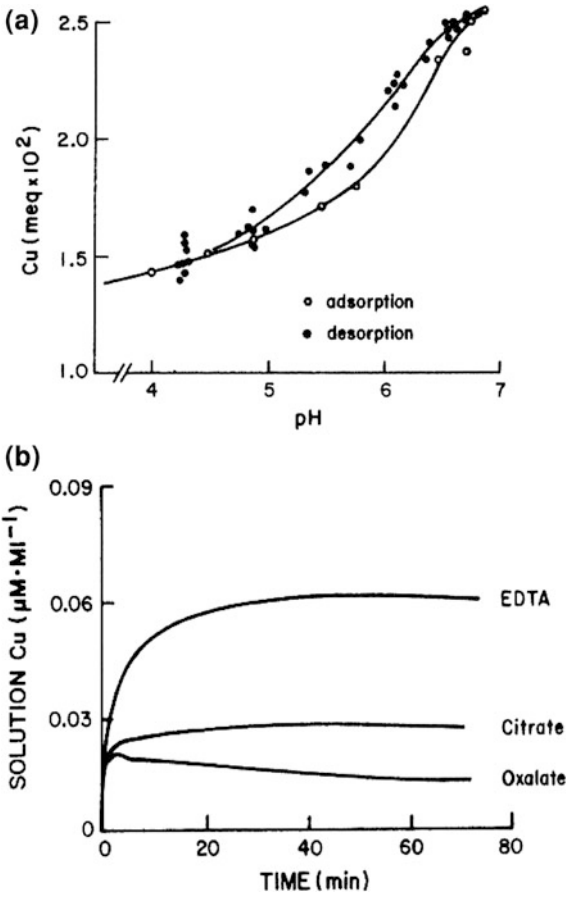

Fig. 8.47 Sorption of Cu^{2+} on montmorillonite as a function of **a** pH and **b** time-dependent release of soil-absorbed Cu by EDTA, citrate, and oxalate (Calvet 1989; Lehman and Harter 1984)

A difference in the rate of adsorption and desorption of Cr(VI) by alluvium was also observed in a batch experiment (Fig. 8.46b). On the basis of these two experiments, Stollenwerk and Grove (1985) concluded that the quantity of Cr(VI) adsorbed by alluvium is a function of its concentration as well as of the type and concentration of other anions in solution. The Cr(VI) adsorbed through nonspecific processes is desorbed readily by a Cr-free solution. Stronger bonds that are formed between Cr(VI) and alluvium during specific adsorption result in very slow release of this fraction. The Cr(VI) desorption from the alluvium material illustrates the hysteresis process that results from chemical transformation of a portion of contaminant retained in the subsurface.

The release rate of "nondesorbable," metallic cation contaminants adsorbed on the solid phase can be examined in terms of three environmental factors—pH, the presence of another metallic cation, and ligand presence—all of which vary substantially in subsurface aqueous solutions. A decrease in pH favors the release of cationic metals adsorbed on surfaces. An example of pH effects on Cu^{2+} release

for a montmorillonite clay is given in Fig. 8.47a (Calvet 1989). Lehman and Harter (1984) studied the kinetics of copper desorption from soils when various ligands (Na_2-oxalate, Na_3-citrate, and Na_4-EDTA) were added to copper-contaminated samples, in stoichiometric amounts relevant to the Cu addition (i.e., for a charge ratio of 1:1 Cu/ligand). Figure 8.47b shows the time-dependent release of Cu adsorbed on soil in solutions where the three organic cations are present. It is clear that each ligand in the subsurface environment affects Cu desorption differently; Cu release is enhanced in the presence of the EDTA ligand compared to citrate and oxalate. It also appears that Cu readsorbed onto the surface, in the case of Cu-oxalate. An additional factor to consider is the competition among metallic cations for sorption sites. Metals bound through surface complexation can be displaced by other cations.

Sequential disposal of heavy metals on land surfaces may control the pathway of their retention and release in the soil–subsurface system. An example of Pb and Cd retention on and release from soil material is given by Appel et al. (2008). The authors discuss behavior of these heavy metals when added sequentially or concurrently to three tropical soils: oxisol, ultisol, and mollisol. The retention/release patterns of monometal sequential addition of Pb > Cd or Cd > Pb in the three soils are presented in Fig. 8.48.

The differences in sorbed and exchanged Pb, when Pb was added to the soils before Cd as compared to when it was applied after Cd, were insignificant despite the fact that differences were observed between the soils. In contrast, the trend for Cd was different. In the case of oxisol—characterized by a high surface area—a significant decrease in the adsorbed Cd occurred when Cd was added to the soil after Pb application. Lead, which is much less exchangeable than Cd, inhibited Cd sorption. The authors attribute this behavior mainly to chemical characteristics of the heavy metals. Due to its relatively high electronegativity, low pK_h, and small hydrated radius, Pb was sorbed in preference to Cd. Cadmium was retained on the sorption sites of the soil–subsurface mineral phase to a greater extent than when it was added prior to Pb. Appel et al. (2008) suggested that at a contaminated site receiving successive amounts of Pb and Cd at different times, Cd may be more mobile when introduced into soil after Pb.

Retention of organic contaminants on subsurface solid-phase constituents in general is not completely reversible, so that release isotherms differ from retention isotherms. As a consequence, the extent of sorption depends on the nature of the sorbent. Subsurface constituents as well as the types of bonding mechanisms between contaminants and the solid phase are factors that control the release of adsorbed organic contaminants. Saltzman et al. (1972) demonstrated the influence of soil OM on the extent of hysteresis. Adsorption isotherms of parathion showed hysteresis (or apparent hysteresis) in its adsorption and desorption in a water solution. In contrast, smaller differences between the two processes were observed when the soils were pretreated with hydrogen peroxide (oxidized subsamples) to reduce initial OM content. The parathion content of the natural soils was greater (8 % in Golan soil, 24 % in Meron soil, and 31 % in Bet-Guvrin soil) than the oxidized subsamples. Natural peat retained two to three times more parathion than

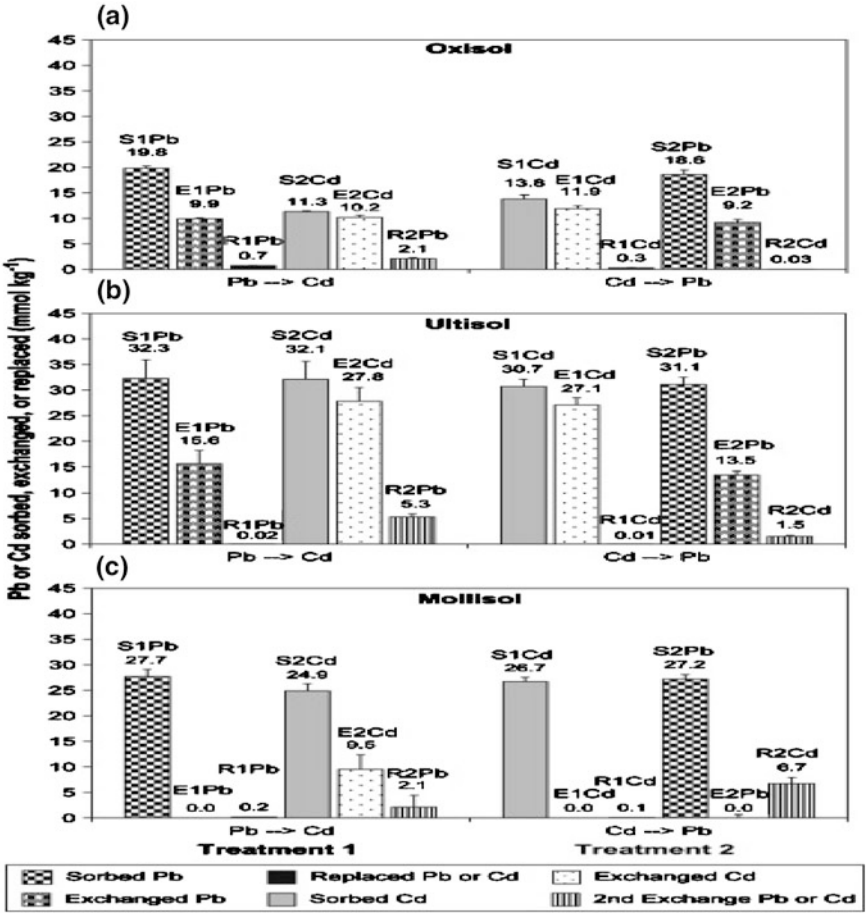

Fig. 8.48 Monometal sequential addition of Pb → Cd or Cd → Pb to the **a** Oxisol, **b** Ultisol, and **c** Mollisol soils. *S*, *E*, and *R* represent the amount of sorbed, exchanged, or replaced metal, respectively. The numbers following the letter designations indicate the order of metal addition to the soils (Appel et al. 2008)

the oxidized one. This behavior shows that parathion–organic complexes are stronger than parathion–mineral ones. Assuming that changes in OM content are solely responsible for changes in contaminant desorption, it is possible to estimate desorption curves for mineral and organic fractions. Figure 8.49 shows the calculated parathion desorption in water solutions from the (a) mineral and (b) organic fractions of Golan and Meron soils. The slopes of the desorption curves of the mineral fraction are rather steep (especially for Golan soil), indicating that adsorption is totally reversible. In the range of the concentration studied, only very small amounts of parathion appear to be released from the OM.

The properties of both OM and clay minerals may affect the release of contaminants from adsorbed surfaces. Zhang et al. (1990) report that desorption (in aqueous

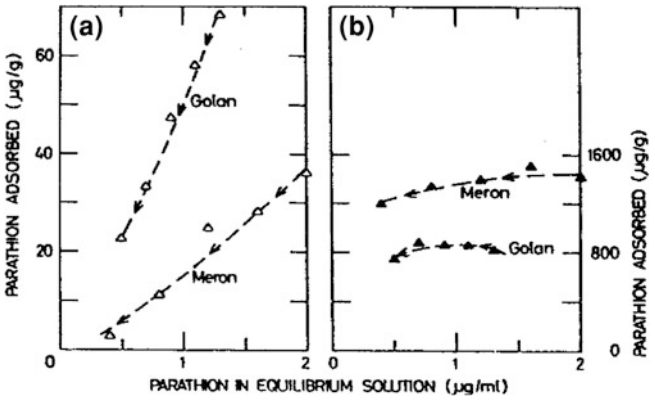

Fig. 8.49 Calculated parathion desorption from the **a** mineral and **b** organic fractions of Golan and Meron soils. Saltzman et al. (1972). Copyright 1972 American Chemical Society

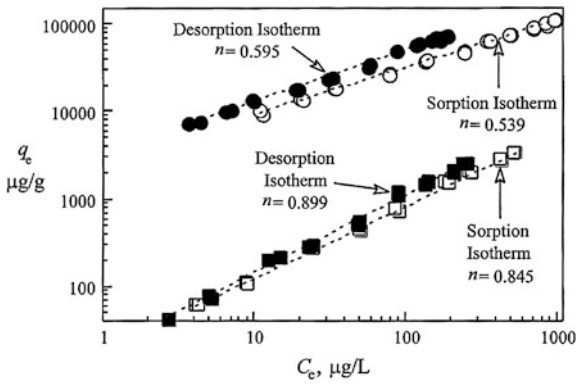

Fig. 8.50 Phenanthrene adsorption–desorption hysteresis observed for Lachine and Chelsa humic acid aggregate; the hysteresis index is given by *n*. Reprinted from Huang et al. (2003). Copyright 2003 with permission of Elsevier

solution) of acetonitrile solvent from homoionic montmorillonite clays is reversible, and hysteresis appears to exist except for K^+-montmorillonite. This behavior suggests that desorption may be affected by the fundamental difference in the swelling of the various homoionic montmorillonites, when acetonitrile is present in the water solution. During adsorption, it was observed that the presence of acetonitrile affects the swelling of different homoionic clays. At a concentration of 0.5 M acetonitrile in solution, the layers of K^+-montmorillonite do not expand as they would in pure water, while the layers of Ca^{2+}- and Mg^{2+}-montmorillonite expand beyond a partially collapsed state. The behaviors of K^+-, Ca^{2+}-, and Mg^{2+}-montmorillonite are different from the behavior of these clays in pure water. Na^+-montmorillonite is not affected by acetonitrile presence in an aqueous solution.

The heterogeneity of subsurface OM also may influence the release of adsorbed organic contaminants. Huang and Weber (1998) present adsorption–desorption isotherms of phenanthrene for a kerogen (Lachine) and a humic acid (Chelsea).

We see from Fig. 8.50 that both sorbents exhibit adsorption–desorption hysteresis. Compared to the humic acid, the kerogen exhibits a greater degree of hysteresis, as indicated by a higher hysteresis index.

The quality of desorption water is another factor affecting the release of organic contaminants from adsorbed surfaces. For example, Barriuso et al. (1992) demonstrated that DOM in desorbing aqueous solutions increases the release of atrazine and carbetamide adsorbed on soils. Desorption of diquat and paraquat herbicides was also affected significantly by the salt concentration of the aqueous extract (Kookana and Aylmore 1993). Both Ca^{2+} and Na^{+} cations compete for sorption sites with these herbicides, but Na^{+} is not as influential as Ca^{2+}. Desorption of diquat was higher than that of paraquat for all salt concentrations.

8.6 Bound Residues

Formation of bound residues is related mainly to the fate of crop protection chemicals and other toxic waste organics in the biologically active soil surface, during and after chemical redistribution in the subsurface over long periods of time.

Bound residues are those chemicals retained in the subsurface matrix in the form of the parent organic contaminant or its metabolites; these residues remain after subsequent extractions, during which the nature of the compound or of the matrix is not altered by the extraction procedure. An example of sequential extraction of pesticide residues from soil, to define the nonextractable contaminant or the bound residue, is described in the laboratory experiment protocols presented by Mordaunt et al. (2005). Six pesticides (atrazine, dicamba, isoproturon, lindane, paraquat, and trifluralin) with various properties were added to an agricultural soil from Terrington, United Kingdom (17 % clay, 2–2.5 % OM, pH 8), and kept under controlled environmental conditions for 90 days. The soil was sampled six times, submitted to sequential solvent extraction procedure, and analyzed for pesticide content during the incubation period. The following steps for sequential extraction were performed:

1. Extraction in 0.01 M $CaCl_2$, and shake for 24 h.
2. Acetonitrile: water (9:1) shake extraction for 24 h.
3. Methanol shake extraction for 24 h.
4. Dichloromethane shake extraction for 24 h.
5. Added ^{14}C-activity combusted to $^{14}CO_2$.

Step 1 simulates the readily available soil fraction, steps 2–4 indicate potentially available soil fractions, and step 5 yields the unextracted residue and completes the mass balance. Note that the solvent used becomes increasingly nonpolar during the extraction sequence. Summary data for the six studied compounds are presented in Fig. 8.51.

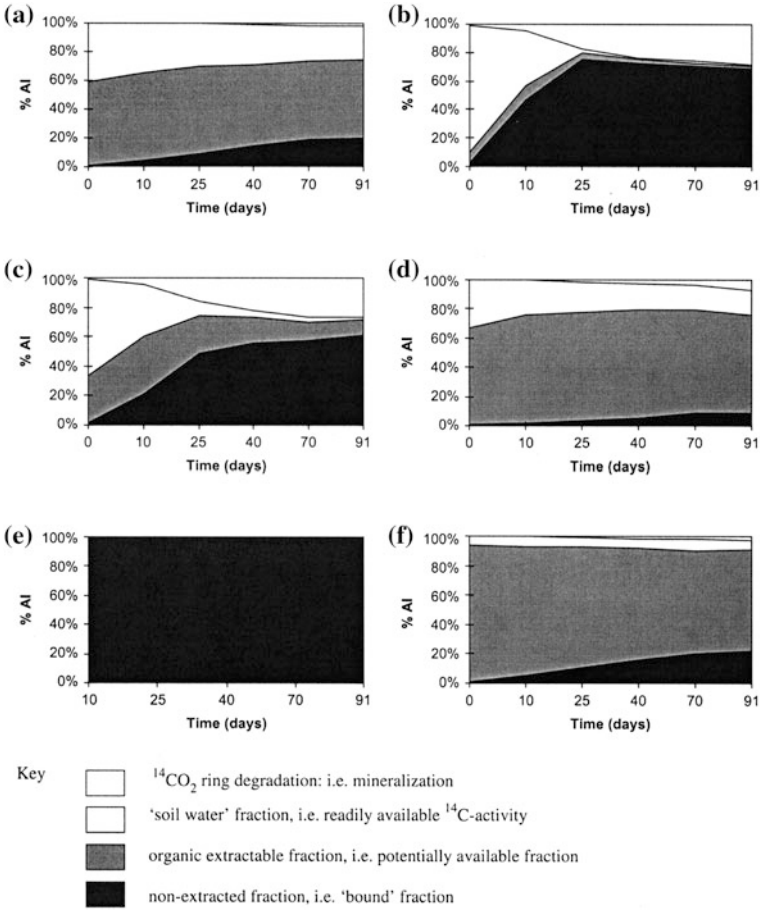

Fig. 8.51 Summary data of pesticide residues in the soil environment, showing the distribution between mineralization and extractability: **a** atrazine, **b** dicamba, **c** isoproturon, **d** lindane, **e** paraquat, and **f** trifluralin. Reprinted from Mordaunt et al. (2005). Copyright 2005 with permission of Elsevier

Mordaunt et al. (2005) categorized three classes of pesticide behavior: type A (atrazine, lindane, and trifluralin), in which ring degradation was limited as well as the formation of nonextractable residues; type B (dicamba, isoproturon), in which 25 % of ^{14}C-activity was mineralized and a large portion became nonextractable after 90 days; and type *C* (paraquat), in which a large portion of contaminant was found nonextractable after 90 days. These results illustrate the effect of extraction sequence by organic solvents on the extractable portion of contaminant from soils. However, because the soil matrix is altered during the extraction procedure, the data cannot be used to define the amount of pesticides remaining in soils as bound

Table 8.12 Reduction in compound availability for soil microbial degradation as a result of aging

Compound	Soil	Aging period (*d*)
Naphthalene	Colwood loam	365
Naphthalene	Mt. pleasant silt loam	68
Phenanthrene	Mt. pleasant silt loam	110
Phenanthrene	16 soils	200
Anthracene	Lima loam	203
Fluoranthene	Lima loam	140
Pyrene	Lima loam	133
Atrazine	Ravenna silt loam	90
Atrazine	16 soils	200
4-Nitrophenol	Lima loam	103
4-Nitrophenol	Edwards muck	103

Reprinted with permission from Alexander (2000). Copyright 2005 American Chemical Society

residues. Use of solvents milder than those used in this experiment lead to different bound residue values.

The effect of native soil microorganisms on formation of bound residues is illustrated by the study of Gevao et al. (2005) on formation and release of "nonextractable" ^{14}C-dicamba. The impact of microorganisms was determined by following the behavior of this compound under sterile and nonsterile regimes during 90 days of incubation, using a mild extraction solvent (0.01 M $CaCl_2$ aqueous solution). The reported results indicate that, one day following the treatment, about 5 % of the added contaminant was not extractable. The fraction of nonextractable dicamba increased exponentially to a maximum between 14 and 21 days after application, followed by a decrease that led, at the end of the experiment (90 days), to about 65 % nonextractable contaminant. This behavior characterizes the nonsterile soil. Different patterns appeared in a sterile incubation: A gradual increase in the amount of nonextractable residue was formed, reaching about 20 % of the initial activity two weeks following treatment. After this period, there were no significant changes in the amount of nonextractable residues formed for the entire incubation period. Additional treatment (e.g., fresh soil added to aged soil) led to the hypothesis that microorganisms play a dual role in the formation and eventual release of nonextractable residues. When a pesticide is added to a catabolically active soil, the degrading microorganisms convert the pesticide to one or more metabolites, which are capable of interacting with subsurface OM. In the case of dicamba, the major metabolite (3, 6 dichlorosalicylic acid) is adsorbed to a much greater extent than the parent compound; this strong adsorption of the metabolite prevents its extraction in $CaCl_2$ solution. As the concentration of the available portion of added pesticide drops, the microbes revert to utilizing subsurface OM for their energy needs. The microbes consume subsurface OM as their primary substrate, so the bound pesticide–metabolite molecules are freed from their entrapment with humic macromolecules.

As they persist or age, organic contaminants in the subsurface become progressively less available. In a review on contaminant bioavailability during aging, Alexander (2000) shows evidence that organic compounds aged in the field are less bioavailable than the same compounds added freshly to samples of the same soil. Table 8.12 compiles the time required for a number of contaminants to become less available for microbial degradation as result of aging. Bioavailability to microorganisms decreases with time, until reaching a value below which further decline is not detectable. The time required to reach this value varies among soils, compounds, and environmental conditions.

Sequestration is considered as the decrease in availability of a compound, for uptake by a living organism and for nonvigorous extraction by an organic solvent. Nam et al. (1998) studied phenanthrene sequestration by fresh and aged soil OM, where the contaminant presence was determined by both bioavailability (e.g., mineralization by an added bacterium) and mild solvent extraction (1-butanol) procedures. Sequestration of phenanthrene as measured by bacteria-induced mineralization was appreciable in samples with >2 % organic C and was not evident in samples with <2 % organic C. Phenanthrene aged 200 days was more slowly degraded than the freshly added compound in soils with >2 % organic C. However, only a small effect was evident when the soil organic C was <2 %. Mild extraction with 1-butanol showed that the quantity removed by the solvent diminished as the compound persisted and the rate of decline in extractability generally diminished with decreasing organic C. Subsequent extraction by Soxhlet led to complete recovery of the compound, showing that the decline in availability comes from sequestration and does not reflect a loss of phenanthrene during aging.

It is questionable whether or not the value obtained by bioassays or the sequestration value can be used to define contaminant-bound residues. Aging–sequestration relationships in the subsurface, as determined through bioavailability, may provide an answer for short-term assessment of the contamination status at a specific site. To predict long-term hazards caused to the subsurface by organic contaminants of anthropogenic origin, where potential changes in environmental parameters may occur, the use of a reliable solvent extraction of bound residues is required

8.7 Contaminants in Urban Geosystems

Land surface deposits in the urban environment comprise a mixture of natural earth materials and disposed residues during many years of human activity. The term “urban geochemistry” was initially used by Thornton in the 1990s and reactivated recently by Jartun and Ottensen (2011) and Lyons and Harmon (2012). Urban geochemistry is characterized by intense toxic chemical disposal on a soil–subsurface landscape already disturbed by previous anthropogenic manipulation. The redistribution of contaminants in an urban environment differs from that occurring in a natural geosystem, due to differential impact of microrelief, water,

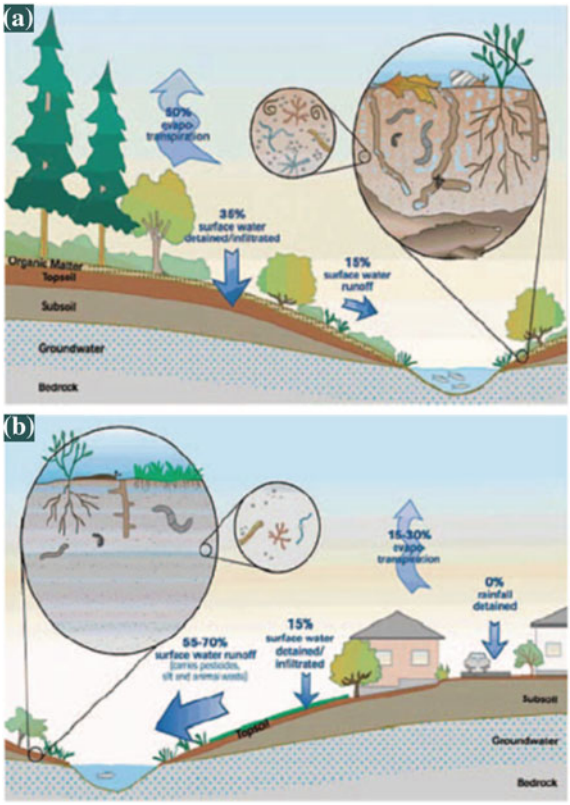

Fig. 8.52 The movement of water into a soil depends on land surface slope, vegetation, degree of surface loading, and soil texture, structure, density, and compaction. More water moves into the soil zone on natural landscapes compared to urban landscapes with disturbed soils. These schematic drawings compare the generalized disposition and movement of incoming water on a natural plant-covered landscape **a** with that in a disturbed urban landscape and **b** with limited vegetation and abundant impervious surfaces (Lyons and Harmon 2012; modified after Scheyer and Hipple 2005)

and vegetation (Fig. 8.52). Urbanization strongly affects the physical and hydrological regime of a natural soil–subsurface and may completely change the pathway of disposed contaminants.

Two specific groups of chemical contaminants that are retained in soil–subsurface systems are heavy metals and metalloids, and petroleum hydrocarbons. Several examples involving these chemicals are discussed here, being representative of urban contamination.

Arsenic contamination of soil–subsurface systems is of great environmental concern. Chirenje et al. (2003) examined arsenic contamination in urban and nonurban areas in Florida (USA). Arsenic presence was determined in 440 urban and 448 uninhabited locations; the distribution of arsenic concentrations is presented in Fig. 8.53. In general, arsenic concentrations in urban areas were higher than those in uninhabited areas. The differences between the two urban sites are due to their specific land uses. The authors noted that soil arsenic concentration in the nonurban areas showed significant correlation with natural soil properties, because they were exposed to a lower disturbance than urban soils. As a

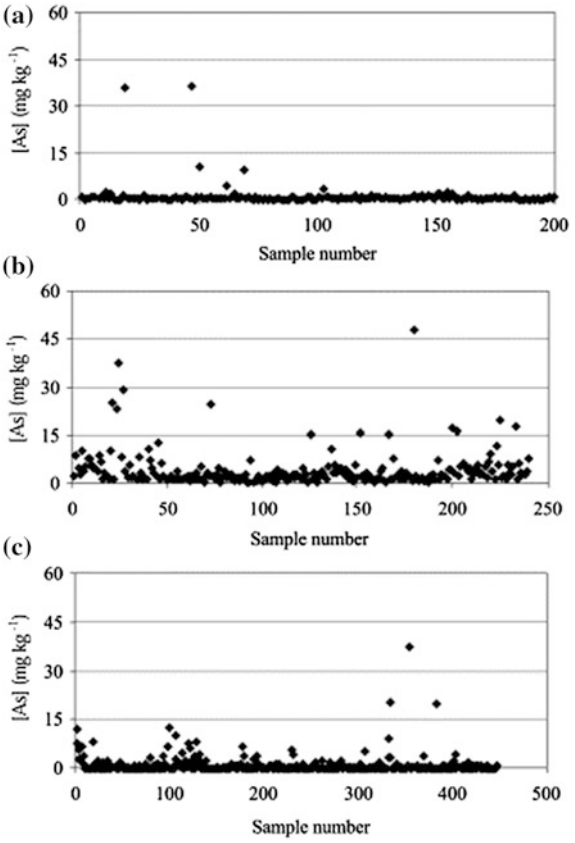

Fig. 8.53 Soil arsenic concentration (raw data) distribution in **a** Gainesville ($n = 200$), **b** Miami ($n = 240$), and **c** nonurban areas ($n = 448$) in Florida (Chirenje et al. 2003)

consequence, arsenic concentrations in urban soils showed greater variation than those from relatively undisturbed nonurban soils.

The potential adsorption of Cd, Cu, Cr, Pb, and Zn heavy metals on a "typical" mixed brownfield deposit from Scotland (UK) is reported by Markiewicz-Patkowska et al. (2005). The urban soil was collected from 15 points within a derelict area formerly used as a mix of residential and workshop/warehouse activities. The soil sample had a sandy loam texture and neutral/slightly acid pH. Fragments of brick, OM, and demolition wastes were clearly visible, suggesting that 10–15 % of the bulk was of anthropogenic origin. The sorption of heavy metals from single and multielement solutions, as a function of their initial concentration and pH, is presented in Fig. 8.54. It is found that adsorption of Cu from a single-element solution was over four times greater than adsorption from a multielement solution, due to competitive effects. In the case of Cr and Zn, release of metal from soil to solution was observed. The adsorption capacity at pH 2 occurred in the order Cr > Cu > Pb > Cd, and at pH 7 Cd > Zn, with precipitation affecting Cu and Pb

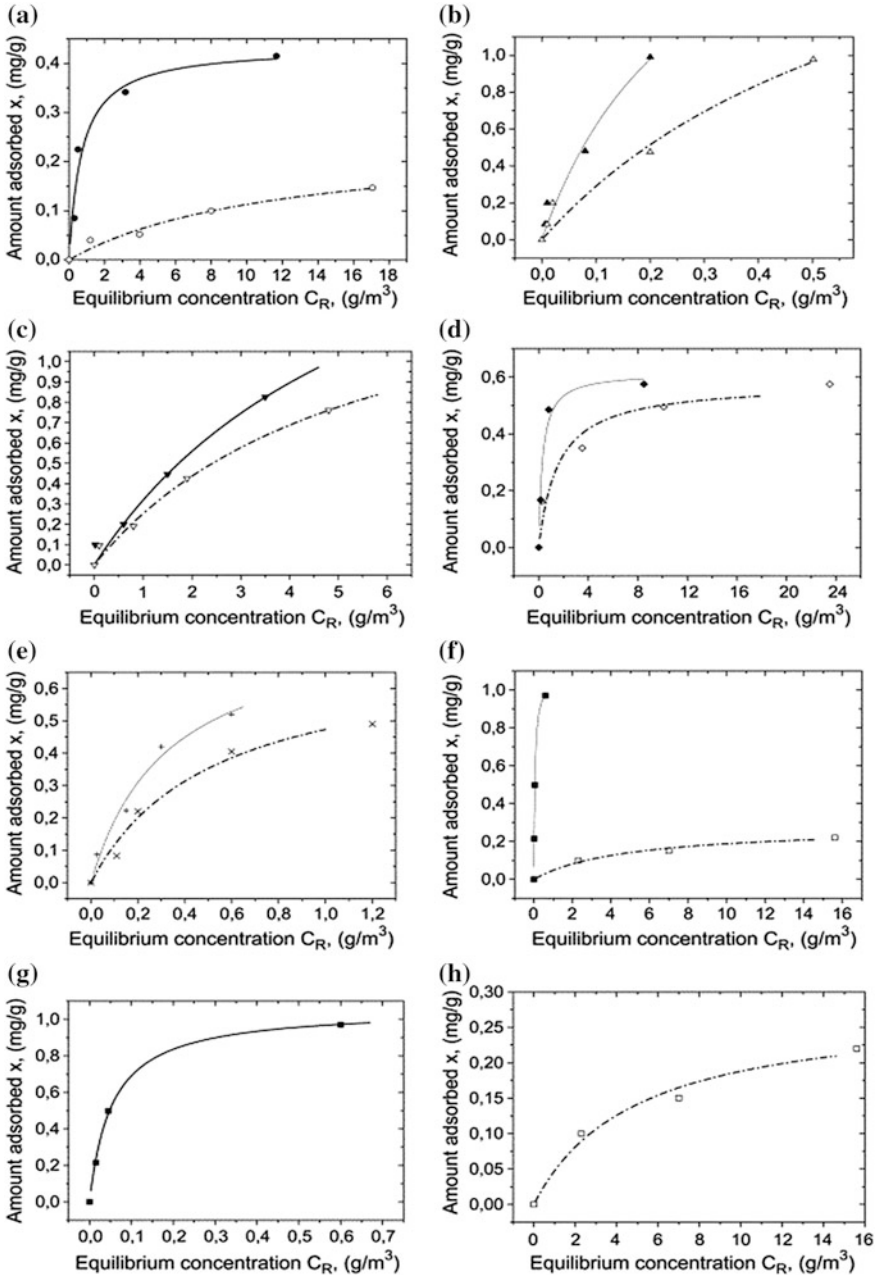

Fig. 8.54 Langmuir adsorption isotherms for the selected metals, at different pH values, adsorption from single- and multielement solutions. Experimental data (*points*), approximation function (*lines*): **a** Cd, pH 2, single (*black circle*), multi (*open circle*), **b** Cd, pH 7, single (*black up-pointing triangle*), multi (*open up-pointing triangle*), **c** Cr, pH 2, single (*black down-pointing triangle*), multi (*open down-pointing triangle*), **d** Pb, pH 2, single (), multi (*open diamond*), **e** Zn, pH 7, single (+), multi (×), and **f** Cu, pH 2, single (*black square*), multi (*open square*) (Markiewicz-Patkowska et al. 2005)

Table 8.13 Range and median of detected PAHs in three urban soils (modified after Morillo et al. 2008)

Compound	Range (and median) (μg/kg, dry weight basis)		
	Glasgow	Ljubljana	Torino
Naphthalene	16.5–940 (68.1)	17.7–38.6 (28.8)	15.3–79.4 (30.0)
Acenaphthene	9.10–848 (25.0)	0.005–19.9 (9.07)	5.69–74.2 (8.82)
Fluorene	13.3–750 (38.1)	6.60–54.3 (10.9)	7.22–241 (11.7)
Phenanthrene	187–9,736 (1379)	21.9–2,776 (84.4)	22.7–2,670 (75.9)
Anthracene	28.6–1,352 (136)	6.02–30.5 (12.0)	5.10–370 (11.6)
Fluoranthene	141–7,249 (1125)	16.1–872 (101)	12.6–3,560 (47.9)
Pyrene	184–7,835 (1124)	15.4–248 (94.9)	9.62–3,460 (71.8)
Benzo[a]anthracene	109–3,928 (680)	11.5–158 (51.7)	8.23–2,040 (40.9)
Chrysene	154–5,002 (856)	12.8–209 (72.3)	8.70–2,430 (41.0)
Benzo[b]fluoranthene	92.1–2,984 (525)	5.21–203 (56.4)	4.68–2,020 (30.7)
Benzo[k]fluoranthene	63.0–1,400 (292)	12.7–90.8 (34.6)	10.4–1,240 (25.8)
Benzo[a]pyrene	132–3,627 (657)	18.4–186 (70.9)	14.1–3,170 (44.5)
Dibenzo[a, h]anthracene	16.7–399 (70.0)	6.23–25.4 (10.9)	5.09–153 (10.8)
Benzo[g, h, i]perylene	117–3,884 (544)	12.8–187 (36.8)	11.9–1,640 (52.8)
Indeno[1, 2, 3-c, d]pyrene	158–2,827 (424)	0.04–185 (66.2)	0.047–364 (63.3)
Σ15 PAHs	1,487–51,822 (8,337)	218–4,488 (791)	148–23,500 (704)

behavior. The urban soil studied displayed some enhanced adsorption as compared to agricultural soils, probably due to the presence of anthropogenic materials.

Contamination of the soil–subsurface environment by PAHs is of major interest due to their potential health hazards. The highest concentration of PAHs occurs in urban areas near point sources and in soils with high OM. A survey of PAH concentrations in European cities was performed by Morillo et al. (2008). Glasgow (UK), Torino (Italy), and Lubljana (Slovenia) were selected for this study, and the same methodology for soil sampling, extraction, and chemical analysis was employed. Median PAH concentrations resulting from analysis of 20 samples in each city are presented in Table 8.13. Despite the wide range of values in PAH concentrations, it is clear that in Glasgow urban soils, the contamination is about 10 times higher than in the other cities studied. The three predominant PAHs were phenanthrene, fluoranthene, and pyrene, representing about 40 % of the total compounds found in the urban soils. Based on these results, the authors consider that PAH contamination of the urban soils is due to pyrogenic origin and is affected by climatic conditions, natural OC of the soil, and proximity to the contamination sources.

Polychlorinated naphthalenes (PCNs) are extremely toxic compounds including congeners with chlorine substitutions in the 2-, 3-, 6-, and 7-positions. These contaminants are found both in urban and rural environments. Krauss and Wilcke (2003) studied the fate of PCNs in soils, investigating their occurrence in urban and rural environments. Their study comprised 49 topsoils from various locations

Table 8.14 Sums of the concentrations of PCNs, PCBs, and PAHs in urban soils of Bayreuth and rural soils under different land use (medians and ranges) (Krauss and Wilcke 2003)

Land use	*n*	Σ35 PCNs (μg/kg)		Σ12 PCBs (μg/kg)		Σ20 PAHs (μg/kg)	
		Median	Range	Median	Range	Median	Range
Urban sites							
Alluvial grassland	10	1.6	0.35–5.7	14.8	3.3–58.1	2.7	0.38–20.7
House garden	10	3.6	0.29–15.4	14.8	2.8–158	10.9	0.81–17.7
Park	9	0.46	0.10–3.1	5.5	0.82–13.7	1.9	0.76–10.5
Roadside	9	0.90	0.28–4.7	14.3	2.2–91.9	2.3	0.63–186
Industrial	7	1.9	0.67–15.0	21.9	2.3–70.2	10.3	2.4–48.9
Agricultural	4	0.10	nd[a]–0.51	1.6	1.1–7.6	0.64	0.28–2.2
Urban area	49	1.3	nd–15.4	13.0	0.82–158	3.4	0.28–186
City center[b]	17	0.74	0.23–7.4	8.7	1.5–20.7	2.7	0.63–20.7
Outskirts[b]	14	0.92	nd–5.6	10.3	0.82–58.1	1.2	0.28–7.2
Rural sites							
Agriculture	6	0.13	nd–0.29	1.6	1.1–2.6	0.30	0.19–0.69
Alluvial grassland	3	0.44	0.07–0.82	1.8	1.3–5.0	0.37	0.16–2.1
Rural area	9	0.13	nd–0.82	1.7	1.1–5.0	0.34	0.16–2.1

[a] Not detected
[b] Without house gardens, industrial sites, and roadside soil

within the city of Bayreuth (Germany) and 9 agricultural soils in the vicinity of the city. It was found that PCN concentrations were five times lower in the rural area than in the central part of the city, characterized by the same natural soil. Table 8.14 shows PCN concentrations in comparison with polychlorinated biphenyls (PCBs) and PAHs found in both urban and rural soils. The human impact on soil contamination is confirmed by the highest concentrations occurring in industrial sites and in house gardens. The increase in PCN ad PCB concentrations in the rural soils may be explained by the more volatile lower molecular weight compounds being easily transported in gaseous phase from urban to rural areas (Krauss and Wilcke 2003).

References

Alexander M (2000) Aging, bioavailability and overestimation of risk from environmental pollutants. Environ Sci Technol 34:4259–4265

Appel C, Ma QL, Rhue RD, Reve W (2008) Sequential sorption of lead and cadmium in three tropical soils. Environ Pollut 155:132–140

Babiarz CL, Hurley JP, Hoffman SR, Andren AW, Shafer MM, Armstrong DE (2001) Partitioning of total mercury and methylmercury to the colloidal phase in freshwaters. Environ Sci Technol 35:4773–4782

Bang JS, Hesterberg D (2004) Dissolution of trace element contaminants from two coastal plain soils as affected by pH. J Environ Qual 33:891–901
Barriuso E, Baer U, Calvet R (1992) Dissolved organic matter and adsorption-desorption of difemuron, atrazine and carbetamide by soils. J Environ Qual 21:359–367
Bar-Yosef B, Afic I, Rosenberg R (1989) Fluoride sorption and mobility in reactive porous media. In: Bar Yosef B, Barrow NJ, Goldschmid J (eds) Inorganic contaminants in the vadose zone. Springer, Heidelberg, pp 75–89
Bennett B, Larter SR (1997) Partition behaviour of alkylphenols in crude/oil brine systems under subsurface condition. Geochim Cosmochim Acta 61:4393–4402
Bergaoui L, Lambert JF, Prost R (2005) Cesium adsorption on soil clay: macroscopic and spectroscopic measurements. App Clay Sci 29:23–29
Buerge-Weirich D, Hari R, Xue H, Behra O, Sigg L (2002) Adsorption of Cu, Cd, and Ni on goethite in the presence of natural ground ligands. Environ Sci Technol 36:328–336
Burns IG, Hayes MHB, Stacey M (1973) Some physico-chemical interactions of paraquat with soil organic materials and model compounds. II. Adsorption and desorption equilibria in aqueous suspensions. Weed Res 13:79–90
Calvet R (1989) Adsorption of organic chemicals in soils. Environ Health Perspect 83:145–177
Chaney RL (1989) Toxic element accumulation in soils and crops protecting soil fertility and agricultural food chains. In: Bar Yosef B, Barrow NJ, Goldschmid J (eds) Inorganic contaminants in the vadose zone. Springer, Heidelberg, pp 140–159
Charlatchka R, Cambier P (2000) Influence of reducing conditions on solubility of trace metals in contaminated soils. Water Air Soil Poll 118:143–167
Chirenje T, Ma LQ, Chen M, Zillioux EJ (2003) Comparison between background concentrations of arsenic in urban and non-urban areas of Florida. Adv Environ Res 8:137–146
Cho HH, Choi J, Goltz MN, Park JW (2002) Combined effect of natural organic matter and surfactants on the apparent solubility of polycyclic aromatic hydrocarbons. J Environ Qual 31:275–280
Coulibaly KM, Borden RC (2004) Impact of edible oil injection on the permeability of aquifer sands. J Contam Hydrol 71:219–237
Donovan WC, Logan TJ (1983) Factors affecting ammonia volatilization from sewage sludge applied to soil in a laboratory study. J Environ Qual 12:584–590
Dror I, Kliger L, Laufer A, Hadas A, Russo D, Yaron B (1999) Behavior of atrazine and terbuthylazine in an irrigated field: I. Soil and management spatial variability. Agrochimica 43:21–29
Dror I, Gerstl Z, Prost R, Yaron B (2000) Behavior of neat and enriched volatile petroleum hydrocarbons mixture in the subsurface during leaching. Land Contam Reclam 8:341–348
Dror I, Gerstl Z, Prost R, Yaron B (2002) Abiotic behavior of entrapped petroleum products in the subsurface during leaching. Chemosphere 49:1375–1388
Dror I, Amitay T, Yaron B, Berkowitz B (2003) A "salt-pump" mechanism for induced intrusion of organic contaminants from marine sources into coastal aquifers. Science 300:950
Engel MH, Macko SA (1993) Organic geochemistry: principles and applications. Plenum, New York
Fine P, Yaron B (1993) Outdoor experiments on enhanced volatilization by venting of kerosene components from soil. J Contam Hydrol 12:335–374
Flühler H, Polomski J, Blaser P (1982) Retention and movement of fluoride in soils. J Environ Qual 11:461–468
Foster KL, Mackay D, Parkerton TF, Webster E, Milford L (2005) Five-stage environmental exposure assessment strategy for mixture: gasoline as a case study. Environ Sci Technol 39:2711–2718
Galin Ts, Gerstl Z, Yaron B (1990) Soil pollution by petroleum products. III. Kerosene stability in soil columns as affected by volatilization. J Contam Hydrol 5:375–385
Gerstl Z, Yaron B (1981) Attapulgite-pesticide interactions. Residue Rev 78:69–99
Gevao B, Jones KC, Semple KT (2005) Formation and release of non-extractable ^{14}Dicamba residues in soil under sterile and non-sterile regimes. Environ Pollut 133:17–24

Giles CH, MacEwan TH, Nakhwa SN, Smith D (1960) Studies in adsorption. Part XI. A system of classification of solution adsorption isotherms and its use in diagnosis and adsorptive mechanism and measurements of specific area of solids. Chem Soc J 3:3973–3993

Gobran G, Miyamoto S (1985) Dissolution rate of gypsum in aqueous salt solutions. Soil Sci 140:89–94

Green CH, Heil DM, Cardon GE, Butters GL, Kelly EF (2003) Solubilization of manganese and trace metals in soils affected by acid mine runoff. J Environ Qual 32:1323–1334

Haitzer M, Aiken GR, Ryan JN (2002) Binding of mercury(II) to dissolved organic matter: the role of the mercury-to-DOM concentration ratio. Environ Sci Technol 36:3564–3570

Hargrove WL (1986) The solubility of aluminum-organic matter and its implication on plant uptake aluminum. Soil Sci 142:179–181

Hayden NJ, Voice TC, Wallace RB (1997) Residual gasoline saturation in unsaturated soil with and without organic matter. J Contam Hydrol 25:271–281

Hayes MHB, Mingelgrin U (1991) Interactions at the soil colloid-solution interface. In: Bolt GH, De Boodt MF, Hayes MF, McBride MB (eds) NATO ASI series—applied science—series F vol 190. Kluwer, Dordrecht, pp 324–401

Huang W, Peng P, Yu Z, Fu J (2003) Effects of organic matter heterogeneity on sorption and desorption of organic contaminants by soils and sediments. Appl Geochem 18:955–972

Huang W, Weber WJ Jr (1998) A distributed reactivity model for sorption by soils and sediments: slow concentration-dependent sorption rate. Environ Sci Technol 32:3549–3555

Jarsjo J, Destouni G, Yaron B (1994) Retention and volatilization of kerosene: laboratory experiments on glacial and postglacial soils. J Contam Hydrol 17:167–185

Jartun M, Ottensen RT (2011) Urban geochemistry. In: Harmon RS, Parker A (eds) Contribution of geochemistry to the study of the earth frontiers in geochemistry. Wiley, Hoboken, pp 221–237. doi:10.1002/9781444329957.ch11

Jayaweera GR, Mikkelsen DS (1991) Assessment of ammonia volatilization from flooded soil systems. Adv Agron 45:303–357

Johnston AE, Goulding KWT, Poulton PR (1986) Soil acidification during more than 100 years under permanent grassland and woodland at Rothamsted. Soil Use Manage 2:3–10

Karlson U, Frankenberger WT (1988) Determination of gaseous Se-75 evolved from soil. Soil Sci Soc Am J 52:678–681

Khachikian C, Harmon TC (2000) Nonaqueous phase liquid dissolution in porous media: current state of knowledge and research needs. Trans Porous Media 38:3–28

Kookana RS, Aylmore LAG (1993) Retention and release of diquat and paraquat herbicides in soils. Austral J Soil Res 31:97–109

Krauss M, Wilcke W (2003) Polychlorinated naphthalenes in urban soils: analysis, concentrations, and relation to other persistent organic pollutants. Environ Pollut 122:75–89

Lai KM, Johnson KL, Scrimshaw MD, Lester JN (2000) Binding of waterborne steroid estrogens to solid phases in river and estuarine systems. Environ Sci Technol 34:3890–3894

Lee LS, Strock TJ, Sarmah AK, Rao PSC (2003) Sorption and dissipation of testosterone, estrogens, and their primary transformation products in soils and sediment. Environ Sci Technol 37:4098–4105

Lehman RG, Harter RD (1984) Assessment of copper-soil bond strength by desorption kinetics. Soil Sci Soc Am J 43:769–772

Lin ZQ, Schemenauer RS, Cervinka V, Zayed A, Lee A, Terry N (2000) Selenium volatilization from a soil—plant system for the remediation of contaminated water and soil in the San Joaquin Valley. J Environ Qual 29:1048–1056

Lindsay WL (1979) Chemical equilibria in soils. Wiley, New York

Liu C, Zachara JM, Smith SC, McKinley JP, Ainsworth CC (2003) Desorption kinetics of radiocesium from subsurface sediments at Hanford Site USA. Geochim Cosmochim Acta 67:2893–2912

Loffredo E, Senesi N (2006) Fate of anthropogenic organic pollutants in soils with emphasis on adsorption/desorption processes of endocrine disruptor compounds. Pure App Chem 78:947–961

Lyons WB, Harmon RS (2012) Why urban geochemistry? Elements 8:439–444
Maqueda C, Undabeytia T, Morillo E (1998) Retention and release of copper on montmorillonite as affected by the presence of pesticide. J Agric Food Chem 46:1200–1204
Markiewicz-Patkowska JA, Hursthouse A, Przybyla-Kij H (2005) The interaction of heavy metals with urban soils: sorption behaviour of Cd, Cu, Cr, Pb and Zn with a typical mixed brownfield deposit. Environ Inter 31:513–521
Master Y, Laughlin RJ, Stevens RJ, Shaviv A (2004) Nitrite formation and nitrous oxide emissions as affected by reclaimed effluent application. J Environ Qual 33:852–860
McBride MB (1989) Reactions controlling heavy metals solubility in soils. Adv Soil Sci 10:1–47
McBride MB (1994) Environmental chemistry of soils. Oxford University Press, Oxford
Melkior T, Yahiaoi S, Motellier S, Thoby D, Tevissen E (2005) Cesium sorption and diffusion in Bure mudrock samples. Appl Clay Sci 29:172–186
Mordaunt CJ, Gevao B, Jones KC, Semple KT (2005) Formation of non-extractable pesticide residues: observations on compound differences, measurement and regulatory issues. Environ Pollut 133:25–34
Morillo E, Romero AS, Madrid L, Villaverde J, Maqueda C (2008) Characterization and sources of PAHs and potentially toxic metals in urban environments of Sevilla (Southern Spain). Water Air Soil Pollut 187:41–51
Mulder J, van Grinsven JJM, Breemen N (1987) Impacts of acid atmospheric deposition on woodland soils. III. Aluminum chemistry. Soil Sci Soc Am J 51:1640–1646
Nam K, Chung N, Alexander M (1998) Relationship between organic matter content of soil and the sequestration of phenanthrene. Environ Sci Technol 32:3785–3788
Ni N, El-Sayed MM, Sanghvi T, Yalkowsky SH (2000) Estimation of the effect of NaCl on the solubility of organic compounds in aqueous solutions. J Pharm Sci 89:1620–1625
Park SK, Bielefeldt A (2003) Equilibrium partitioning of non-ionic surfactant and pentachlorophenol between water and a non-aqueous phase liquid. Water Res 37:3412–3420
Peck AM, Hornbuckle KC (2005) Gas-phase concentrations of current-use pesticides in Iowa. Environ Sci Technol 39:2952–2959
Prost R, Gerstl Z, Yaron B, Chaussidon J (1977) Infrared studies of parathion attapulgite interaction. In: Behavior of pesticides in soils. Israel-France symposium INRA, Versailles, pp 108–115
Qin H, Yakoyama Y, Fan Q, Iwatani H, Tanaka K, Sakaguchi A, Kanai Y, Zhu J, Onda Y, Takahashi Y (2012) Investigation of cesium adsorption on soil and sediment samples from Fukushima Prefecture by sequential extraction and EXAFS technique. Geochem J 46:297–302
Ross DS, Sjogren RE, Bartlett EJ (1981) Behavior of chromium in soils: IV. Toxicity to microorganisms. J Environ Qual 10:145–148
Rytwo G, Tropp T, Serban C (2002) Adsorption of diquat, paraquat and methyl green on sepiolite: experimental results and model calculations. Appl Clay Sci 20:273–282
Saltzman S, Kliger L, Yaron B (1972) Adsorption-desorption of parathion as affected by soil organic matter. J Agric Food Chem 20:1224–1227
Saltzman S, Yariv S (1976) Infrared and X-ray study of parathion montmorillonite sorption complexes. Soil Sci Soc Am J 35:700–705
Sanudo-Wilhelmy SA, Rossi FK, Bokuniewicz H, Paulsen RJ (2002) Trace metal levels in groundwater of a coastal watershed: importance of colloidal forms. Environ Sci Technol 36:1435–1441
Scheyer JM, Hipple KW (2005) Urban soil primer. United States Department of Agriculture, Natural Resources Conservation Service, National Soil Survey Center, Lincoln, Nebraska. http://soils.usda.gov/use
Schmidt TC, Kleinert P, Stengel C, Goss KU, Haderlein SB (2002) Polar fuel constituents—compound identification and equilibrium partitioning between nonaqueous phase liquid and water. Environ Sci Technol 36:4074–4080
Song J, Peng P, Huang W (2002) Black carbon and kerogen in soils and sediments. I. Quantification and characterization. Environ Sci Technol 36:3960–3967

Sorensen H, Pedersen KS, Christensen PL (2002) Modeling gas solubility in brine. Org Geochem 33:635–642
Sparks DL (2005) Sorption–desorption, kinetics. In: Hillel D et al (eds) Encyclopedia of soils in the environment. Elsevier Ltd, Oxford, pp 556–561
Spencer WF, Cliath MM (1969) Vapor densities of dieldrin. Environ Sci Technol 3:670–674
Spencer WF, Cliath MM (1973) Pesticide volatilization as related to water loss from soil. J Environ Qual 2:284–289
Sposito G, Martin Neto L, Yang A (1996) Atrazine complexation by soil humic acids. J Environ Qual 25:1203–1209
Sterling MC Jr, Bonner JS, Page CA, Ernest ANS, Autenrieth RL (2003) Partitioning of crude oil polycyclic aromatic hydrocarbons in aquatic systems. Environ Sci Technol 37:4429–4434
Stollenwerk KC, Grove DB (1985) Adsorption and desorption of hexavalent chromium in an alluvial aquifer near Telluride, Colorado. J Environ Qual 14:150–155
Strawn DG, Sparks DI (2000) Effects of soil organic matter on the kinetics and mechanisms of Pb(II) sorption and desorption in soil. Soil Sci Soc J 64:144–156
Stumm W, Morgan JJ (1996) Aquatic chemistry, 3rd edn. Wiley, New York
Taylor AW, Spencer WF (1990) Volatilization and vapor transport processes. In: Cheng HH (ed) Pesticides in the soil environment (Soil Sci Soc Amer Book Ser 2). Madison, Wisconsin, pp 213–369
Tengen I, Doerr H, Muennich KO (1991) Laboratory experiments to investigate the influence of microbial activity on the migration of cesium on a forest soil. Water Air Soil Poll 57(58):441–449
Thomas GW, Yaron B (1968) Adsorption of sodium from irrigation water by four Texas soils. Soil Sci 106:213–220
Thorpe KL, Cummings RI, Hutchinson TH, Scholze M, Brighty G, Sumpter JP, Tyler CR (2003) Relative potencies and combination effects of steroidal estrogens in fish. Environ Sci Technol 37:1142–1149
Tsai WT, Lai CW, Hsien KJ (2003) Effect of particle size of activated clay on the adsorption of paraquat from aqueous solution. J Coll Interface Sci 263:29–34
Turner A (1996) Trace-metal partitioning in estuaries: importance of salinity and particle concentration. Mar Chem 54:27–39
Turner A, Millward GE, LeRoux SM (2001) Sediment-water partitioning of inorganic mercuries in estuaries. Environ Sci Technol 35:4648–4654
Turner A, Martino M, Le Roux SM (2002) Trace metal distribution coefficients in the Mersey Estuary UK: evidence for salting out of metal complexes. Environ Sci Technol 36:4578–4584
Undabeytia T, Morillo E, Ramos AB, Maqueda C (2002) Mutual influence of Cu and a cationic herbicide on their adsorption–desorption processes on two selected soils. Water Air Soil Poll 137:81–94B
van Grunsven HJM, van Riensdijk WH, Otjes R, van Beemer N (1992) Rates of aluminum dilution in acid sandy soils observed in column experiments. J Environ Qual 21:439–447
Vinten AJ, Mingelgrin U, Yaron B (1983) The effect of suspended solids in waste water on soil hydraulic conductivity I. Suspended solid labeling method II. Vertical distribution of suspended solids. Soil Sci Soc Am J 47:402–412
Waite DT, Cessna AJ, Grover R, Kerr LA, Snihura AD (2004) Environmental concentrations of agricultural herbicides in Saskatchewan, Canada: bromoxynil, dicamba, diclofop, MCPA, triluralin. J Environ Qual 33:1616–1628
Wolters A, Linnemann V, Herbst M, Klein M, Schaffer A, Vereecken H (2003) Pesticide volatilization from soil: lysimeter measurements versus predictions of European registration models. J Environ Qual 32:1183–1193
Xiang HF, Banin A (1996) A solid-phase manganese fractionation changes in saturated arid-zone soils: pathways and kinetics. Soil Sci Soc Am J 60:1072–1080
Xiao B, Yu Z, Peng P, Song J, Huang W (2004) Black carbon and kerogen in soils and sediments. 2. Their role in phenanthrene and naphthalene sorption equilibria. Environ Sci Technol 38:5842–5852

Xu D, Zhou X, Wang X (2008) Adsorption and desorption of Ni^{2+} on Na-montmorillonite: effects of pH, ionic strength, fulvic acid, humic acid addition sequences. Appl Clay Sci 39:133–141

Yaron B (1978) Organophosphorus pesticide-clay interactions. Soil Sci 125:412–417

Yaron B, Dror I, Graber E, Jarsjo J, Fine P, Gerstl Z (1998) Behavior of volatile organic mixtures in the soil environment. In: Rubin H, Narkis N, Carberry J (eds) Soil and aquifer pollution. Springer, Heidelberg, pp 37–58

Yaron B, Saltzman S (1978) Soil-parathion surface interactions. Residue Rev 69:1–34

Yaron-Marcovich D, Dror I (2007) Berkowitz B (2007) Behavior and stability of organic contaminant droplets in aqueous solutions. Chemosphere 69:1593–1601. doi:10.1016/j.chemosphere.2007.05.056

Zhang ZZ, Sparks DL, Pease RA (1990) Sorption and desorption of acetonitrile on montmorillonite from aqueous solutions. Soil Sci Soc Am J 54:351–356

Zhong L, Mayer AS, Pope GA (2003) The effects of surfactant formulation on non-equilibrium NAPL solubilization. J Contam Hydrol 60:55–75